Department of Precision and Microsystems Engineering

In-situ spectral calibration module for an earth observation satellite
Devabhaktuni Chakravarthy

TUDelft Delft University of Technology

TNO

Challenge the future

In-situ spectral calibration module for an earth observation satellite

by

Devabhaktuni Chakravarthy

to obtain the degree of Master of Science
at the Delft University of Technology,
to be defended publicly on Thursday October 28, 2021 at 10:30 AM.

This thesis is confidential and cannot be made public until October 28, 2023.

An electronic version of this thesis is available at `http://repository.tudelft.nl/`.

Abstract

With climate change being a prime source of concern around the world, air pollution is a topic that requires special attention. Therefore, it is of utmost importance to track and measure the emissions in our environment for detecting the sources and understating the climate change so as to figure out possible solutions. Despite ongoing development, the current LEO and GEO satellite instruments have a long prolonged global survey, revealing the pollution trends at a broad scale, but there is still a lack of high-resolution data to pinpoint pollution sources.

For this, John Hopkins University (Applied physics lab) and NASA are now developing a new earth atmospheric monitoring mission called Compact Hyperspectral Air Pollution Sensor (CHAPS) to address it at a local scale. Presently, TNO is carrying out the design study for this system by employing both freeform optics and additive manufactured mechanics. The mission objective is to perform targeted local measurements of the atmosphere on a daily basis by providing high spatial and temporal resolution possible in UV-VIS wavelength range.

In order to characterize, quantify, and monitor emissions from urban areas, power plants, and other anthropogenic activities, it is important to collect accurate and precise data and calibrate the optical instrument. But the data often received from the sensor is not reliable due to the operational and the non-operational conditions leading to cross-sensitivity, change in the trajectory, and optomechanical errors. For this, an on-board calibration system is developed to perform continuous calibration of the science product, that is compatible with both the instrument and the satellite platform and is robust to the variable operating conditions. This requires a stable system that achieves a good performance that is insensitive to thermal and mechanical disturbances, in order to meet the strict specifications.

As opposed to conventional methods, additive manufacturing, enables new possibilities for developing Optomechanical structures because of the layer-wise manufacturing technique. This manufacturing process is widely touted as a foundation for the next industrial revolution as it offers profound advantages like shorter lead time, lower wastage of materials, and higher geometric complexity that can be useful for multi-functional and multi-material structures. It can also facilitate good strength, significant mass reduction, and better dimensional homogeneity and stability. At the same time, additive manufacturing is not an easy process and requires new design strategies and solutions for overcoming the existing constraints.

The prime research objective is to investigate the optomechanical design of the spectral calibration module applying a kinematic approach. The second research objective is to investigate design and the potential improvements when applying additive manufacturing. The present case study demonstrates and evaluates the preliminary phase of the calibration module design study, thus providing the key ingredients for the realisation of the full system.

Acknowledgement

Contents

List of Figures

List of Tables

Nomenclature

Acronyms

3D	Three Dimensional
ACT	Across Track Direction
ALT	Along Track Direction
AM	Additive Manufacturing
APL	Applied Physics Lab, John Hopkins University, USA
CAD	Computer-aided Design
CHAPS	Compact Hyperspectral Air Pollution Sensor
CTE	Coefficients Of Thermal Expansion
CVCM	Collected Volatile Condensible Material
DOF	Degree Of Freedom
FEM	Finite Element Method
FS	Factor Of Safety
GEO	Geosynchronous Equatorial Orbit
HSI	Hyperspectral Imager
LEO	Low-Earth Orbit
LOS	Line Of Sight
MS	Margin Of Safety
NA	Numerical aperture
NASA	National Aeronautics and Space Administration
RML	Recovered Mass Loss
RSS	Root Sum Squared
SLM	Selective Laser Melting
TO	Topology Optimization
TROPOMI	TROPOspheric Monitoring Instrument

<div align="right">1</div>

Introduction

This chapter starts by discussing the impact of air pollution and the methodology commonly employed for monitoring. Later a brief introduction is provided about the Instrument, and finally, the research goals and the structure of the thesis are presented.

1.1. Background And Motivation

Worldwide air pollution is still a major and increasing problem with protracted suffering of the ecosystem. According to the World Health Organisation, air pollution is the accountable for more than 7 million premature deaths every year. Therefore, it is of utmost important to track and measure the emissions in our environment for post analysis and modelling. One of the methods to gather such information is through earth observation via satellites which are non-disruptive,and can provide data with high sensitivity, resolution and global coverage. These satellites comprises sensors with spectrographic systems which are used to separate and measure the spectral components emitted from the physical, chemical and biological system of the planet. With the help of these spectral components, information regarding NO_2, SO_2, O_3 etc. content which are the prime drivers for air pollution can be extracted. Previous satellite missions were able to determine air pollution but have lacked the power to differentiate individual sources and were not providing daily measurements. Current geostationary satellites do operate during the whole day but lack global coverage of the area [3].

Compact Hyperspectral Air Pollution Sensor (CHAPS) is a Hyperspectral Imager (HSI) which makes use of the recent technological advancement to solve these problems. This project is proposed and currently being developed by APL (Applied physics Lab, John Hopkins University, USA) and NASA (National Aeronautics and Space Administration). CHAPS uses freeform optics in a form factor suitable for accommodation on a small satellite or hosted payload. It will make measurements of air pollution at unprecedented spatial resolution from low Earth orbit (1 x 1 km^2) and will characterize, quantify, and monitor emissions from urban areas, power plants, and other anthropogenic activities [3]. The use of free form optics and additive manufacturing techniques reduce the weight, volume and cost of the system. The high resolution provides cloud free observations, effectively discredited point sources and better understanding of the emission mixing, transformation and transportation. This instrument will fly on a cubesat, thus requiring the instrument to be small. The platform size must be within 6U(6 Liters) with 4U available for payload. Figure 1.1 below provides a quantitative comparision of CHAPS with respect to other previous satellite missions in terms of mass and resolution.
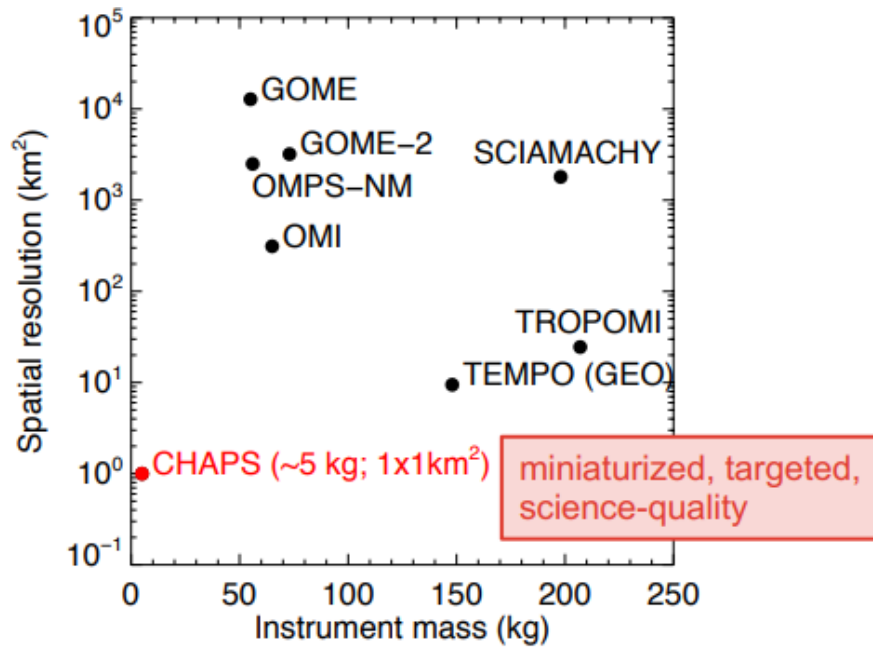
Figure 1.1: Comparison Chart [43]

For exploring the full capability of this system an airborne demonstrator is being designed with similar requirements before tackling numerous earth science objectives. As shown in the Figure 3.13 below, This demonstration setup will be installed and tested on an airplane before installing it into the main satellite. This will be done after controlled testing of the instrument. This HSI system will consist of a telescope, collimator, calibration, grating and an imager subsystem.
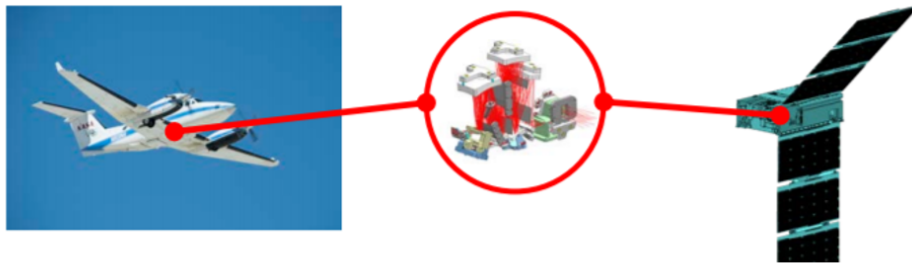
Figure 1.2: Instrument Development [43]

TNO (Netherlands Organisation for Applied Scientific Research) is an independent research organization that anchors on answering explicit questions related to applied physics which are both practicable and innovative. It focuses on nine different domains including defense, industry, robotics e.t.c. The Opto mechatronics and space system departments located in the delft, which is the home for many innovative instruments including the TROPOMI and GAIA is carrying out this design study for the APL, with their prime focus on the design and fabrication of the optics and the mechanical structure.

Due to the high sensitivity of optical components combined with harsh operating conditions in space and limited volume requirements, these systems have to accommodated with utmost precision and rigidity. The very nature of such systems compels the designers to have a good understanding of the requirements and work as a team. The mechanical housing of such instruments should be stiff, thermally stable and should be able to position the components despite the dynamics loads during the launch and thermal loads while orbiting around the earth [27].Hence a comprehensive study to

understand the underlying mechanism and a thorough examination of the conditions is needed for designing a quality mechanical structure.

1.2. Thesis Objective

This study focuses on developing a feasible concept design to enable the on-board verification of the science product produced by the CHAPS instrument. That is done understanding the physics developed on the CHAPS and using that information to correlate with a known reference. For generating a known reference, a spectral calibration module is employed. The following are the general thesis objectives:

1. Optomechanical Design the spectral calibration module for the CHAPS instrument applying kinematic approach to satisfy the requirements.

2. Investigate the impact and potential of additive manufacturing for the design of this complex miniature optical system.

3. Perform optical sensitivity analysis to determine the mechanical requirements and design drivers under structural and thermal load cases.

1.3. Approach and Report Structure

This thesis describes the design process and analysis of the calibration module for the CHAPS Instrument. The calibration module monitors the instrument response, using the sun spectrum on either side of the spatial image. The focus is mainly on the optomechanical design aspects, employing a system-level approach by developing different concepts using conventional design principles to provide a foundation for the instrument while exploiting the positive assets that Additive Manufacturing (AM) provides. The broad scope and the technical requirements focus on the optical sensitivity, design assembly procedure, manufacturability, and multi-physics simulation modeling. Finally, after successfully meeting the pertaining requisites, some concluding remarks, plausible advancements, and suggestions for further research are given in recommendations. This report consists of seven chapters, and the contents are stated below for the reader's reference:

1. **Introduction**: A brief overview of the project background and for a more in-depth understanding of the system is presented.

2. **Sensors and Calibration System**: A short overview of the categories of sensors and calibration methods are presented. A brief introduction regarding the CHAPS Module. This will be elaborated by illustrations and details regarding the various subsystems and their components.

3. **Spectral Calibration Unit**: A detailed description regarding the components, their respective sensitivities, environmental constraints, and performance requirements were generated. These would tailor designing aspects of the spectral calibration optomechanical fuselage.

4. **Conceptual Design**: Here, an emphasis was made on the selection of the component materials and their respective mounting strategies. Later, Six assembly concepts were generated where the most suitable concept was selected based on a preliminary error budget and a pugh matrix.

5. **Detailed Design**: Based on the information collected from the Pugh Matrix, minor changes and refinements were proposed during this period for improved performance. The second part of the section describes the approach used for designing the module. This is where the actual component mount is designed. For example, in the case of a lens, It kicks off with a basic flexure design and calculations the boundaries the flexure has to meet. Similarly, all the component mounts were designed. Next, a complete assembly 3D model with further refinements

6. **Performance Analysis**: This chapter walks through each requirement and shows that the proposed design fulfills most of the requirements. Also, An adverse analysis was conducted to analyze the structure in the worst-case scenario. A method for focus compensation was also provided for the alignment of the optics.

7. **Conclusion, Recommendations, and Outlook**: This chapter concludes and proposes recommendations for future work. Further, an outlook is provided to understand the importance of AM in the Optomechatronics and Space System industry.

2

Sensors and Calibration System

2.1. Sensors For Earth Observation

The launch of Terra satellite in the year 1999, marked the beginning of the Earth observing system era [29]. The use of these remote sensing sensors for acquiring data from the earth's atmosphere persistent from then. Depending on the interaction between the sensor and earths atmosphere, sensing can be subdivided into 2 types: passive and active sensors. Passive sensors (Optical) in general, just try to capture the electromagnetic radiations that are emitted without interacting with the environment. Active sensors (Radar) on the other hand, transmit signals and then receives responses from the object it has interacted with. These sensors can be further subdivided based on their ability to scan and image depending on the mapping process of information. Figure 2.1 below summarizes broad range of sensors that can be applicable for remote sensing. Although passive sensors only operate during the day time, they purely depend on external sources for detection. Active sensors on the other hand need to actively probe for detection.
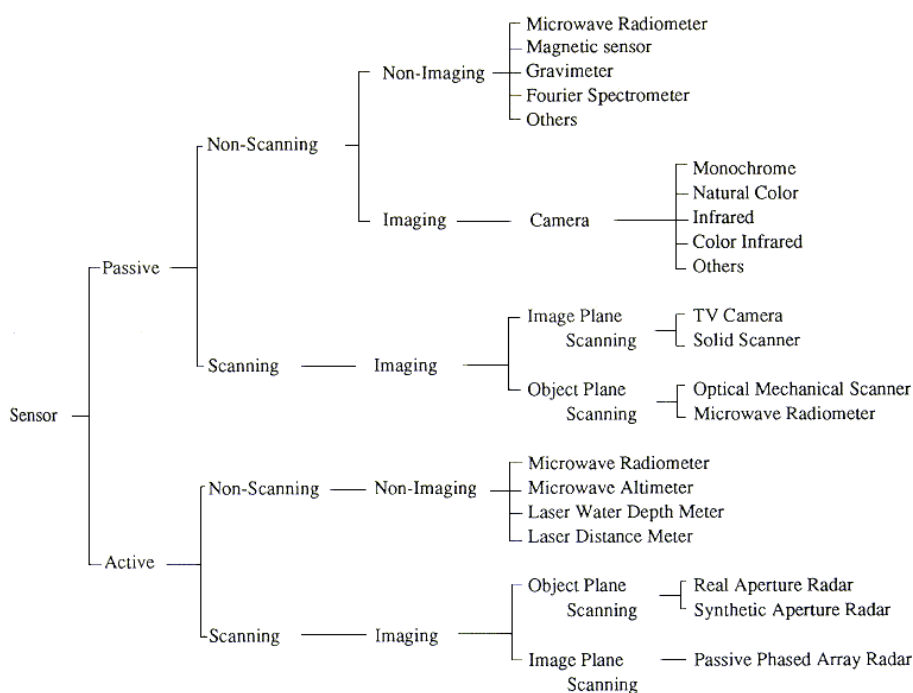
Figure 2.1: Classification of sensors [6]

In order to have a better visualization of the surveillance data and provide situational context, it is important to have sensors which can provide a wider converge of area. For these reasons, scanning system and framing systems are generally regarded as a favourable option. This combined with imaging sensors have unlocked the capability to produce images with full coverage of the desired area and also have a build up on the current images for a better supervision. Optical sensors of this type in general are composed of 6 different components:

1. **Optical System**: It provides a means to capture and direct the radiations(in the form of light) to the spectrographic elements.

2. **Spectrographic system**: Here the directed light is dispersed based on wavelength with the help of a prism or a diffraction grating. Certain filters such as absorption, interference, polarization filters etc. can also be used depending on the scientific experiment that the instrument will perform.

3. **Scanning system**: This module is used for scanning areas. It consists of a mirror which rotates or oscillates during the operation and is placed perpendicular to the flight direction to enlarge the field of view, by changing the view periodically during operation.

4. **Detector system**: The dispersed spectrum is converted into electrical signals with the help of optical electronic detectors. The electrical signals are then amplified, recorded and analysed to produce an image

5. **Reference system**: Since these sensors are typically susceptible to drift, it is important to consider the impact on the recorded electrical signals.Therefore, a light source or thermal source are often used to interpret the signals.

6. **Support equipment**: This includes solar panels, electrical subsystem and radio/ communication modules. The electrical signals thus produced are stored here.

Typically, these scanners are generally differentiated by the type of scanning mechanisms used and the arrangement of the pixels in the instrument architecture. Figure 2.2 below illustrates 4 different types of optical sensors that enable a wider surface coverage.

(a) **Push Broom Sensor**: Also referred to as Along Track Scanner, this architecture exploits the motion of the platform to create two-dimensional images. Here, the linear detector is arranged perpendicular to the flight direction. That would allow the scanner to scan successive lines, thus eliminating the need of moving part.

(b) **Wrisk Broom Sensor**: Also referred to as Across Track Scanner, this Optomechanical device employs a rotating mirror to collect measurements.

(c) **Framing Sensor**: Also regarded as imagers, these sensors use additional optics or detectors to record signals of different wavelength bands using filters. They have a simpler design compared to the above two sensors. However, these sensors are capable of capturing only limited intensity of light [26].

(d) **Windowing Sensor**: Has a similar design compared to the framing sensor. However, these sensors capture distinct images with no integration in between [26].

The push broom approach is generally favoured due to the fact that they receive stronger signal and have a longer exposure for each pixel compared to wrisk broom sensor. Also no image patching is required in this case. It also requires the least amount of data to avoid occlusions as the optical system provides the best field of view in this case. Although it has clear advantages over other sensors, it does have some drawbacks. The system has to be very stable in terms of measurement drift over time and location due to the varying sensitivities of the detector. This can be corrected with the help of a calibration system. Also, it requires wider field of view to obtain the same swath (broad strip of an area) as for the corresponding wrisk broom scanner.
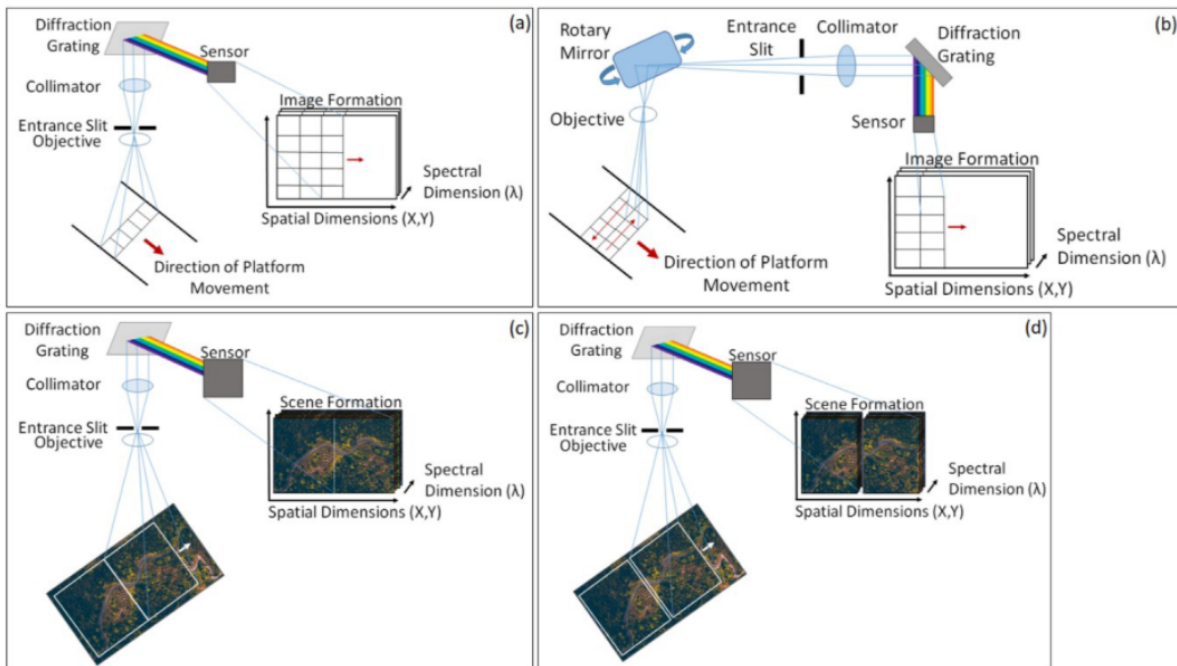
Figure 2.2: Schematic design of each sensor[26]

Push broom scanners in general can be further categorized into four types [35]:

- **Monochromatic scanners**: Only one linear array of CCD is in this case. This scanner is generally used for rapid data acquisition, processing and interpretation of the image.

- **Multi-spectral scanners**: These scanners have an array of detectors thus, allowing the system to produce color images.

- **Hyperspectral scanners** : A Spectrographic system is installed into these sensors. This will enable the instrument to create large number of images with different spectral bands.

- **3-Line scanners**: This is a special kind of scanner which generates 3 strip images overlapping over one another(i.e forward, nadir and backward pointing). This can help in producing mutispectral images with color or false color images as their secondary products.

While multi spectral scanners have been available for quite some time, hyperspectral imaging has opened the door to a more accurate scene analysis. With recent advances in spatial and spectral resolutions, data can now be represented in three dimensional hyperspectral data cube where each slice can represent a multiple bands [26].

2.2. Space Instrument Calibration

Often the data received from the sensors are not completely reliable. There is always some deviation present which is primarily due to sensitivity of the detector, change in the trajectory of the system, or lack of extracting the physical unit from the data. Calibration is the process of determining the parameters needed to comprehend and explain a sensor's output. The calibration process quantifies the sensor's response to an input, characterizes the interactions and dependencies between the optical and electronic components, and discovers and evaluates any systematic errors that may occur. Calibration increases the likelihood of mission success by ensuring that the sensor will meet mission requirements and interpret data correctly to make accurate mission decisions. Successful implementation of a calibration system depends on 5 criteria [44]:

- Calibration planning should begin early in the sensor design process.

- Aspects regarding performance, cost and schedule should be mapped out before implementation.

- Measurements carried out by the calibration system should be traceable.

- Testing should be carried out of the whole instrument to estimate the performance.

- Both pre- and post launch calibrations should be carried out for a instrument.

As illustrated in Figure 2.3 below, The calibration and validation process consists of five steps: instrument characterization, instrument calibration, calibration verification, data quality assessment, and data product validation [4]. Summation of the above steps with the operation factors can provide a fully calibrated and validated system.
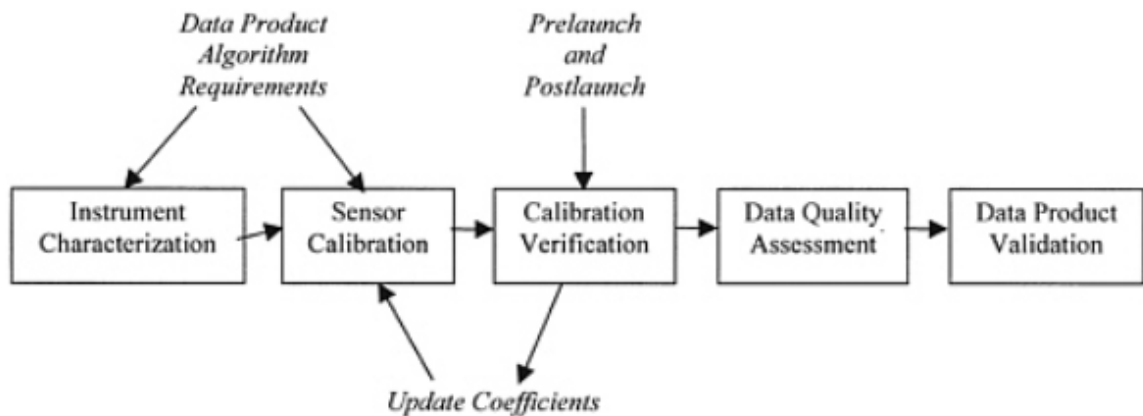
Figure 2.3: Steps involved in Calibration and validation process [4]

Since these earth observation instruments are unique and have no specific standard guidelines to meet, the instrument themselves, but also the calibration systems are generally different in designs and operation. Typically Calibration system consists of both on-ground and on-board components. During the on-ground phase, the instrument is tested with well-versed scenarios. This is done on both instruments as a whole and components separately. The system is then characterized based on the response. Measurements usually include radiometric calibration, polarization characterization, spectral calibration, temporal calibration and slit function characterization. This provides an initial key data base for reference. The on-board calibration source aims to monitor and provide an update to the key data base of satellite instruments to validate the final science product measurement. The apparent variations in results are caused by time and space mismatches, differences in the resolution, accuracy and repeatability limitations, and physical measurement differences [45].

2.3. Compact Hyperspectral Air Pollution Sensor

The CHAPS is a HSI used for measuring trace gases from low earth orbit. This instrument will be capable of providing accurate measurements of key atmospheric constituents such as NO_2,SO_2, O_3, CH_2O, CHOCHO, aerosol and clouds. This means the system must measure a broad spectrum of the earth's reflected radiance. Therefore a spectral range of 300 to 500 nm is considered. CHAPS is a very small instrument which can fit into miniaturized satellites like CubeSat but can provide an unmatched spatial resolution up to 1X1 km^2. Unlike most other earth observation instruments, this instrument will make a targeted observation of the pollution hotspots rather than global surveys. This will help in unravelling the key contributor of the emission by allocating point sources in the specific region and will also help us in understanding the mixing of these emission, their transport, and transformation. As shown in the figure 2.4 below, the high spatial resolution can provide a more cloud-free observation compared to the previously analogous Instruments like TROPOspheric Monitoring Instrument (TROPOMI).
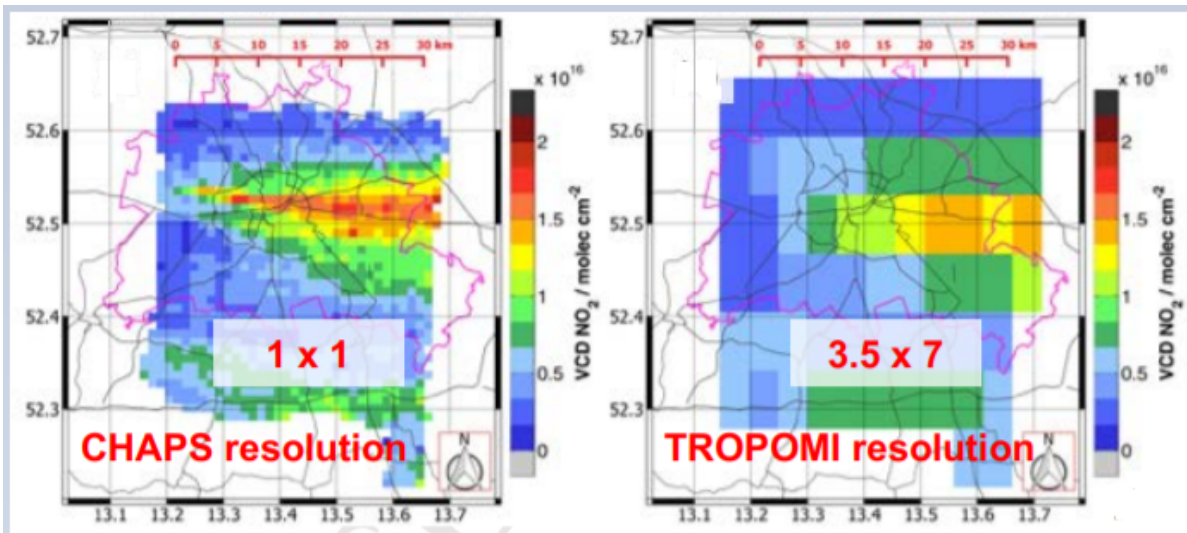
Figure 2.4: Comparison between CHAPS and TROPOMI based on spatial resolution (km^2) [43]

This push broom telescope spectrometer combination will fly in the lower orbit region, anywhere between 400 and 600km. Figure 2.5 below describes the orientation of CHAPS instrument. The direction of flight will be in the narrow image dimension,i.e along-track (ALT) direction. The broad image dimension is perpendicular and is therefore referred to as across-track (ACT) direction. The detector samples the ACT dimension spatially and ALT dimension spectrally.
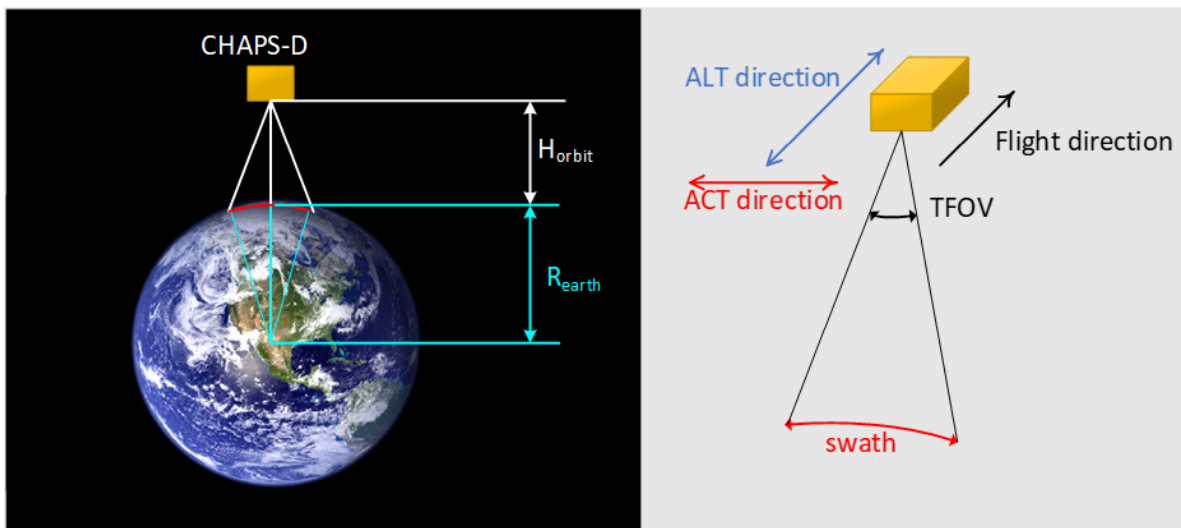
Figure 2.5: Orientation of CHAPS Instrument

As this system has to be installed in a CubeSat, the size of the instrument must be very small. Since the platform was considered to be 6U, the instrument should be less than 4U. For creating such a small spectrometer, freeform mirrors are used. These mirrors will not only miniaturize the instrument but will also provide a wider spectral and spatial range. An optical system including freeform mirrors have been selected in the CHAPS, because of the superior abberation correction compared to regular mirrors. Further, exploring the option of AM will also provide a potential reduction in the volume. Compared to the traditional processes, mechanical parts of significantly greater complexity can be produced. This method also provides significant advantages in terms of cost, manufacturing time, mass and part number.

The Optical design of the CHAPS is shown in the figure 2.6 below. This Instrument constitutes **five** subsystems. Firstly the **telescope** subsystem which, consists of 2 freeform mirrors, images a line on

the earth.The area of the Earth that will be imaged will be broad in one dimension, the swath, and narrow in the other dimension. The incoming beam then passes through a fold mirror which directs the rays onto a spectrometer entrance slit. This slit here acts as a performance evaluator, which evaluates the resolution and the location of the spot received from the telescope. The image of the entrance slit is collimated by a **collimater** mirror. This subsystem aligns the direction of the rays and will limit the size of the beam spatial cross-section. The collimated light falls on a **diffraction grating**. The grating diffracts the light with an angle depending on the wavelength. Past the grating collimated light with a wavelength dependent angle is imaged by the **imager subsystem** so that different wavelengths land at different ALT / dispersion positions on the detector. The detector then samples the images in two dimensions, with the x-axis measuring the spatial direction and the y-axis measuring the spectral direction. Samples taken at a different timescale are combined together to generate two-dimensional images.
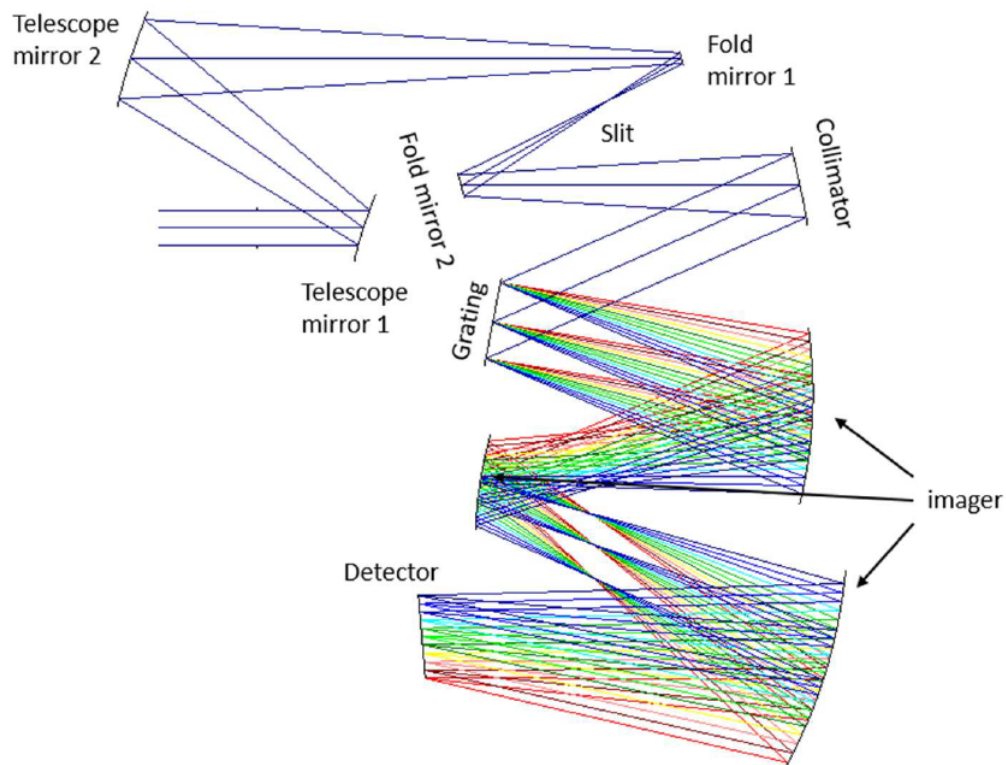
Figure 2.6: Optical Design of the CHAPS instrument

2.4. Scientific Background

The calibration system is to be designed for the CHAPS instrument and therefore, it is essential to know about the CHAPS design drivers. The environment of the calibration module is quite similar to the main system. The drivers include the assumptions made regarding the scientific measurement, environment and performance of the calibration system as well as down flowed requirements coming from the parent system. This leads us to the next step, to consider the choices made on the optical system of CHAPS, the detector and the grating. The table 2.1 below provides the information regarding the overall system assumptions and choices made.

Some important points to be noted:

- An altitude of 400-600 km was considered because targeted resolution versus field of view, and a lifetime of at least 15 years.

- The platform speed is important because it determines the frame rate and the number of samples taken in a given time period.

- The zenith angle was selected the same as earth to reduce uncertainty, thus improving the measurements. This angle is between -90 and 90 degrees because of the change in zenith angle w.r.t earth because of the day and night shift. For example, the angle is almost zero during sunrise and sunset but changes to 90 during the day and -90 during the night.

- An swath of 100 km was considered because this could provide the adequate coverage of the urban environment.

- An spatial X spectral coverage of 1x1 km^2 was considered because this would provide the adequate isolation of individual pollution sources which is very useful transport and transformation modelling with effectively separate clustered point sources.

- A signal-to-noise ratio of 500 must be achieved at the reference radiance, while the detector should not be saturated at the maximum radiance.

- Selecting the detector was mandatory before designing the optical system because it determines the image size and F numbers to be created at the end of the imager subsystem. This detector was able to satisfy the current requirements of the SNR. Below is an illustration of the distribution made on the detector. It can be seen that a total of 0.18 mm is allocated for the calibration images on the either side of the detector real-estate.
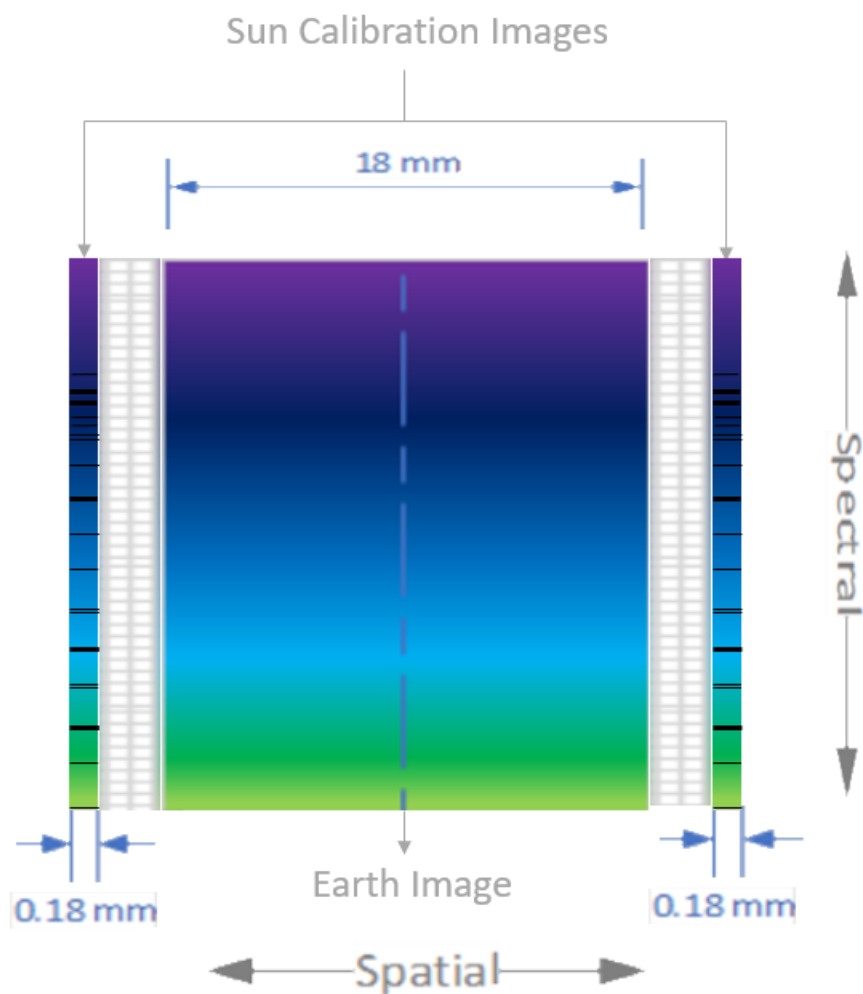
Figure 2.7: Image distribution on the detector real estate

- The Grating determines to a large extend, the sensitivity of the design. This is important as it determines the scientific, spectral and radiometric performances of the instrument.

Table 2.1: Design Drivers for CHAPS Instrument Overall

	Parameter	Value	Remarks
General Parameters:	Orbital Altitude	400 km - 600 km	based on Flexibility of deployment
	Platform Speed	7.22 km/s @ 400 km 6.91 km/s @ 600 km	
	Zenith Angle for diffuser	−90° to +90°	same as that of earth
	Swath Width	100 km	Total Field Of View: > 14.24°
	Spatial X Spectral Sampling	1x1 km^2	For adequate isolation ALT=0.095° ACT= 0.143°
Performance Parameters	Spectral Range	300 nm - 500 nm	Sun Spectrum (UV-B, UV-C, VIS)
	Spectral Stability	0.1 nm	For a proper initial starting point for spectral calibration algorithm
	Spectral-Spatial Co-registration Alignment	< 20%	
	Signal To Noise Ratio at reference radiance (SNR)	> 500	Determined by KNMI analysis
	Reference Radiance	2.5E+13 ph/s/cm^2/nm/sr	Determined by KNMI analysis
	Maximum Radiance	1.7E+14 ph/s/cm^2/nm/sr	Determined by KNMI analysis
Detector	Number Of Pixels	2048 X 2048	CIS120 from Teledyne/E2V Total Size = 20.48 mm X20.48 mm
	Pixel Size	10 μ m	
	Calibration Image size	20 mm X 0.18 mm	On both the sides of the earth image Spectral Image size = 20 mm Spatial Image Size = 0.18 mm
Grating	Groove Density	1200	Company: Edmund Optics
	Blaze Wavelength	250 nm	Construction: Ruled Grating

These assumptions, mission-level and system-level decisions have let to the CHAPS optical design described in section 2.2. That design will be out-of-scope for the calibration sub-system, but is of course is of vital information because of the mechanical, optical and thermal interfaces and shared environments.

<div style="text-align: right; font-size: 3em;">3</div>

Spectral Calibration Unit

3.1. Calibrations Used For CHAPS

As pointed out before, push broom scanners have a critical disadvantage of requiring the system to be very stable in terms of measurement drift over time and location due to the varying sensitivities of the detector. Else, it can lead to stripes in the image data and deviations in the spectral scale as shown in the figure 3.1 below. Therefore, there is a need for a calibration instrument to avoid such errors during its operation.
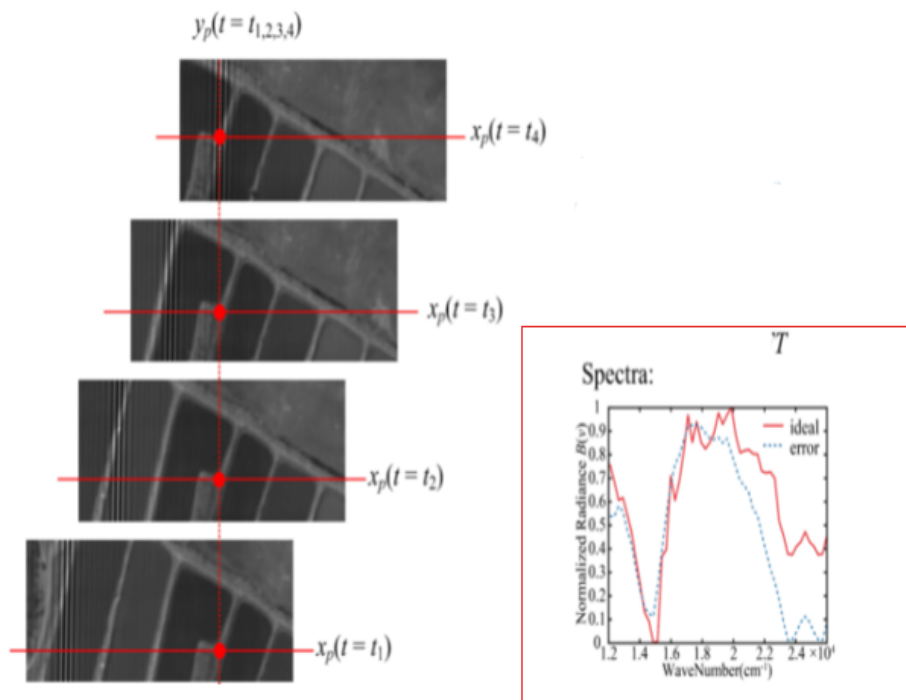
Figure 3.1: Error generated on the image data due to sensitivity of the scanner [22]

After the data has been collected by the instrument, it is important to calibrate the system to produce a physical unit and correct for aberrations. In this case, two **calibration systems** are used here.

1. Since these systems are influenced by several factors such as illumination, absorption, and scattering, the data received by the instrument is variable and hard to predict. To correct this, a

radiometric correction is required. The **radiometric calibration** is done both on ground and on board. As shown in the Figure 3.2 below, this system comprises two diffusers: The main diffuser and a monitoring diffuser. Here the monitoring diffuser is used to observe the main diffuser. The light from both the diffusers will enter the system via the pupil. This system will then normalize the intensity of the generated wavelength to the wavelength of a reference image. For a robust instrument, the mechanism is eschewed, which is generally the case for conventional instruments. Instead, a secondhand approach of using ground targets was employed for calibration, and two diffusing surfaces are installed in the pupil so that one surface will be illuminated longer than the other.
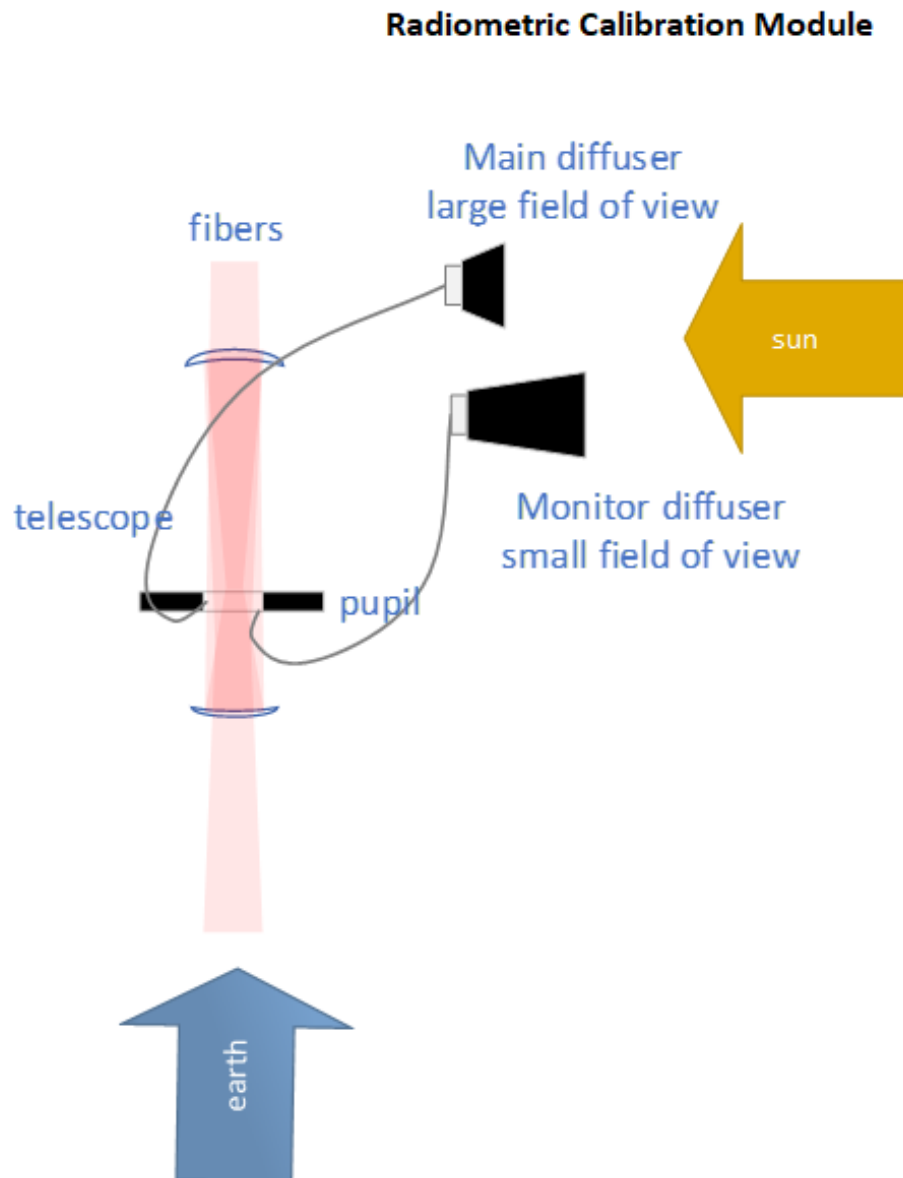
Figure 3.2: Radiometric Calibration Module

2. Detector position tolerances and non-linearity in the spectrograph causes deviations in the wavelength scale of the image. Therefore spectral light sources with peaks are used to calibrate the system [36]. For this resolution, sun Fraunhofer lines can be used. Fraunhofer lines are dark, narrow absorption lines that are caused due to the absorption of photons from the source to the

detector. This provides a structure for the registration of the spectrum. This, in addition to a monitoring path next to the side of the spatial image, can provide a **spectral calibration** module. As shown in the Figure 3.3 below, a diffuser placing the sun will transfer the solar irradiance to a radiance able to fill the required etendue. This will also reduce the flux so the radiance is comparable to the earth radiance. These sun radiance are transferred through a fiber towards the slit. Even though the optical path will degrade radiometrically, it will not hamper the Fraunhofer lines, thus maintaining the validity of the calibration module.
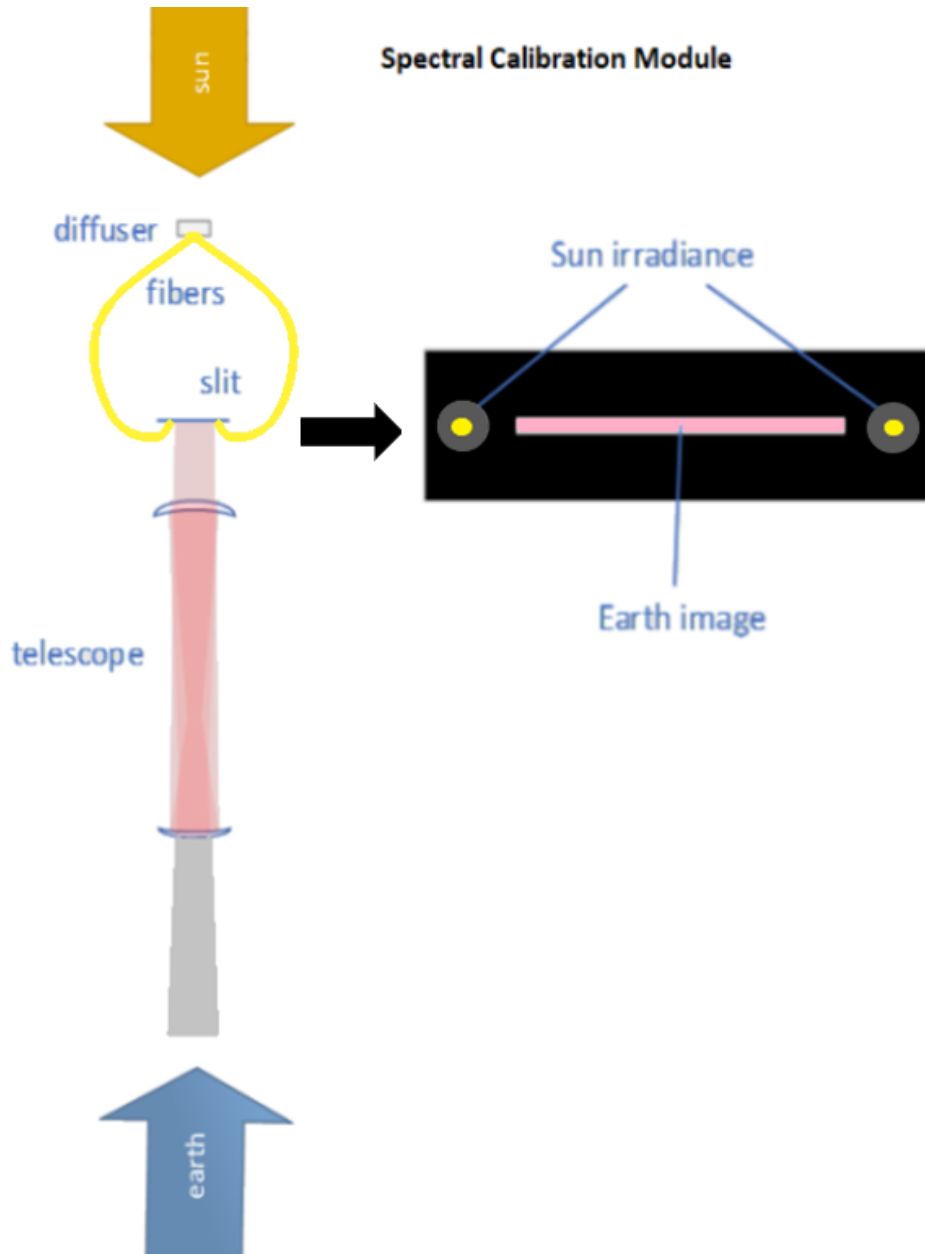
Figure 3.3: Spectral Calibration Module

3.2. Optical Design

As shown in Figure 3.3 sunlight is captured by the diffusers and is transferred by fibers towards the two extremities of the slit. Since these rays are used as a reference for monitoring, it is of utmost importance to maintain the path of solar irradiance on the detector with the required precision. For maintaining this

precision and to synchronize the NA of the fiber with the NA of the measurement passing through the slit, it is necessary to filter the rays from noise and interceptions. Therefore an 4f optical system is adopted here that changes the light coming from the fiber into source beams next to the ends of the slit, as shown in the figure 3.4 below. A 4f system is an optical relay that usually consists of 2 similar lenses, placed at a distance twice the focal length (f). This system works on the convolution theorem from the Fourier transform, where a convolution in the spatial domain is equivalent to multiplication in the frequency domain. If a point source of light is positioned on-axis in the first lens's input plane, a uniform, collimated field is formed in the first lens's output plane. When the collimated field is multiplied by the FT plane mask and Fourier transformed by the second lens, the output plane field is simply feature which must be identified and placed within the input plane[10]. In this case the baseline design does not include a filter or stop between the two lenses, but it uses a aperture on SL1 to capture the relatively homogeneous region (in terms of light intensity) of the beam exiting the fiber.
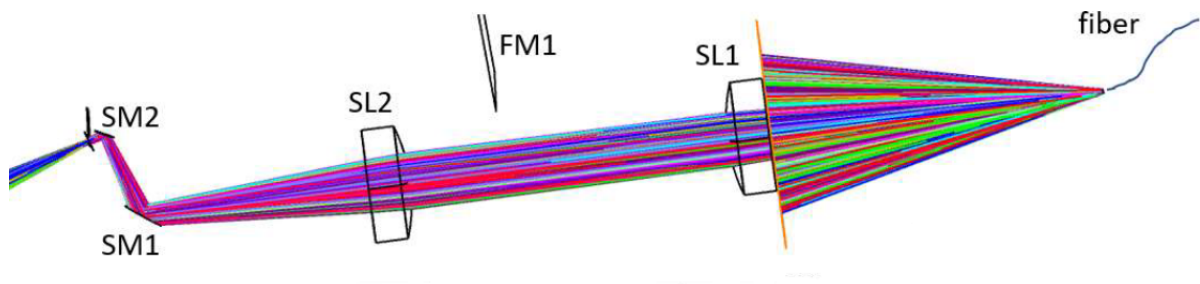
Figure 3.4: Optical design of the Spectral Calibration Module

Considering that the light from the fiber ferrule is in use for monitoring the sun's light in order to compare it to the earth's light, it is crucial to maintain a similar f-number.The earth light in the slit has an f-number of F/7 by F/8. The aperture is designed circular with F/7, because that makes alignment easier and enables the use of off-the-shelf lenses with respect to rotation around the optical axes and optical analysis have shown that the aberration and stray light is acceptable. The system consists of two Plano-convex lenses (SL1 and SL2) with their convex side facing each other. The SL1 and SL2 lens are placed such that their back focal points coincide with the fiber end and the slit respectively. In order to physically place the optical system close to the slit and to the CHAPS mirrors, 2 folding mirrors (SM1 and SM2) are placed such that they are used to fold the system to the desired position even with the folding the system is challengingly compact.

Two different Optical designs of the spectral calibration system were designed. Other than the different folding paths, both the modules are almost identical in performance from a purely optical point of view.

- The horizontal version is designed in such a way that the system is positioned to the side of fold mirror 1 and above collimater mirror.
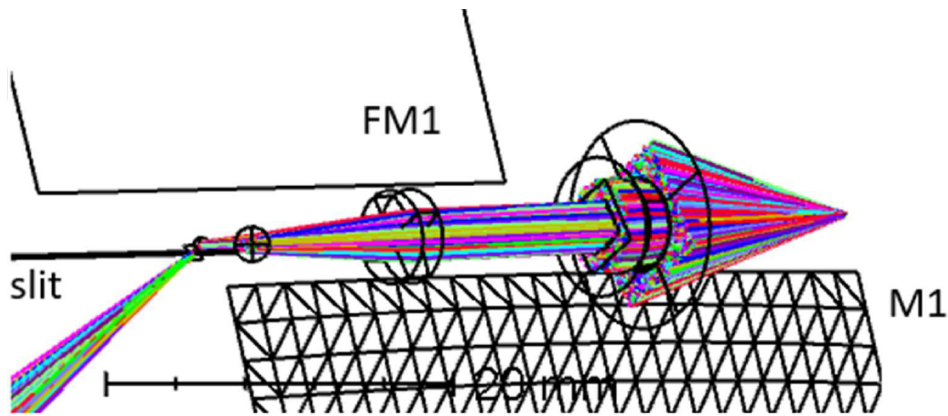
Figure 3.5: Horizontal version of the spectral calibration module

- The vertical version is perpendicular to the previous version, positioned between fold mirror 1 and collimator mirror.
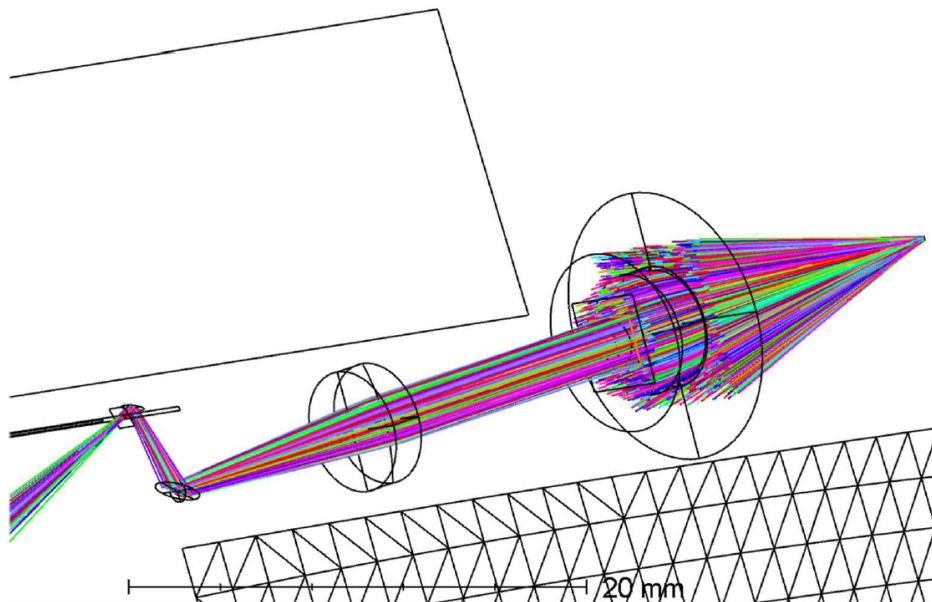
Figure 3.6: Vertical version of the spectral calibration module

3.3. Optical Component Sensitivity

Now that we have an optical design, it is time to create a support structure for placing the components in the correct position in a way that the system will not be affected in any operational environment and additionally survives all non-operation environments. The mechanical design of the spectral calibration module is mainly driven by optical component sensitivity, optical performance stability, strength and dynamic performance, and by the strong wish to enable assembly on machine tolerances without adjustment mechanisms. This subsection will mainly focus on the sensitivity with respect to displacement and rotations of the optics, while the next subsection will cover aspects regarding the optomechaical requirements.

An optical element, in general, is sensitive and can be perturbed axially, laterally, and angularly. These aberrations arise mainly due to misalignment, surface roughness, an irregular radius of curvature, extreme operating conditions, and displacement in the location and can result in line-of-sight(LOS) errors, blurriness, and distortion in the image, leading to a degradation in quality. These aberrations, in

general, can be classified into two types: first-order and third-order. [17] provides a detailed description of each of these aberrations. From here on, we will only restrict ourselves to first order aberrations.

The Spectral calibration system incorporates multiple elements placed at different orientations and locations. Therefore, it is important to create a model, which not only can locate the final image of the optical system but can also illustrate the effect of each component perturbation on the overall system. [20] has developed an integrated model based on linear systems theory that can conduct optical analyses and assist in the thermal and structural deformations also. Here, in this case, only rigid body motions are considered. The formulation used here is for the mapping of structural displacements caused by disturbances in matrix representation as shown below with resultant expressed in terms of change in optical path difference in the image plane. To generate these linear sensitivity matrices, the ray-trace model was used. A ray transfer matrix can be denoted by the equation given below where $r_i = [Y \quad \theta]$ with Y and θ as the distance and angle respectively. r_{i+1} is the linear transformation of the incoming ray, M_i is the component specific transfer matrix and E_i is the influence of the misalignment for that particular component.

$$\begin{bmatrix} r_{i+1} \\ 1 \end{bmatrix} = \begin{bmatrix} M_i & E_i \\ 0 & 1 \end{bmatrix} \cdot \begin{bmatrix} r_i \\ 1 \end{bmatrix} \tag{3.1}$$

The process begins with the perturbation of a single structural DOF by a small amount such that the system has a response. Then a ray tracing is performed to determine the effect of that perturbation on the image plane. In this way, all the DOFs were examined using the same method. Few assumptions were considered before proceeding towards the analysis for this particular problem. Firstly, All the components were considered to be circularly symmetric and the meridional rays should contain on the z-axis. Also, the slit structure was used as a reference and is considered to be stable. Finally, only the y axis and z-axis are considered in the matrix with an assumption that x and y have similar sensitivities with just a change in dimensions.

A ray transfer matrix can be denoted by the equation (derived from [8] and [7]) given below where $r_i = [Y \quad \theta]$ with Y and θ as the distance and angle respectively. r_{i+1} is the linear transformation of the incoming ray, M_i is the component specific transfer matrix and E_i is the influence of the misalignment for that particular component. Below is a table providing the details regarding the component matrix.

Table 3.1: General Misaligned ray transfer matrix

Element	Matrix	Remark
Fiber End	$\begin{bmatrix} 1 & 0 & 0 \\ 0 & \frac{n_f}{n_o} & 0 \\ 0 & 0 & 1 \end{bmatrix}$	n_f and n_o are the refractive index of the fiber and outside respectively
Lens	$\begin{bmatrix} a & b & \alpha e + \beta E + \delta(1 - m^2) \\ c & d & \gamma e + \delta E \\ 0 & 0 & 1 \end{bmatrix}$	ABCD = [Curved refraction · propagation through thickness · Flat refraction] e and E are the translation and rotation δ and m are the focus deviation and magnification
Mirror	$\begin{bmatrix} 1 & 0 & 2\delta sin\varphi \\ 0 & 1 & -2\theta \\ 0 & 0 & 1 \end{bmatrix}$	$Sin\varphi$ is the initial angle δ is the deviation on the z axis θ is the rotation in y axis
Space Propagation	$\begin{bmatrix} 1 & d - \delta/cos\varphi & 0 \\ 0 & 1 & 0 \\ 0 & 0 & 1 \end{bmatrix}$	$cos\varphi$ is the initial angle δ is the deviation on the z axis d is the distance between the components
Rotation Matrix	$\begin{bmatrix} cos(\delta) & -sin(\delta) & 0 \\ sin(\delta) & cos(\delta) & 0 \\ 0 & 0 & 1 \end{bmatrix}$	δ is the rotation angle

Figures below shows the displaced of each component and the effects of it. The initial condition of the component and respective system will be the same and is shown in figure a. Figure b is the sensitivity given due to the misalignment of the plane of the module. Figure c shows the sensitivity

while the mirror is misaligned parallel over the optical axis. The tilt of the component is illustrated in figure d. In tables shown below, the sensitivities are given in numbers where top row specifies the the displacements of the component in Translations (x, y, and z) and rotations (Rx, Ry, and Rz). The first column specifies the error in position, change in the angle and change in the z-axis. The numerical value generated are a resultant of ±1micrometer change in height, ±0.1 degree change in angle and ±1micrometer shift in the z-axis. The same methodology was applied o each and every component that was considered for the study.

- **Fiber**:

Table 3.2: Sensitivity table Fiber (μm and mrad)

Fiber	Δ x	Δ y	Δ z	Rx	Ry	Rz
Δ y	1.2	1.2	0	0.15	0.15	0
Δ θ	0.03	0.03	0	0.01	0.01	0
Δ z	0	0	2	0	0	0

(a)   Nominal

(b) Δx and Δy sensitivities

(c) Δz sensitivity

(d)Rx and Ry Sensitivities
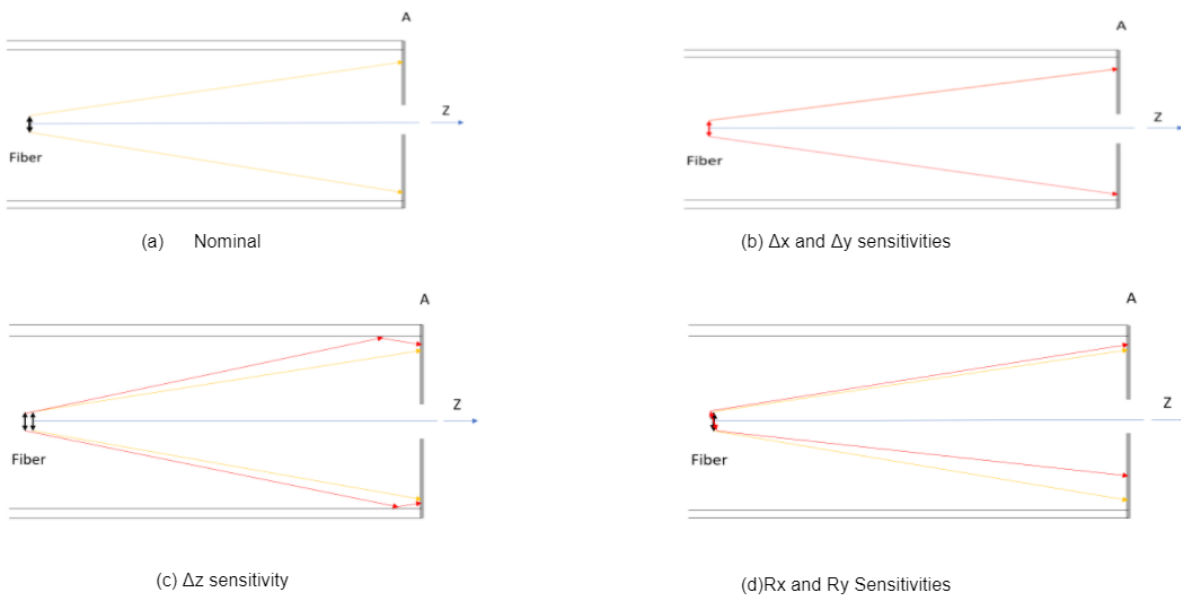
Figure 3.7: Sensitivity Figures Fiber

- **Aperture**:

Table 3.3: Sensitivity table Aperture (μm and mrad)

Aperture	Δ x	Δ y	Δ z	Rx	Ry	Rz
Δ y	0.3	0.3	0	0.01	0.01	0
Δ θ	0.05	0.05	0	0.035	0.035	0
Δ z	0	0	0.49 w.r.t SL1	0	0	0

(a)   Nominal   (b) Δx and Δy sensitivities

(c) Δz sensitivity   (d)Rx and Ry Sensitivities
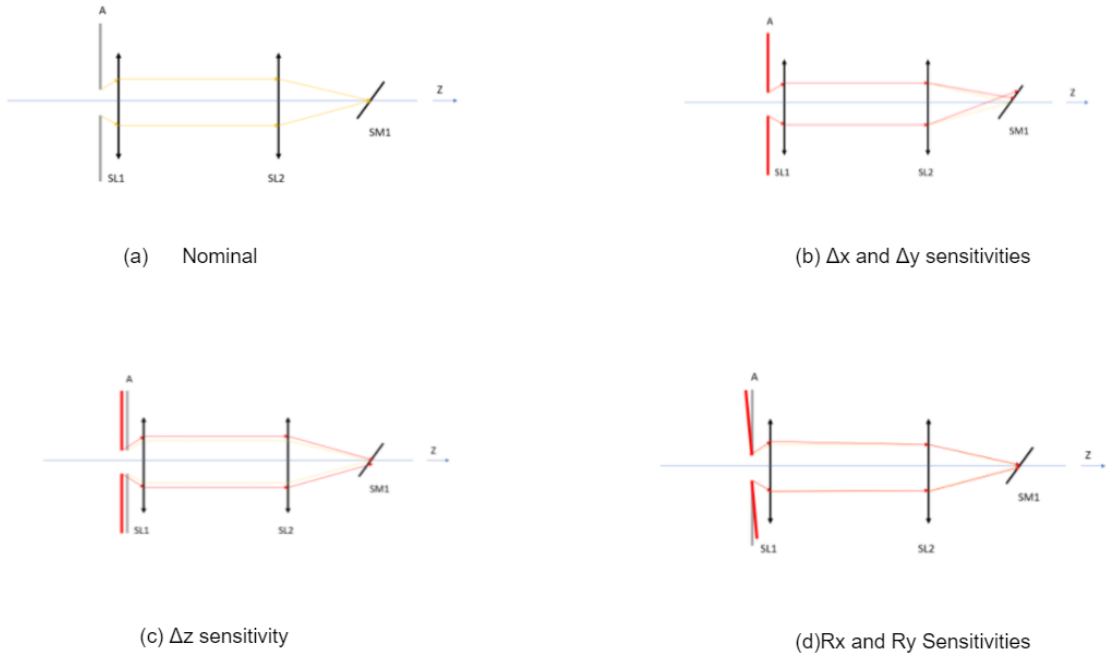
Figure 3.8: Sensitivity Figures Aperture

• **SL-1 Lens**:

Table 3.4: Sensitivity table SL1 (μm and mrad)

SL1	Δ x	Δ y	Δ z	Rx	Ry	Rz
Δ y	0.7	0.7	0	0.2	0.2	0
Δ θ	0.09	0.09	0	0.035	0.035	0
Δ z	0	0	2.4027 w.r.t SL2	0	0	0

(a)   Nominal   (b) Δx and Δy sensitivities

(c) Δz sensitivity   (d)Rx and Ry Sensitivities
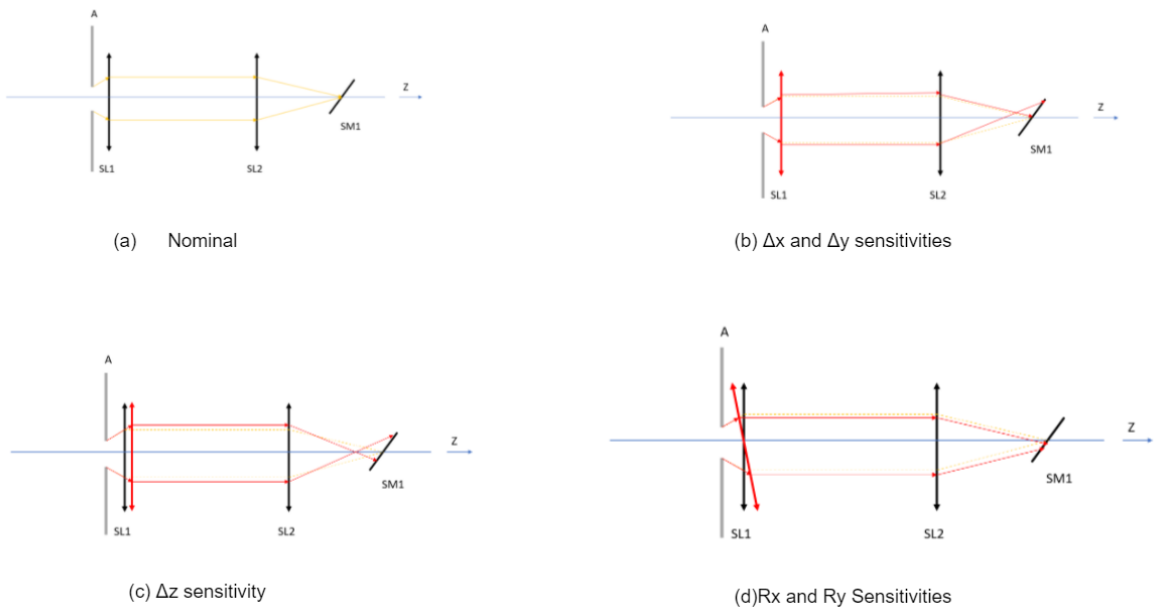
Figure 3.9: Sensitivity Figures SL1

- **SL-2 Lens**:

Table 3.5: Sensitivity table SL2 (μm and mrad)

SL2	Δ x	Δ y	Δ z	Rx	Ry	Rz
Δ y	0.6	0.6	0	0.06	0.06	0
Δ θ	0.212	0.212	0	0.035	0.035	0
Δ z	0	0	0.84 w.r.t SM1	0	0	0

(a)   Nominal

(b) Δx and Δy sensitivities

(c) Δz sensitivity

(d)Rx and Ry Sensitivities
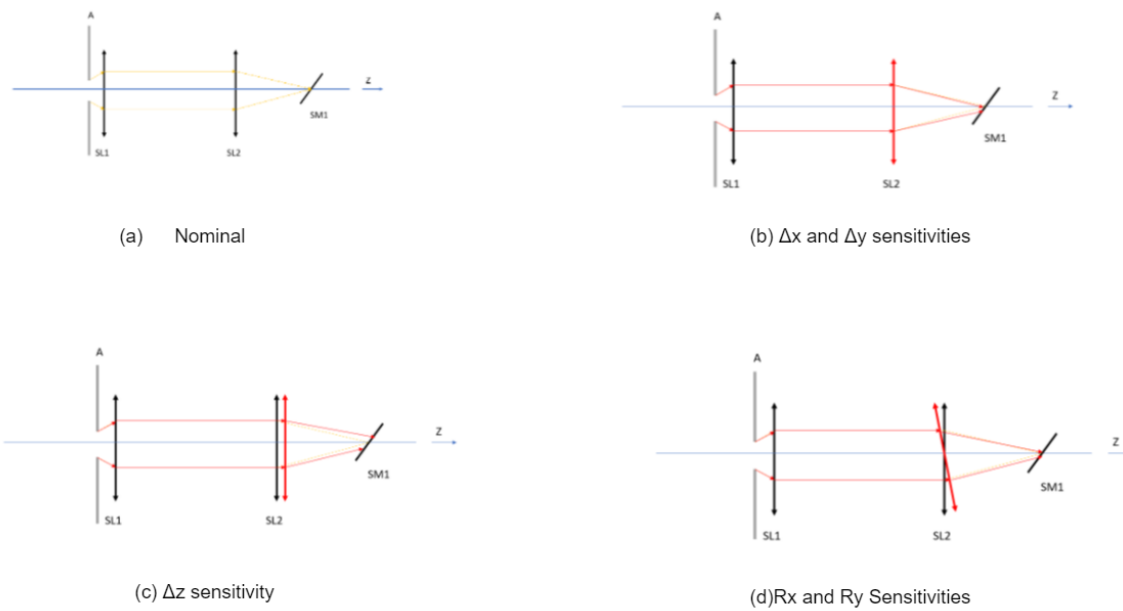
Figure 3.10: Sensitivity Figures SL2

- **SM-1 Mirror**:

Table 3.6: Sensitivity table SM1 (μm and mrad)

SM1	Δ x	Δ y	Δ z	Rx	Ry	Rz
Δ y	0	0	0	0.2	0.2	0
Δ θ	0	0	0	0.2	0.2	0
Δ z	0	0	2	0	0	0

(a)   Nominal

(b) Δx and Δy sensitivities

(c) Δz sensitivity

(d)Rx and Ry Sensitivities
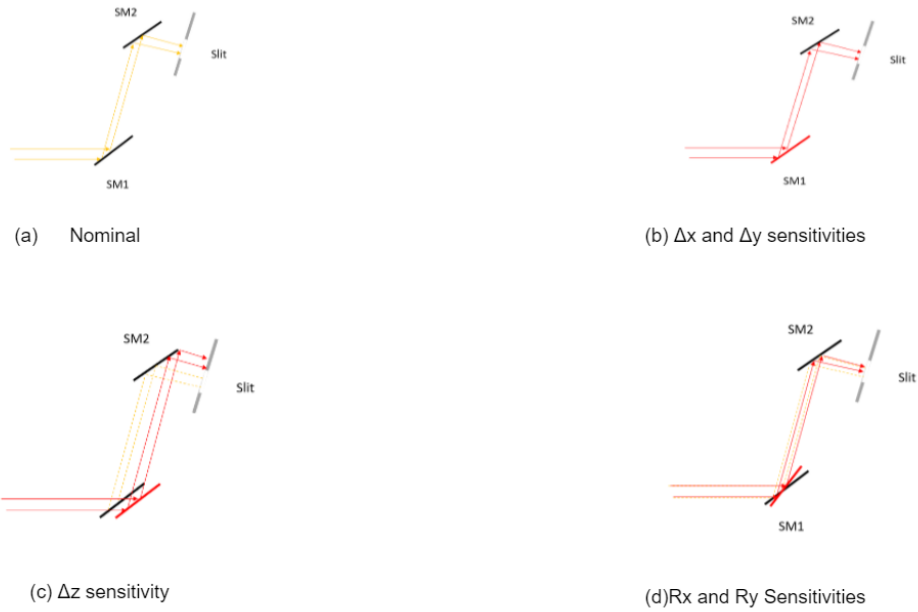
Figure 3.11: Sensitivity Figures SM1

- **SM-2 Mirror**:

Table 3.7: Sensitivity table SM2 (μm and mrad)

SM2	Δ x	Δ y	Δ z	Rx	Ry	Rz
Δ y	0	0	0	0.2	0.2	0
Δ θ	0	0	0	0.2	0.2	0
Δ z	0	0	2	0	0	0

(a)   Nominal

(b) Δx and Δy sensitivities

(c) Δz sensitivity

(d)Rx and Ry Sensitivities
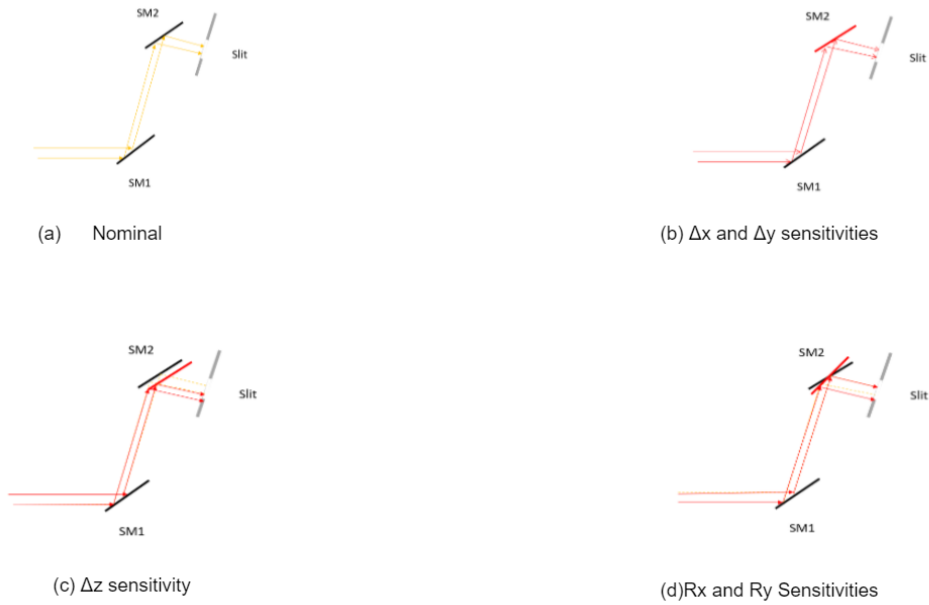
Figure 3.12: Sensitivity Figures SM2

3.4. Optomechanical Requirements

As pointed out earlier, The mechanical design of the spectral calibration module is mainly driven by requirements on optical performance stability, strength and dynamic performance, and by the strong wish to enable assembly on machine tolerances without adjustment mechanisms. It is also crucial to consider the loads that are acting due to the environmental conditions. These two criteria, along with the weight and cost constraints, provide a preliminary description of what the end product must do and how well it must perform in order to be appropriate.

The Design loads, optomechanical requirements, and safety factor for survival are summarized in Table 3.7. For ease of understanding and better representation of the particular requirement, The table is divided and numbered based on the input.

Note: To avoid bewilderment, standard earth gravity in D1 is mentioned as G and grams in O4 is mentioned as g.

Table 3.8: Optomechanical Design Loads and Requirements

Input	Req No	Parameters	Value	Remarks
Design Loads	D1	Shock and Vibration	150 G	In Three Orthogonal Directions
	D2	Isothermal Temperature	293.15 K ±5 K	
	D3	Gradient Temperature	3 K/m	From ground to space and Operating Conditions
	D4	Assembly Tolerences	±0.1 mm	
	D5	Gravity Release	2 G	
	D6	Launch Survival	150 G	
Optomechanical Performance and Design Constraints	O1	Eigenfrequency of the Calibration	> 600 Hz	Due to Shock and Vibrations
	O2	Main Frequency of the Instrument	> 200 Hz	Due To Shock and Vibration
	O3	Stability	< 0.05 mm	w.r.t. Thermal Temperature
	O4	Total Mass	< 200 g	Including the Optics and Adjustment Mechanism
	O5	Available Volume	< 16000 mm^3	Space between the FM1 and M1
	O6	Cost	< €10000	Including Manufacturing and Parts bought from suppliers
Safety Factors For Survival	S1	Mirror Fracture	> 2.5	
	S2	Lens Fracture	> 2.5	
	S3	Adhesive Breakage	> 3	
	S4	Flexure Yield	> 1.25	
	S5	Flexure Buckling	> 10	

(D1): **Shock and Vibration**: This mainly occurs due to the impact created by the rocket and the py-roshock generated during seperation of vehicle stages. The shock and vibration loads also come from the extreme operating conditions and have three orthogonal directions with a value of 50 G in each direction.This value was derived from the Miles' equation, where knowledge of the resonant frequency can provide an estimate of loads due to vibration and shock in one dimension.

$$G_{RMS} = (\pi/2 \cdot f_n \cdot Q \cdot [ASD])^{0.5} [2]$$ (3.2)

where natural frequency (f_n) of the system was considered to be 200 Hz, amplification factor (Q) was considered to be 50 (based on discussions with designers of similar instruments) and the input spectral density at natural frequency was considered to be 0.16 G^2 /Hz.

(D2): **Operating Temperature**: The whole instrument is maintained at a temperature range of $20C$ with a thermal control subsystem installed in the satellite. This control, in general, is achieved using a black painted electronic box and heaters. Electronic box provides radiation with low solar absorptance and high emittance to reject extra heat and is placed on the cold side of the satellite, such that it acts as a radiator. If the temperature of the system falls drastically, then emergency heaters are used and the stability requirement O3 temporarily does not have to be satisfied.[18]

(D3): **Gradient Temperature**: The temperature gradient of the system will be kept 3 K/m or below, by the thermal control system of the instrument and the satellite platform. The absorption of sunlight and the low temperatures in space causes this gradient.

(D4): **Assembly Tolerance**: Tolerances on parts lead to mismatches between mating surfaces during assembly. Optical performance needs to be met even considering these tolerances. Additionally, fixing such as fastening by bolts will apply forces on the components and need to be considered during performance and survival load cases.

(D5): **Gravity Release**: During manufacturing and calibration of the system, there is gravity, but when it is operating the system will be in free fall and will therefore not experience the gravity deformation any more. Because of the lack of gravity deformations, the satellite will deflect compared to its state during calibration on Earth. The system will deflect compared to its state during calibration on Earth. Including a comfortable margin, 2G is considered.

(D6): **Launch Survival**: This is generated by launcher engine vibration and aerodynamic loadings while transporting the instrument to the lower orbit region.

(O1): **Eigenfrequency of the Calibration system**: The Eigen frequency of the calibration module has to be more than 600 Hz order to safely separate calibration sub-system eigenmodes from dynamics of the instrument and to limit susceptibility to vibration sources that are active during operation (such as gyroscopes).

(O2): **Main Frequency of the instrument**: The natural frequency of the rocket delivering the instrument is around 90-100 Hz, with a constraint on the mass of the instrument to be less than 3.5 kg. In order to limit susceptibility to launcher dynamics and shocks the instrument's lowest eigenfrequency is designed to be greater, but close to 200Hz. This is not a responsibility of the calibration sub-system, but can be used for design and estimates.

(O3): **Stability**: Due to the rapid changes in the temperature of the module, a minimum limit has to apply so that the system still performs according to the specifications. Therefore a limit of 50 microns of decenter of the calibration spot with respect to the aperture next to the slit has been taken to be considered stable.

(O4): **Total Mass**: A total mass of less than 200 g is allocated to the module. This will include all the components, structural housing, and adjustment mechanisms. If infeasible, the instrument team needs to be notified as soon as possible, such that dynamical performance can be re-evaluated.

(O5): **Volume**: There is a volume constraint because of the limited available real estate between the Fold mirror 1 and collimator as shown the figure3.13. Therefore both spectral calibration modules have to be built within the volume of 16000 mm^3.
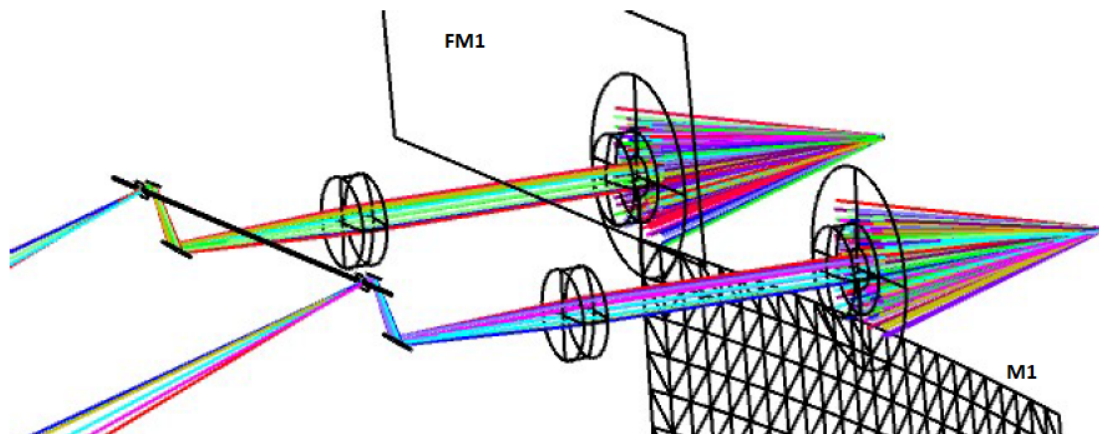
Figure 3.13: Volume between the Fold mirror1 and Collimator

(O6): **Cost**: A budget of €10000 has been allocated. This includes parts brought from the suppliers, manufacturing of components, and housing structure. It excludes design and analysis rates.

(S1 - S5): **Safety Factors For Survival**: The values for safety factors were selected based on the European cooperation for space standards[1]. This includes values for mirror fracture, lens fracture, adhesive breakage, flexure yield, and flexural buckling.

$$FS = \sigma_{yieldstress}/\sigma_{Designstress} \tag{3.3}$$

$$MS = FS - 1 \tag{3.4}$$

Where FS and MS are the factor of safety and the margin of safety respectively. These values are only important for the survival of the system.

4
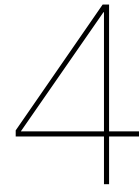
Conceptual Design

4.1. Material Selection

Given the specifications and constraints as well as the concept design for the optical system, the general appeal would be to proceed into the preliminary design phase for the optomechanical structure. However, the optical components in this case are merely represented as a lens or a mirror with axial separation and location, but have concrete radii, thickness or the material type. So, the ideal next step would be provide a definitive dimensions and material properties for the given optical elements.

A typical optical space instrumentation device, consists of a large number of components made of and linked by a variety of materials. In general, all sorts of material classes (glasses, ceramics, metals, crystals Etc) can be considered for optical instruments. The criteria that affect the selection of materials for such interdisciplinary designs include spectral range, stray light requirements, mass, structural rigidity, allocated budget, and thermal design constraints. Therefore, this usually requires materials with high dimensional stability, homogeneity, surface finish, and the least amount of weight for high stiffness. But, this is not the case in real life situations because:

a) It is highly unlikely to have a complete assembly made of one material.

b) Some extent of dimensional instability (temporal, thermal, thermo-mechanical and hysteresis) do exists in all components.

c) There is always a tolerance involved for machined components.

d) Often there is a difference between manufacturing and operating conditions.

Alternatively, compensation is often applied to reduce impact of the requirements and enable adjustment of the system to a tolerable level based on as-manufactured performance. Some potential sources and the controlling strategies of these dimensional instabilities are mentioned in [34]. But the most important methods would be to select the most insensitive locations or to use to use materials with similar mechanical and thermal property profiles. In the first case, strategies like thermal center can be employed for the whole system but it becomes increasingly difficult for complex systems with multiple components. Therefore, the other method seems to be the ideal method in such a scenario. By combining materials with different coefficients of thermal expansion (CTE) and varying the length, points in a system can be designed to be fixed concerning each other while the rest of the system deforms around it.

For the sake of lucidity, the parts used in the calibration module are categorized into five types: Lens, Mechanical structure, Mirrors, Ferrule and Adhesives:

- **Plano-Convex Lenses**: The choice of materials is primarily dependent on the wavelength, refractive index, mechanical, thermal, and dispersion properties. Glasses, crystalline materials, and plastics are the most common type of elements used for the lens. For this particular system, both the lenses should have UV-VIS transmission capability with a spectral wavelength of 300-500 nm and an effective focal length of 18 mm. Fused silica from Edmund optics [5] was chosen for this reason. Being said that, Fused silica also has a low index of refraction, low coefficient of thermal expansion, low inclusion content.

- **Mechanical structure**: Mechanical structure usually include the support and connect structures for the optical components. The choice of materials is primarily dependent on the stiffness, dimensional stability, manufacturing preference, and relative thermal expansion with optics. Materials like aluminum, beryllium, and titanium are most commonly used for space applications. Beryllium, known for its higher conductivity and better compatibility for extreme temperatures, has a reputation as being hazardous and has high thermal expansion and low micro yield strength. Titanium is also preferred for its compatibility with glass/optical materials, consistency for high-temperature variations, and high strength. Although, this does create a problem in terms of manufacturability and post processing. Therefore, aluminum is considered best in this situation. As shown in the figure 4.1 below, Aluminium and fused silica have similar performance in terms of stiffness and thermal stability for equal mass. Since the overall instrument uses scalmalloy aluminium for the structure, it is cogent to consider the same material in order to have a matching CTE. Plus, scallmaloy aluminium is also printable with SLM methodology.
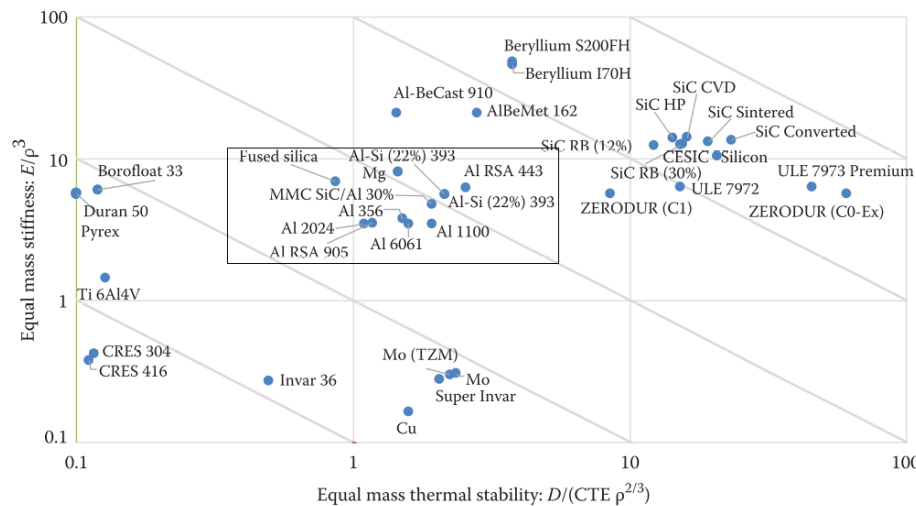
Figure 4.1: Equal mass material comparison for stiffness and thermal stability performance of Aluminium and Fused Silica [32]

- **Mirrors**: Mirror elements usually have a reflective surface and a substrate that supports them. The choice of materials is primarily dependent on the wavelength, thermal, dimensional stability, and constant figure of merit in the operating conditions. A wide variety of material classes including glasses, metals, ceramics, and plastics, are used for reflectors. Aluminum 6061 is preferred in this case because of its low cost, lightweight, high thermal conductivity, high strength, and similar CTE compared to the mechanical structure.

- **Fiber Ferrule**: Fiber ferrule is a stick-shaped optical component that houses fiber cables for assembly to structures. These elements provide low insertion loss, low back reflection, and superior durability with applications ranging from optogenetics to telecommunication and space instruments. These components are made of different materials such as plastics, stainless steel, and ceramics. Although Ceramic Ferrule provides remarkable strength, small elasticity coefficient, easy control of product characteristics, and strong resistance to changes in environmental conditions, they are not compatible with the selected mechanical structure. For this application, Stainless steel from Thor labs [25] was chosen as they provide longer ferrules that are compatible with bonding, press-fitting, and clamping purposes.

- **Adhesive**: The adhesives, in general, are classified based on several parameters like form, load-carrying capability, and type but the ones mostly used for optical systems are classified as structural adhesives. The choice of materials, especially for space instruments, is primarily dependent on the stress-induced during shrinkage, stiffness, coefficient of thermal expansion, and outgassing measures like RML and CVCM (NASA defines that an adhesive with RML< 1 % and CVCM<0.1 % as low out-gassing adhesive). Epoxies, Urethanes, Acrylic, Polyurethane, and Cyanoacrylate adhesives are the major types of structural adhesives. [50] provides a detailed description regarding each type of adhesive and also mentions the most used adhesives in these applications Another important factor to consider while selecting an adhesive is based on the proficiency of the adhesive specialist. Based on all the above mentioned criteria, 3M EC-2216 A/B was selected.

The Table 4.1 below, illustrates all the choices made on each component, regarding both dimensions and material.

Table 4.1: Component Description

Components	General Parameters				Remarks
	Dimensions (mm)	Material	Thickness (mm)	Shape	
Aperture	2.4 (Diameter of the opening)	Scalmalloy aluminum	0.1-0.5	Circular	Distance between the 2 Apertures = 28.40 mm
SL-1 (Lens)	6.00 (Lens Diameter) 8.25 (Curvature Radius)	Fused Silica	1.44 (Edge Thickness) 2.00 (Total Thickness)	Plano Convex	EFL = 18 mm BFL = 16.62 mm Company: Edmund Optics
SL-2 (Lens)	6.00 (Lens Diameter) 8.25 (Curvature Radius)	Fused Silica	1.44 (Edge Thickness) 2.00 (Total Thickness)	Plano Convex	EFL = 18 mm BFL = 16.62 mm Company: Edmund Optics
SM-1 (Mirror)	2.00 (Mirror Diameter)	Aluminum 6061	Depends on the design	Round Shape Flat surface	Fold Mirror Orientation Angle = $54.385°$
SM-2 (Mirror)	1.00 (Mirror Diameter)	Aluminum 6061	Depends on the design	Round shape Flat Surface	Fold Mirror Orientation Angle = $45°$
Fiber Ferrule	2.50 (Outer Diameter)	Stainless Steel	12.7 (Length)	Cylindrical Stick	Fiber = Fused Silica Bore Size = 230 - 440 μ m Flat End Face Company: Thor Labs
Slit	0.4 X0.4 (Side X Side)	Scalmalloy aluminum	0.2 - 0.5	Square	Both the Slits in the either side of the Telescope Slit.

4.2. Mouting of optical components

Mounting is a mechanical component that provides an interface for proper support, position, and orientation to a particular optical element in an instrument. An acceptable mounting design is one in which the effect of tolerance is minimized, and the orientation of each optic is as innocuous to adverse environments as possible throughout its useful life. One important note to remember while designing a mounting structure is that space should be allocated for alternate compensation strategies when assembling the optics. A typical mounting strategy begins with defining the orientation of the optics concerning the ensemble or the mechanical reference(rotational symmetric or asymmetry). Next, determine the constraints that have to be applied for the optics in all the DOF's (both axial and lateral) to a particular limit to avoid birefringence and deformation. Later, an interface has to be provided to support the optics. For reflecting surfaces like mirrors and gratings, these interfaces are usually provided on the other sides of the reflecting surface but in the case of refracting surfaces, this is not usually the case. [47] provides the details regarding the six mounts to lens interface. Finally, After determining the interface to the optics, mounting methodologies are used to lock the position of the optics.

The approach is basically use as few components as you can, place on machining tolerances and use a assembly budget to determine if it complies to the optical tolerances. If not you might consider alignment or a mechanism, but now not yet. With the added advantage of AM, it is more convenient to allocate athermal designs with high complexity, thus further diminishing a need for adjustment mechanism.

From here on, mounting strategies used for each component are discussed similarly as shown in section 4.1. To brainstorm ideas of different concepts, the morphological chart methodology was generated for each of the component. The morphological chart is an design methodology in which mounting strategies of the desired design are listed corresponding to all the possible options or solutions that can fulfill. All the mounting options and strategies collected in this section are directly derived from various Reference papers and past missions with similar requirements and environmental conditions. Further details regrading each methodology is provided in the literature research.

- **Lens**: A lens mount in general aims to create rigid support which is statically determined. The statically determined design provides six degrees of freedom constraint without any over or under constraint in any given axis. The advantages of a static determined structure are that computations are simple, the structure is predictable, and stress on either side of the structure can only displace and not deform the other side. These constraints in each degree of freedom are provided by the interface and preload. But the utilization of a desirable interface or a preload for holding a lens component is mainly constrained by the usage of the area, the weight of the optics, and the environmental conditions. Therefore, it is not possible to create a kinematic mounting in every situation.

  In general, there are two methods available for mounting lenses: Clamping and Bonding. Figure 4.2 below illustrates the different concepts of mounting lens that are applicable for the given requirements. These include methodologies ranging from inexpensive, lower precision techniques to expensive technologies that include both custom-made and off-the-shelf components.
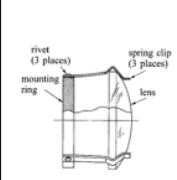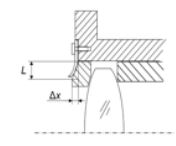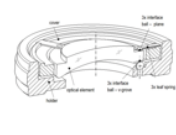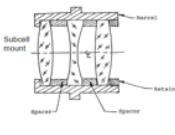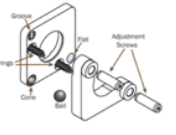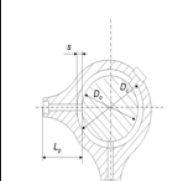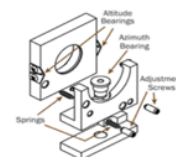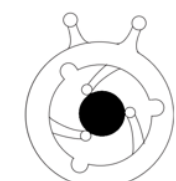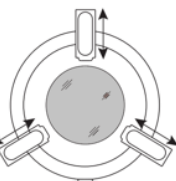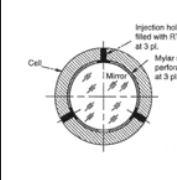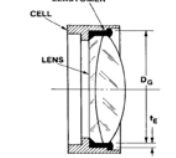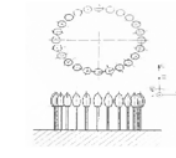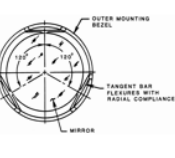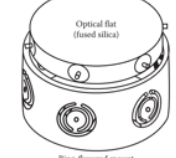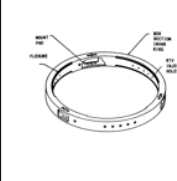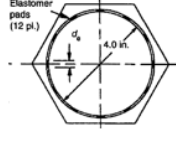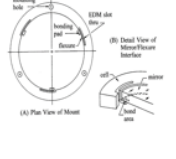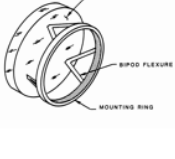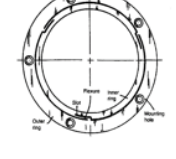
Figure 4.2: Strategies for Mounting Lens

- **Mirrors**:The objective of a mirror is to reflect light and hence contribute as few aberrations to the

wavefront as feasible. A mirror mount keeps the mirror in place throughout operation and transportation, which can be disrupted. As previously stated in the requirements chapter, temperature changes will cause the mirror to expand, and transportation will cause shocks and vibrations. The mount should be able to hold the mirror in place while not transferring extraneous effects into the mirror. In general, the mirror can be self supporting (i.e. can survive without outside assistance, for example, support in the middle) or require a mount. The first case is only possible when we have enough space for allocating higher thickness.

Figure 4.3 below illustrates the different concepts of mounting mirrors, which are categorized as clamping, bonding and hybrid.

Mounting	Concept-1	Concept-2	Concept-3	Concept-4	Concept-5	Concept-6
Clamping						
Bonding						
Hybrid						

Figure 4.3: Strategies for Mounting Mirrors

- **Fiber Ferrule**: Fiber ferrule is a component that houses the fiber which transmits the solar radiation from the diffuser to the slit. As pointed out before these fibers should be placed at the focal point of lens 1. Therefore, it is of utmost importance to mount these components which are robust to environmental conditions. Figure 4.4 below demonstrates different kinds of mechanisms used for mounting a ferrule structure. In [46], the ferrule is mounted by a positioner which attains stability using pure kinematic principles. As shown in concept-1, The main mountable body is clamped to the structure. This is a single mode fiber positioner and allows adjustments in five degree of freedom. Concept-2 is directly mounting the ferrule by press-fitting into the assembly. The concept-3 here employs a feature-based mounting where specific features are created to lock the system into the structure [31]. The concept-4 is created by cannon [13], which uses a compliant mechanism to mount the assembly. The Concept-5 is created by Edmund optics [33], which employs an adjustable mechanism to lock the ferrule position in the assembly. The last concept is a conventional method where the ferrule is directly bonded by using bond pads at the desired location.

Mounting	Concept-1	Concept-2	Concept-3	Concept-4	Concept-5	Concept-6
Fiber Ferrule						

Figure 4.4: Strategies for Mounting Ferrule

- **Slit**: The slit corrects the performance of the rays entering from the telescope and the calibration module and eliminate the off- axis rays, thus being responsible for the input that is used by the remaining spectrometer component. The most common and simplest way to mount a slit is by

creating sharp wedges with a preferred separation and creating extra space immediately to not avoid the outgoing rays. The figure 4.5 below demonstrates the slit assembly incorporated by [21]. It is important to remember that the slits made should have roughness in the order of micrometers to avoid inaccuracies. For maintaining the accuracy in the position and the orientation of the slit, alignment cubes are used for references.
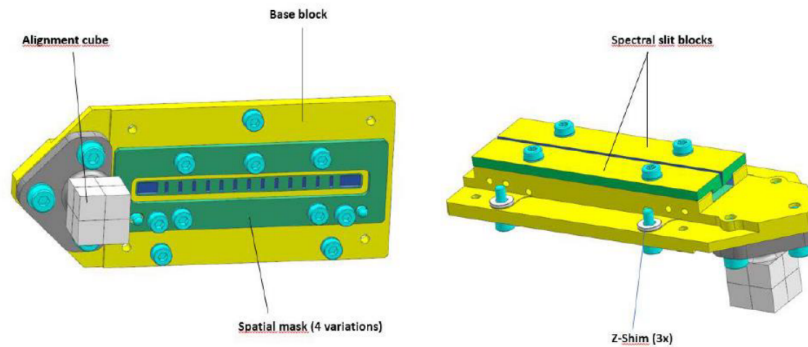
Figure 4.5: Mounting Slit Assembly [21]

4.3. Module Concepts

Now that we have gone through different mounting methodologies for single optical components, the integration of these sub-assemblies is considered. For this, it is crucial to comprise the whole ensemble by maintaining the required alignment and orientation. In general, there are three different kinds of structures present for structural design: Truss, Boom and Barrel design. A rank based comparative study was made between the three structures in [40], where eleven different parameters were considered in determining the best design for an optical system that was deployed in a small Earth Observation satellite. From the figure, it is seen that the barrel structure was the most suitable for the optical design. Since, the requirement criteria and the environmental conditions were similar, the shell type of structure was employed for all the concepts.

Trade-off Crit.	Truss Structure	Boom Structure	Barrel Structure
Mass	3	2	2
Compaction	2	2	2
Thermo-stability	1	3	3
Complexity	2	1	3
Scalability (deploy. leng.)	1	2	3
Scalability (general)	1	2	3
Light Management	1	1	3
Cost	3	2	1
Repeatability	1	3	3
Deployment control	1	3	3
Stiffness	1	1	3
Total	17	22	29

Figure 4.6: Trade Off Matrix [40]

Based on the morphological charts initiated before and the requirement criteria, six new module concepts were generated by combining solutions of each mounting strategy together. Since there is no such utilization of off-the-shelf or existing components, a top-down approach was implemented while designing these components. Top-down is a big picture approach that relies on the black box for assistance and further enhancement. In a top-down method, an overview of the system is presented, with first-level subsystems specified but not detailed. Each subsystem is then refined further, until the entire specification is reduced to fundamental parts. The generated concepts are explained in detail below,

with appropriate images as an aid for better realization.

- **Concept-1**: This concept is a drop-in assembly type where the optics and the mount features that interface with them are produced to specific specifications within specified tolerances and assembled with minimal machining and adjustment.
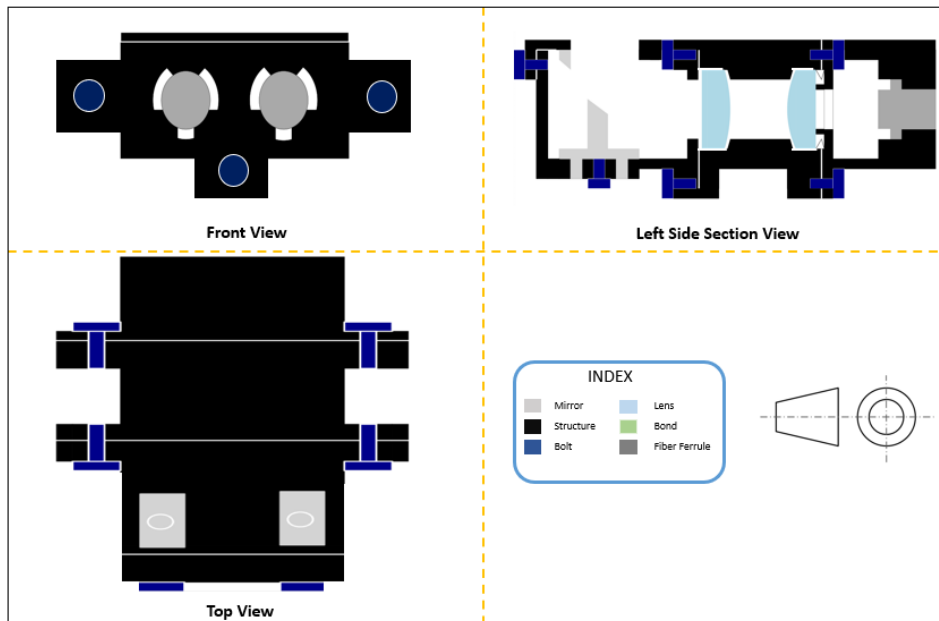
Figure 4.7: Concept-1

As shown in Figure 4.7 above, this concept employs the vertical version and comprises of four main parts. The first part from the right houses the ferrule and the aperture. The ferrule, in this case, is mounted using the concept three principle as shown in Figure 4.4. The second part consists of mounting features for both the lens. Here both the lens are mounted on curved surfaces with the spherical lens-mount interface. The additional space is provided on the plane side for housing spring clips or washers for reliving the stress when encountered with extreme conditions. Also interfaces (aperture and the tip of the third part) are provided for the plane side of lenses to avoid the penalty caused by extreme defocus in the lenses. The third part provides Slots for mounting the SM1 mirror and houses the slit structure. The SM1 mirror is mounted using the concept 3 (in the Clamping Row) principle as shown in Figure 4.3, with few minor changes. Two alignment pins were provided on the SM1 structure for constraining five DOF when inserted into the slot. The sixth DOF is constrained when clamped using a bolt. Finally, The fourth part comprises the SM2 mirror. The fourth component is connected on the backside of the slit structure using bolts. Since all the parts were clamped to one another, it creates an opportunity for the user to reassemble. Although this also reduces reliability and the tolerance generated in this case is very high. This concept is also not suitable for changes as it does not provide additional volume if required.

- **Concept-2**: This concept is a lathe type assembly where the optics interface are custom made by one single machine to fit closely to the outer diameter of the ensemble of optics. Here, it is important to note that precisely manufactured optics (especially on the edges) should be used. As shown in Figure 4.8 below, This is a single component horizontal version design. The whole concept is manufactured using the SLM. The ferrule, in this case, is mounted using the concept number six principle as shown in Figure 4.4. The aperture is installed into the system via the slot that is placed between the two lens holders. The lens and the mirror are mounted using the concept number one (in the Bonding-1 Row) principle as shown in Figure 4.2 and the concept number two (in the Bonding Row) principle as shown in Figure 4.3 respectively. As shown in

the above concept, the aperture and the extrusion provide an interface for the plane side of the lens. The whole component is finally connected using a flange or a threaded structure to the slit plate (which was not designed in this case). This concept provides a distinct advantage in terms of weight and volume for design improvement. Since all the components are bonded here, in this case, it is not possible to reassemble. Also, it is an over-constraint design that can lead to unanticipated deformations. This concept does provide thermal center via bonding at three equidistant points for the lens but it is not the best option available because the considerable analytical effort is substantial, and no provision for active centration during thermal deformations. Finally, this concept does not provide a lot of room for all the post-processing methodologies.
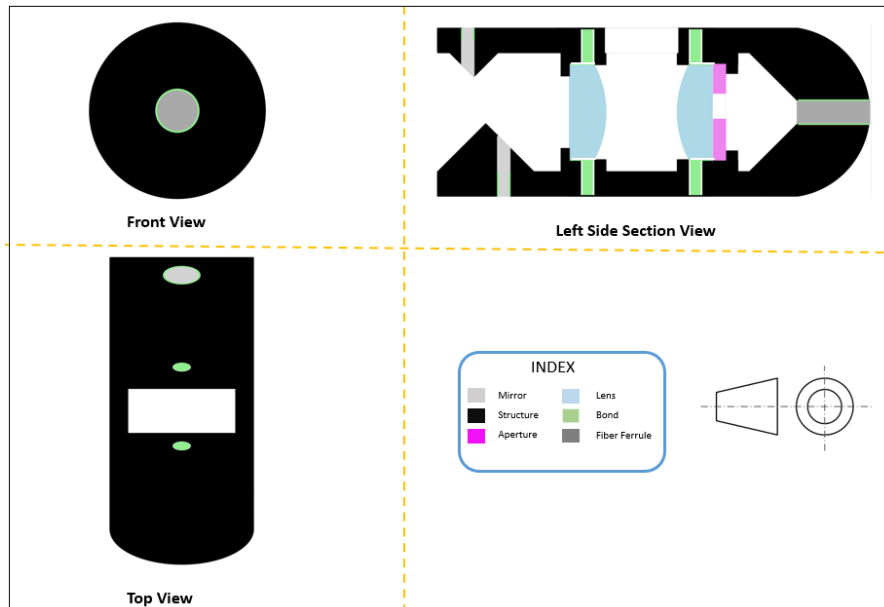
Figure 4.8: Concept-2

- **Concept-3**: This concept is a modular assembly system, where all the mechanical and optical parts are constructed and pre-aligned beforehand as separate modules.
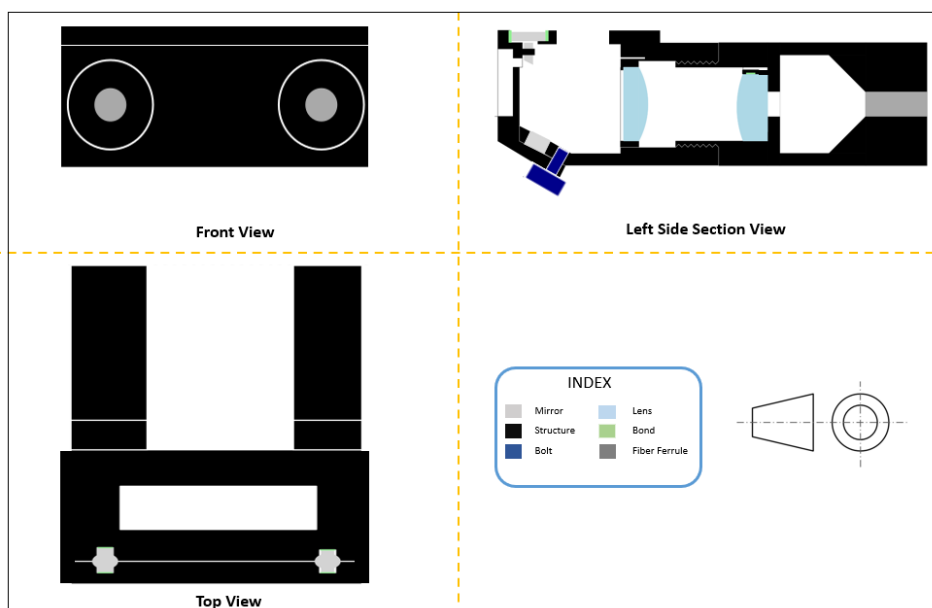
Figure 4.9: Concept-3

As shown in Figure 4.9 above, This concept employs the vertical version and comprises four main parts. The first two-part are tube-like axisymmetric structures, which houses the ferrule, aperture, and SL1 each. The ferrule here is mounted via press fitting, while the aperture is directly printed in the structure itself. The SL-1 lens is mounted using the concept number four (in the Bonding-1 Row) principle as shown in Figure 4.2. A tangential and a flat interface is provided for the lens by the flexure and the aperture respectively. The two parts are then assembled to the third part by threads (M8 size). The third part provides features, interfaces and Slots for mounting SL-2, SM-1, and SM-2. The SL-2 lens is mounted using the concept number three (in the Bonding-2 Row) principle as shown in Figure 4.2. The fourth part comprises the slit and the SM-1 mirror. This part also provides features for mounting the SM-2 mirror. These parts are connected by placing the SM-1 mirrors into the slots and bonding the SM-2 mirror with both the provided interfaces. To constraint all the degree of freedom, this part is also clamped together with the third part. An asymmetric structure is utilized in the case of the SM-2 mirror to avoid errors while assembling.The concept is not completely manufacturable by SLM technique. The fourth part will be manufactured using conventional methods as the SLM does not provide the best surface finish and feature size required for the Slit and the SM1 mirror. Also, the This concept provides a distinct advantage in terms of ease of manufacturing, acceptable tolerances, sufficient volume for design improvement, and active centration for lenses during thermal deformations. Finally, this concept also provides a lot of room for most of the post-processing. Although, it does have a disadvantage for the exact constrained mount design for the SL-1 lens due to lack of post processing capability. Also, with some of the components being bonded, it is not possible to reassemble completely.

- **Concept-4**: As shown in Figure 4.10 below, This is a single component vertical version design. The whole concept is completely manufactured using SLM.
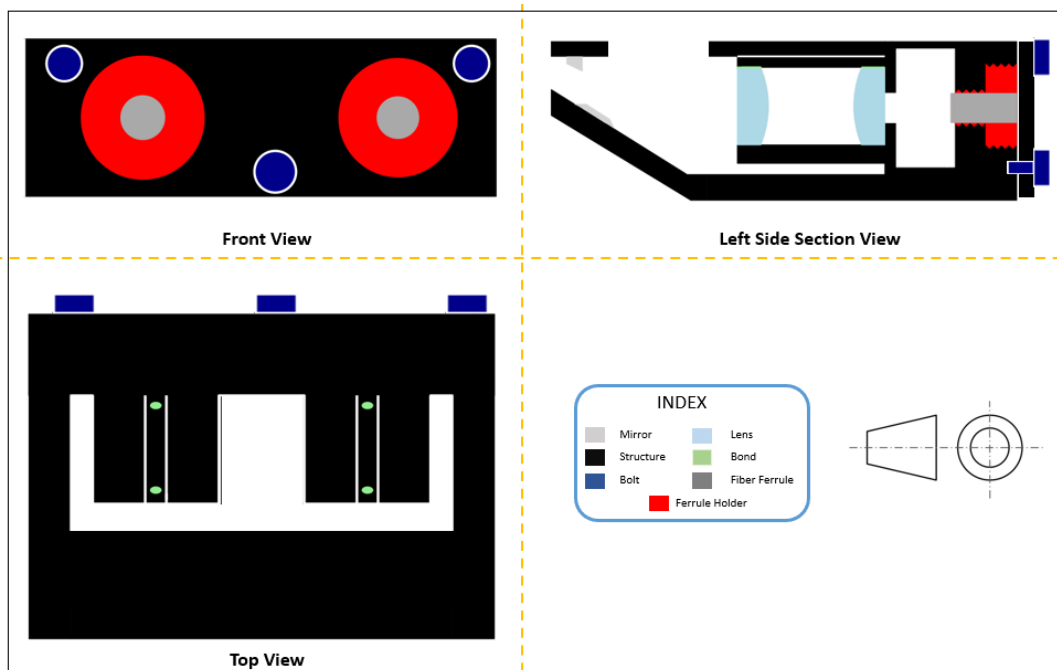
Figure 4.10: Concept-4

The ferrule, in this case, is mounted using the concept number four principle as shown in Figure 4.4. In contrast to the other concepts, both the ferrule are mounted, in this case to the same single structure. The lens here is mounted to the same flexure as shown in the figure 4.11 below. These long flexures, provided at an angle of 120 degrees, are fabricated by creating two long slots on the side of the triangular structure. The SM1 and the SM2 mirrors are printed directly on the structure itself. Contrary to the previous concepts, the whole module is clamped on the ferrule side of the structure with three bolts, thereby constraining all the six DOF. This concept provides

a distinct advantage in terms of ease of manufacturing, weight, thermal center for the lens and eliminates additional alignment features. Although this concept provides active centration, it is an over-constrained design. Also, no support or reference is provided in the z-axis for the SL-2. Since all the components are bonded here, in this case, it is not possible to reassemble. Also, the surface roughness of the mirrors is not good. Finally, the accessibility for the post processing of the mirrors is very poor.
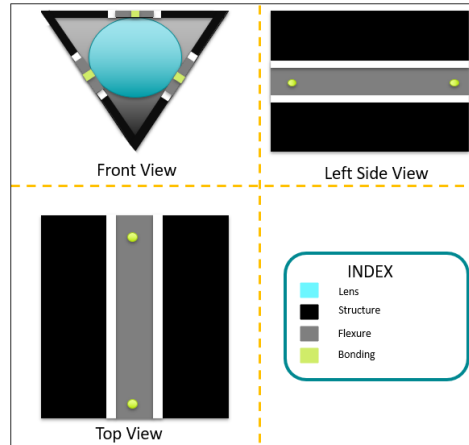
Figure 4.11: Lens mounting strategy in concept-4

- **Concept-5**:As shown in Figure 4.12 below, This concept employs the vertical version and comprises three main parts. Compared to the previous versions, a change has been made in the SL-1 geometric parameters. This way, the assembly procedure was simplified by eliminating the need for designing two different parts.
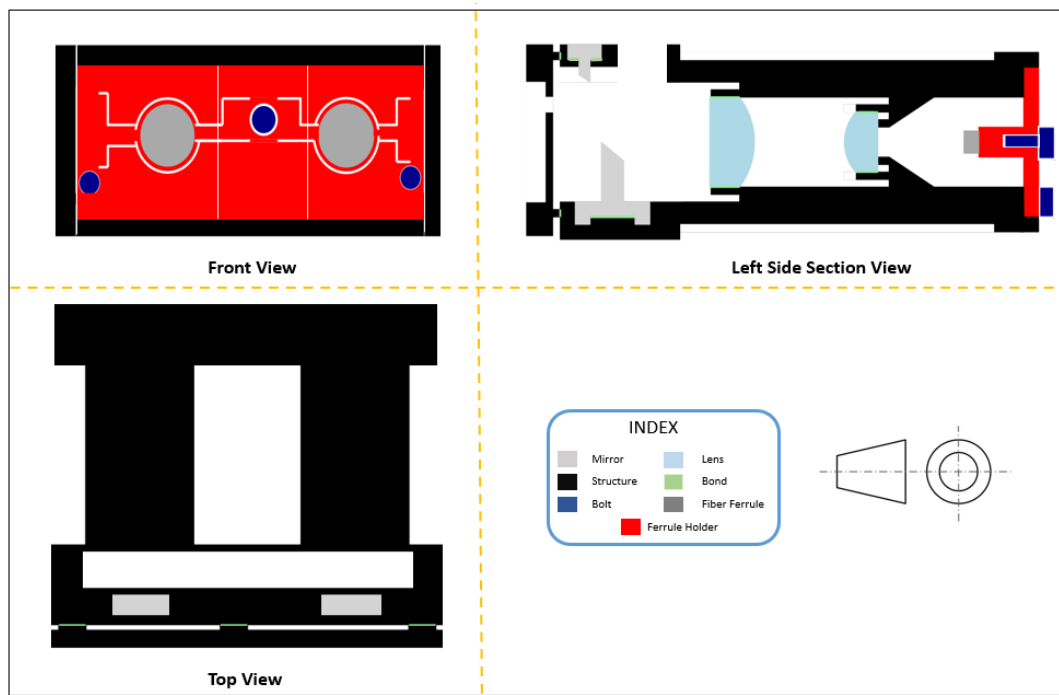
Figure 4.12: Concept-5

The ferrule, in this case, is press-fitted on the first part (a plate-like structure), where features were made to adjust the position and the orientation of the ferrule using a differential screw. The plate

is then fitted into the second part and is constrained (both rotations and translations) using two bolts. The second part comprises the aperture, flexure features for mounting both the lenses and slots for mounting both the mirrors. The lens and the mirror are mounted using the fourth concept (in the Bonding-2 Row) and the first concept(in the Bonding Row) principles as shown in Figure 4.2 and 4.3 respectively. Finally, the third part (which houses the slit structure) is mounted onto the main body using adhesive patches at three different locations (by maintaining the thermal center at the slit). This concept does provide a distinct advantage in terms of manufacturing, assembling, and weight. Also, both the lens are provided active centration and thermal center to compensate for the disturbances. But, it does increase the cost and time of manufacturing the SL-1 lens, as there are no commercially available products with smaller sizes and similar properties. Also, the self supporting feature developed for eliminating the overhang issue on the aperture can lead to errors.

- **Concept-6**:This concept is a subcell assembly system, where all the mounting interfaces are aligned in order. Later, the components are installed in a sequence into the main body of the optomechanical module. These mounting component subcells are retained in the position by clamping or bonding methodologies.
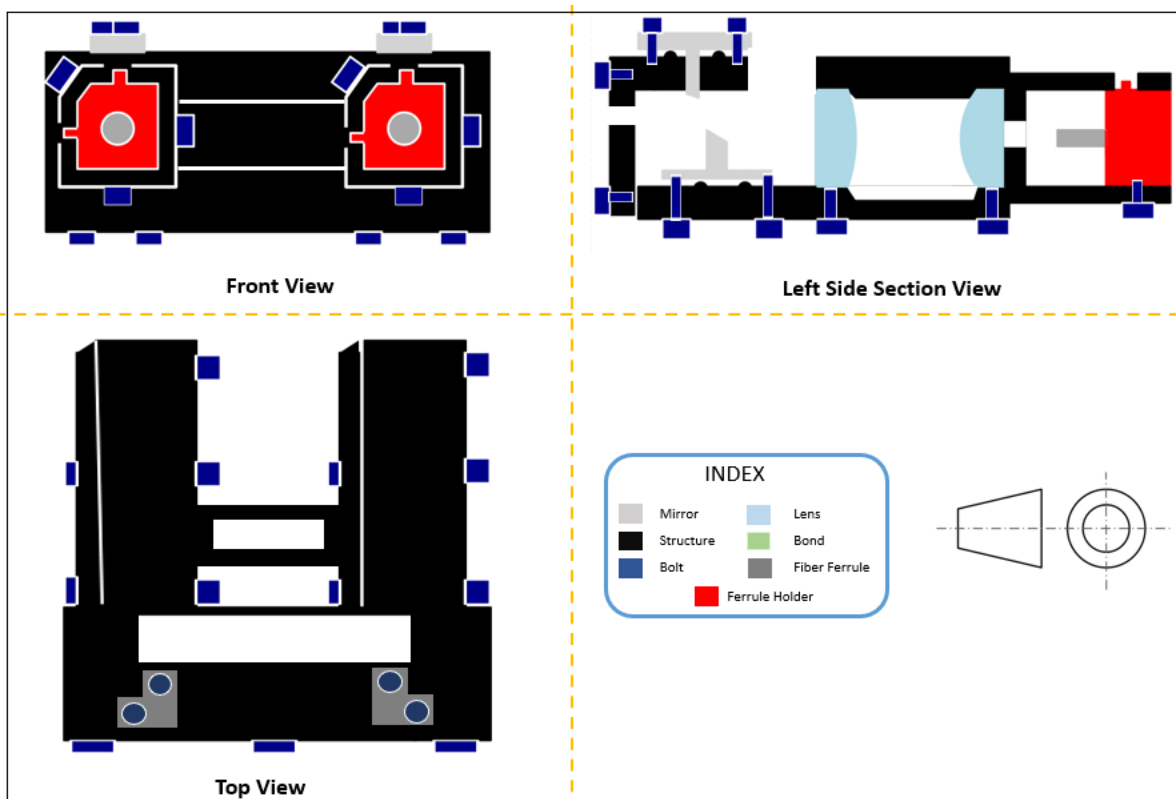
Figure 4.13: Concept-6

As shown in Figure 4.13 above, This is a single body vertical version design with multiple sub-assemblies. The ferrule, in this case, is mounted using the first concept principle as shown in Figure 4.4. Here, the ferrule is mounted by a 3 DOF (two translation and one rotation) positioner which attains stability using pure kinematic principles. The lens components are mounted using the first concept(in the clamping-second Row) principles as shown in Figure 4.2. The two pins at a 90-degree angle put a radial limit on the optical element in this pin mounting approach. A third pin is attached to the existing two at a 135-degree angle. Here, pins are made of low CTE materials, to compensate for the thermal disturbances. This mounting approach prevents lens fracture owing to differential thermal expansion, provides exact lens alignment and so reduces manufacturing tolerances, and keeps hysteresis low. The two mirrors are mounted using the sixth

clamping concept principle as shown in Figure 4.3. Finally, a slit structure is clamped onto the assembly using three bolts to constraint all the DOF. This concept provides a distinct advantage in terms of ease of hysteresis and centration during thermal disturbances. Also, the post-processing for this concept is feasible. But it is not the best concept in terms of weight, cost, assembling, and tolerances. Despite the fact that kinematic mounts provide excellent support for optical elements, point contact is not a viable choice in such environmentally sensitive systems. Finally, it does not accommodate additional volume for design improvements.

4.4. Concept Selection

Given the specifications and constraints, an approximate assembles of parts were created with alternative design approaches. Before finalizing the concept selection, it is essential to see whether the assemblies developed are conforming the requirements. For this, a multilevel budget approach was considered to verify whether the credibility of the design. A Multilevel budget, also known as the error budget is an overall addition of the expected performance impact of the error source. It provides valuable insights regarding the worst offenders and can be used as a reference source for fault-finding in the testing phase. The error budget applies to various groups of error sources like manufacturing, thermo-mechanical, optical design choices, and environmental conditions.

In this situation, the total system's trustworthiness relies on the relative alignment of the components. Since tolerances have a huge impact on how well an optomechanical system works and how much it costs over its lifetime, a preliminary mechanical manufacturing error budget was chosen for the evaluation. Here, an assumption is made to fix the position of the slit as the reference element and formulate an error relative to that point. From section 3.3, the sensitivities are already derived. Now, the standard deviations of errors are multiplied with the respective sensitivities to predict the effect on the performance. Finally, a quadratic addition was done to get the overall effect of the performance. From the requirements, it was evident that a total of 50 microns tolerance was acceptable for each axis. The table 4.2 below provides details regarding the error budget in each of the cases.

Table 4.2: Mechanical Error Budget

Concept	Δx (μm)	Δy (μm)	Δz (μm)	Rx (mil)	Ry(mil)	Rz(mil)	Continue with Concept?
Concept-1	41.018	47.53	65.35	0.25	0.015	0	No
Concept-2	25.01	30.18	39.25	0.28	0.014	0	Yes
Concept-3	39.15	41.98	49.56	0.20	0.014	0	Yes
Concept-4	45.85	43.67	58.37	0.25	0.015	0	No
Concept-5	29.80	30.49	38.98	0.23	0.013	0	Yes
Concept-6	53.97	51.28	49.75	1.510	1.289	0	No

Now that we have three concepts which meet the tolerance requirements, it is important to examine further to determine the best concept. To evaluate this, a concept selection methodology was chosen. The Pugh matrix is an approach that aims to identify the best concepts that can be integrated to improve the design further. One of the concepts is chosen as a reference concept in this process, and the rest of the concepts are compared to it using a selection criterion developed from the design requirements. In this case, concept-2 was chosen as the best concept as it provides a design with the least mechanical tolerances possible. A concept receives a + or a - for meeting a condition more or less efficiently than the reference idea. The concept receives a 0 if it is on the same level as the reference concept. The sum of all pluses, minuses, and zeros is then calculated for each notion, and the concepts are ranked. Since, the selected concept acts as a reference, it was given zero for all the criteria. In this manner, the best concept is selected. Also, improvements are made on the best concept and finally a better module is created in this manner. This methodology was chosen because it provides a systematic approach to concept selection, which decreases bias. Here, factors pertaining to cost, manufacturing time, mounting constraints, overall weight, and centration factors were considered to be prime, as they are inevitable and require the most attention. Some different criterion such as reassembly, AM compatibility, and compatibility with the existing components were also considered to check with the

preference made earlier. Although, it is important to remeber that all the selstion criteria were given equal weightage to aviod uncertainty.

Table 4.3: The Pugh Matrix

Selection Criteria	Concept -2/ Reference	Concept-3	Concept-5
Inclusion of all the given components	0	+	+
Overall Weight	0	+	0
Active centration for components	0	+	+
Reassemble	0	+	-
Component Mounting constraint	0	-	+
Additively Manufacturable	0	-	-
Changes made in the previous component selection	0	0	-
Post processing accessibility	0	-	+
Additional volume for design improvements	0	0	0
Manufacturing time and cost	0	+	-
Design for Manufacturing and assembly	0	+	+
Net Score	**0**	**4**	**2**
Rank	**3**	**1**	**2**
Continue with the Concept?	**No**	**Yes**	**No**

After applying this methodology on a total of twelve different criterion, Concept-3 has received the highest score and was selected for the detailed design phase.

5

Detailed Design

5.1. Concept Refinement

Looking at the selected concept and inferring from table 4.3, it can be seen that the post-processing accessibility for the SL-1 lens mount is not present causing an overly constrained design. Since the cross-section for the flexure is also unpredictable, it will no longer work in an intended manner and might lead to undesirable stress on the optics. Also, the current mount design for the SL-2 lens would not fulfill the true purpose of centration which is needed during thermal distortions. Finally, the mechanical tolerances for the intersection between part 3 and part 4 is comparatively higher. To overcome this concern, refinement of this concept was needed. Four design improvements shown below were made to eliminate the existing problems.

- The mounting for the SL-1 lens was modified by creating an opening at three different positions, as shown in figure 5.1 below. It will provide accessibility for the surface finish and manufacurability of flexures with desired dimensions. A small protrusion is made on the aperture to reduce the area required for surface finishing.
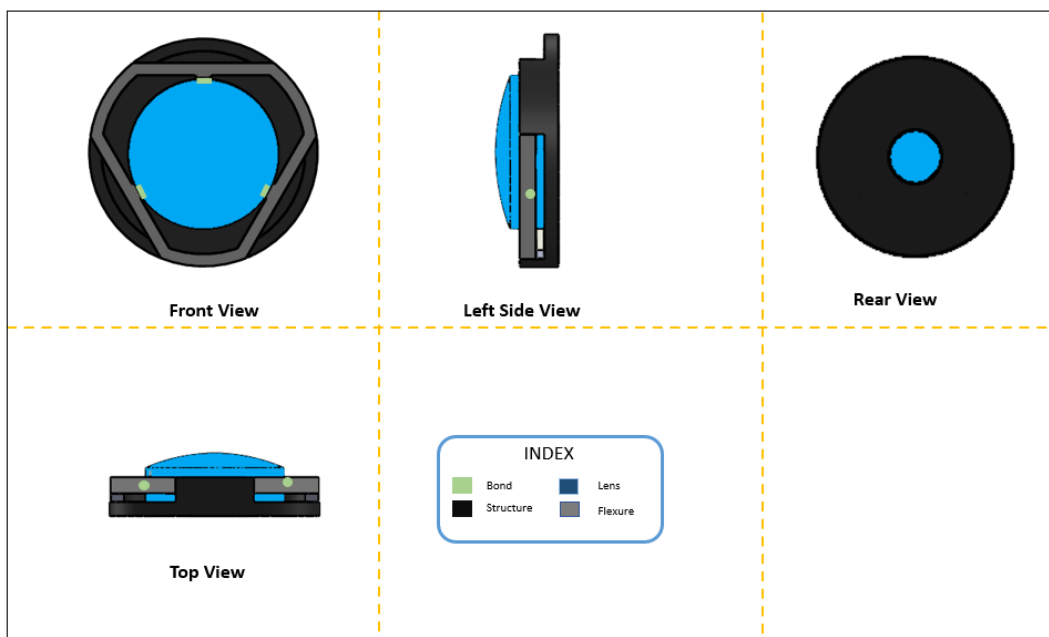
Figure 5.1: Modification for the SL-1 Mount

Also, with the help of these slots, a tangential flexure mount with accurate cross-sections can be manufactured. The lens is bonded at the midpoint of the flexures, located at a separation of 120 degrees. Tangential compliance was essential to prevent stress from spreading toward the lens surface during assembly. A small protrusion was provided at the center of each flexure to provide radial compliance whereby radial expansion of the lens due to thermal loads can be compensated, thus making it an exact constrained design. Due to their monolithic structure, these flexure mounts have no overlapping pieces. Finally, for holding the bond at the desired location, a small feature (with a size of 0.2 mm) was created at the center of each flexure. This will provide a leak-free design with an accurate quantity of the bond.

- The mounting for the SL-2 lens was modified by creating a tube-like structure with three protrusions, each placed at an angle of 120 degrees. Then, the flexures were developed by cutting around the protrusions in u shape using a mill as shown in the figure 5.2 below.
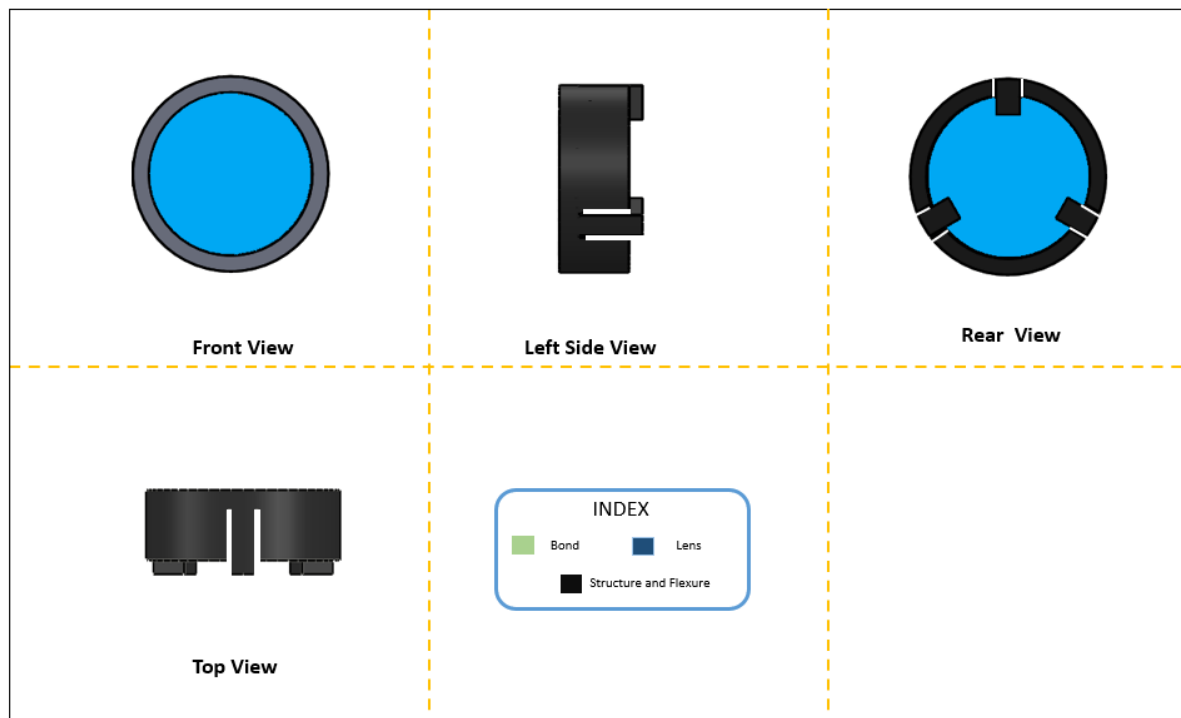
Figure 5.2: Modification for the SL-2 Mount

The flexure blades are constructed integrally within the cell, thus can't be removed or repositioned after installation. These flexures provide isolation by proving thermal center, thus maintaining the position after heavy shocks. Similar to the SL-1 lens mount, a small bath was created on each of these flexures to hold the bond. The lens, in this case, is mounted by aligning it with the protrusion and then adding the glue to bond it at the selected position. Since the mount is an exact constrained design with three flexures constraining two degrees of freedom, the parasitic motions are completely eliminated in this case.

- The previous method used for mounting the SM-2 mirror was to bond the circle with two protrusions structure on either side faces of part 3 and part 4. This was done to avoid shrinkage while curing. Also, a slot was provided for positioning the mirror surface accurately w.r.t slit. This strategy was mainly employed due to the lack of space between the SM-2 and Slit. This did have a disadvantage in terms of mechanical tolerances. Since the component was connected to both parts 3 and 4, the generated tolerance loop was longer. This increases the mechanical tolerances. To avoid this problem, a new method was employed as shown in figure 5.3 below.
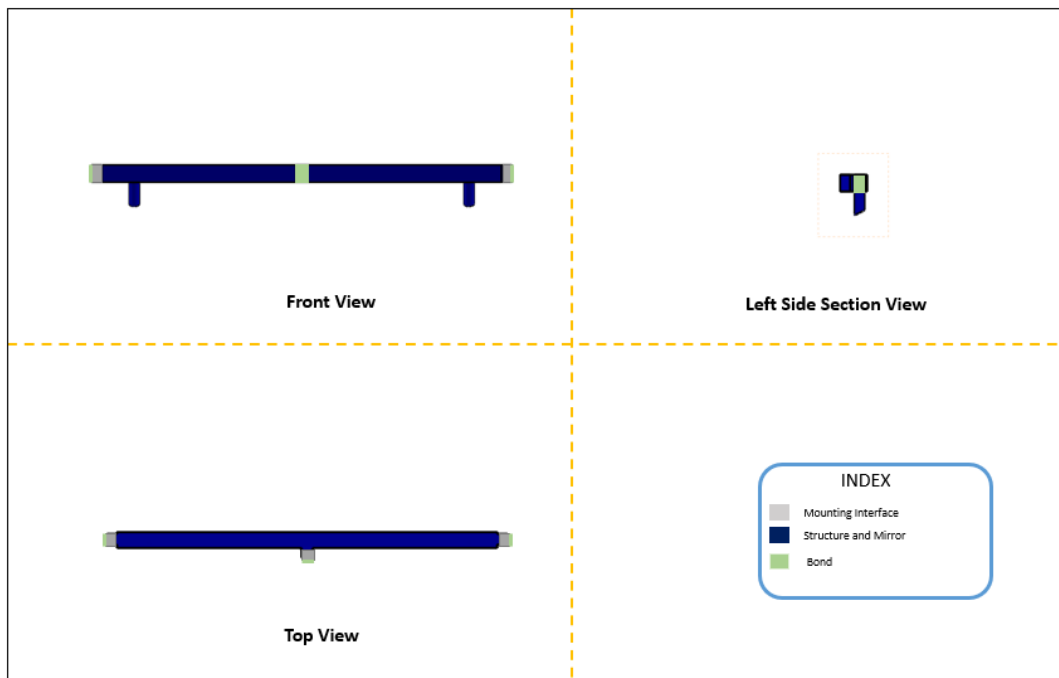
Figure 5.3: Modification for the SM-2 Mount

Here, a long structure with two the SM-2 mirror is proposed. This is the most simple solution as there is no need for multiple different mounts with different attachments. Also, it has the extra benefit of potentially reducing the number of alignment processes because the alignment between the various components is likely to be quite excellent. Finally, it ensures stiff connections for both the mirrors and also in between the mirrors. A small protrusion was provided at the 3 different locations of the structure to maintain the thermal center and, thus making it an exact constrained design.

• Lastly, the Slit and the SM-1 mounting strategy was modified to a semi-kinematic mounting principle, as shown in the figure 5.4 below with slight modifications.
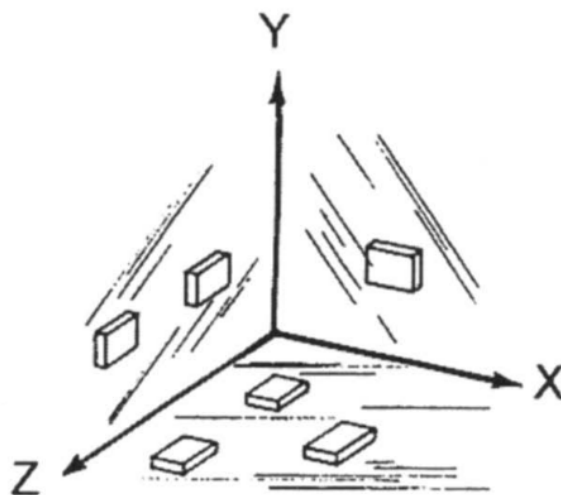
Figure 5.4: Semi-kinematic mounting with small area contacts [48]

Here, two bonding pads were provided on the XY plane, and one bonding pad was provided on the XZ plane as shown in the figure below. It should be noted that the pads have to be machined

carefully so that they are a very accurately angular relationship. The third protrusion on the XZ has been modified in such a way that the bonding areas were all coplanar. As seen previously in the concept-three proposal, parts 3 and 4 are connected by firstly placing the SM-1 mirrors into the slots, thus constraining the three degrees of freedom. Next, adhesive was injected into the bonding pads to constraint the rest three degrees of freedom, thus creating an semi exact constraint design.
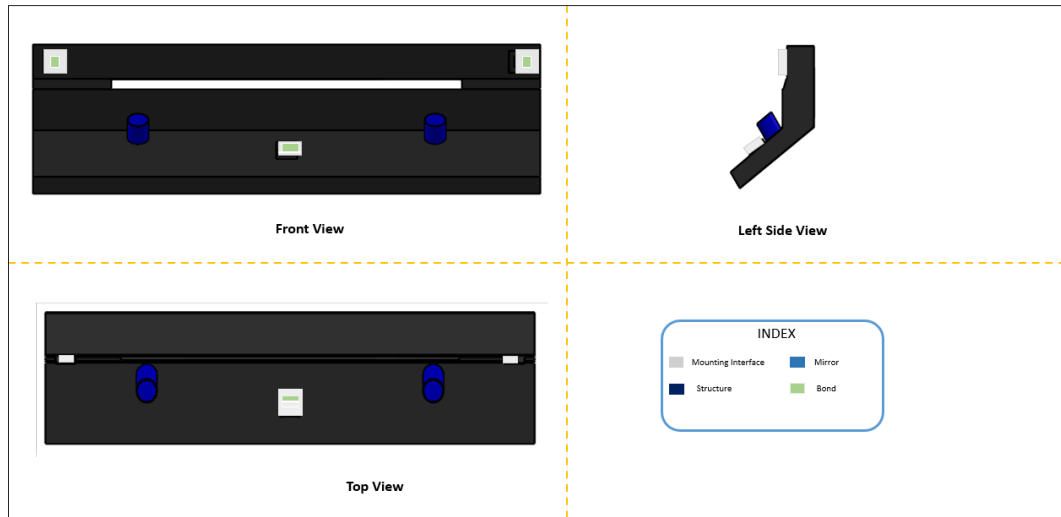
Figure 5.5: Modification for the SM-1 and the slit Mount

5.2. Component Mounting Design

The finalization of the design is supported here by some calculations. The dimensions of the mounting features are limited by the tight packaging of the optical components and the limited available volume. In general, there are two main approaches for designing the mounting mechanisms: Kinematic synthesis and the continuum synthesis approach [28].

a) **Kinematic synthesis**: This is a rigid body kinematic approach where the mechanism is synthesized, connected, and finally analyzed.

b) **Continuum synthesis**: This is a computational method where the expected loading, the desired motions, and force transmission are inputted and, the system is optimized for weight and minimum stresses.

The Kinematic approach does have some disadvantages over the continuum synthesis in terms of potential energy storage for segments and the inability to synthesize the kinematics and dynamics separately. But, it does provide advantages in terms of problem formulation and manufacturability. Also, the continuum approach tends to exploit model weaknesses, contains a lot of control parameters, and requires an appropriate selection of an algorithm for the given problem. Therefore, the kinematic approach was selected for designing this module. From here on, the detailed mounting design for each of the component is shown below.

• **SL-1 Lens**:The method for mounting the SL-1 lens is shown in the figure 5.1. It can be seen that the flexure mechanism is formed by a simple chain of components to produce a defined motion. For designing the flexure mechanism, a screw theory-based compliance analysis approach (as shown in [42]) was implemented. Here, The coordination transformation of screws was used to characterize the connections of the building blocks in a methodical way and the compliance matrices were calculated in a symbolical manner rather than numerically. This method mainly provides advantages in terms of component geometric interpretations, design synthesis, and efficiency compared to the FE model. The flexure considered here had a width of w, the thickness

of t and length of l. Because we're interested in the motion at the middle, the coordinate frame is positioned at the start of the blade flexure.

Let us represent the deformation with a general twist T = $(\theta_x, \theta_y, \theta_z, \delta_x, \delta_y, \delta_z)$ and the loading with a wrench W = $(F_x, F_y, F_z, M_x, M_y, M_z)$ in this case. Both are column vectors. The force here was considered to be 2G in all the three axes and the displacement was derived using the formula (eigenfrequency (f) was considered to be 600Hz):

$$d = \frac{F}{(2 \cdot \pi \cdot f)^2} \tag{5.1}$$

Now, by applying the principle of linear elastic theory (as shown in the figure below), the flexure parameters were derived (Here K is a 6 X 6 Stiffness matrix).

$$W = [K] \cdot T \tag{5.2}$$

$$K = \begin{bmatrix} 0 & 0 & 0 & \frac{l}{G \cdot j} & 0 & 0 \\ 0 & 0 & 0 & 0 & \frac{l}{E \cdot I_y} & 0 \\ 0 & 0 & 0 & 0 & 0 & \frac{l}{E \cdot I_z} \\ \frac{l}{E \cdot A} & 0 & 0 & 0 & 0 & 0 \\ 0 & \frac{l^3}{12 \cdot E \cdot I_y} & 0 & 0 & 0 & 0 \\ 0 & 0 & \frac{l^3}{12 \cdot E \cdot I_z} & 0 & 0 & 0 \end{bmatrix} \tag{5.3}$$

The terms I, E, G, and J are the Moment of inertia, Young's modulus, Shear modulus, and Torsion constant respectively. The Single flexure for the SL-1 mounting mechanism is modeled as a parallel combination of blade parts. Here, $[Ad_j]$ is a coordinate transformation from the jth flexure to the building part in the remaining chain .

$$[K_p] = \Sigma_{j=0}^{2}[Ad_j][K_j][Ad_j]^{-1} \tag{5.4}$$

The overall SL-1 mounting system is formed by three such identical flexures assembled symmetrically in parallel (the same formula as above). [23] provides in detail step-wise calculations done for deriving the parameters. The same method was implemented in this case. From the derived parameters, the maximum stress (referred from [11]) on the optics was calculated using the formula(Here, FS is the factor of safety.):

Table 5.1: Parameters of the tangential flexure mount

SL-1 Lens	Variables(mm)
Thickness	0.5
Length	3.84
Height	0.66

Now that the parameters for the flexure are derived (shown in the table above), it was important to determine the thickness of the bondline. In [19], The equation for determining the optimal bond thickness for mounting a optical component is given below:

$$t = \frac{d_o \cdot (1 - v_b) \cdot (\alpha_c - \alpha_o)}{2 \cdot (1 - v_b) \cdot (\alpha_b - \alpha_o) - \frac{(7 - 6 \cdot v_b) \cdot (\alpha_c - \alpha_o)}{4 \cdot (1 + v_b)}} \tag{5.5}$$

Here. v and d_o are the poisson's ratio of the bond material and the diameter of the optic respectively. α_o, α_b and α_c are the CTE of the optics, bond material and the cell structure material.

Although, this approach was used, it was found that the approach was not beneficial for the stiff-ness and the strength. Also, this approach was not beneficial for large thermal changes in the environment. Therefore an improvised method implemented in [14] and [15], and this resulted in a bond thickness of 0.15mm and a bond diameter of 0.5mm for each spot. Since, the methodol-ogy was very analytically intensive and required non linear modelling, the simulations were done on COMSOL to determine the validity of the designed mount (Results illustrated in detail at the Performance analysis chapter).

• **SL-2 Lens**: The method for mounting the SL-2 lens is shown in the figure 5.2. It can be seen that the flexure mechanism used here is a folded leaf flexure. This flexure creates stiffness in one direction and eliminates parasitic displacements.
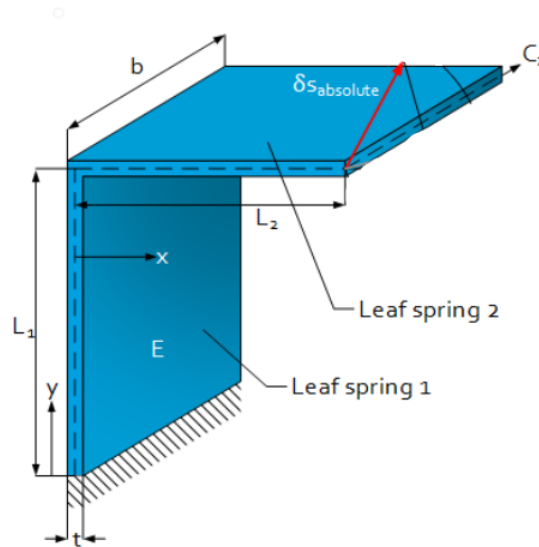
Figure 5.6: Folded Leaf Flexure [11]

For designing this flexure, the same methodology was applied, with minor changes. The reason for using a simpler version is that there is no chain for one single flexure. The flexure considered here has a width of w and a thickness of t. Two lengths L1 and L2, are considered for two different leaf springs (See Figure 5.6). Because we're interested in the motion at the end, the coordinate frame is positioned at the functional body.

Since the requirements for the SL-2 lens are all the similar, the same force and displacement was considered in all the three axes. The stiffness of the folded leaf spring in the stiff direction is (referred from [11]):

$$C_z = \frac{E \cdot t \cdot b^3}{(L_1 + L_2)^3 + 2 \cdot b^2 \cdot (L_1 + L_2) \cdot (1 + v)} \tag{5.6}$$

$$C_b = \frac{E \cdot t \cdot b^3}{(L_1 + L_2)^3} \tag{5.7}$$

$$C_s = \frac{E \cdot t \cdot b}{2 \cdot (1 + v) \cdot (L_1 + L_2)} \tag{5.8}$$

Where C_b and C_s are the bending and the shear stiffness. Once, the correlation was made be-tween each of them, the parameters were derived using the stress formula used below. The table

below provides the dimensions of the flexure.

$$\sigma_{max} = \frac{M_{max} \cdot \frac{1}{2} \cdot t}{I} \tag{5.9}$$

$$M_{Vertical}(y) = F_y \cdot L_1 - F_y \cdot L_2 - F_y \cdot y \tag{5.10}$$

$$M_{Horizontal}(x) = F_y \cdot L_2 - F_y \cdot x \tag{5.11}$$

Table 5.2: Parameters of the folded leafspring mount

SL-2 Lens	Variables(mm)
Thickness	0.6
Length	2.33
Height	0.9

For determining the bond dimensions, the same methodology was implemented shown above. Since, the methodology was very analytically intensive and required non linear modelling, the simulations were done on COMSOL to determine the validity of the designed mount (Results illustrated in detail at the Performance analysis chapter).

- **Fiber Ferrule**: For mounting the Fiber ferrule, press fitting was used as it is simple, economic and also fast compared to the methods. This method also eliminates the use of alignment and mounting tools like metal inserts, adhesives and screws which is beneficial in terms of weight and volume. Although, this structure does have a disadvantage in terms of position accuracy and difference in CTE, these are accepted and monitored to make sure that their effect is considered in the relevant error budgets. To compensate for this effect, small protrusions were made to maintain the position and the constraint the additional movements. To compensate for the stress relax/buildup, grooves were made.
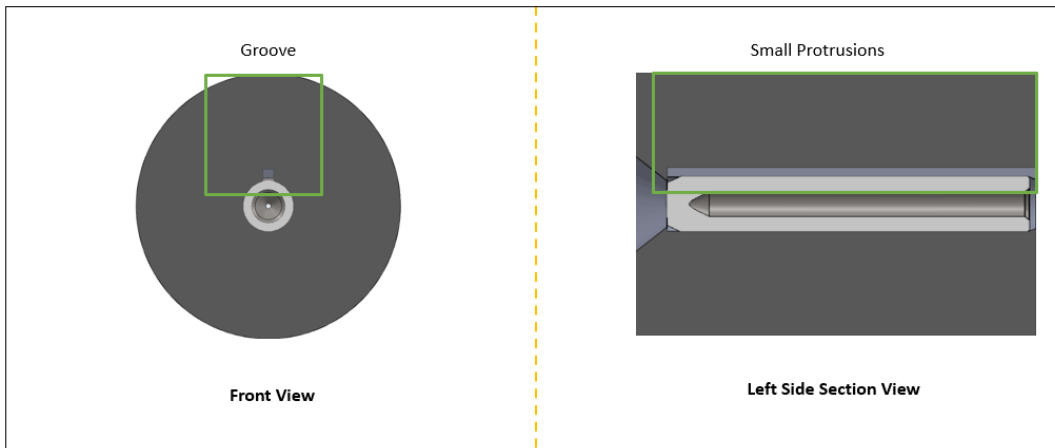
Figure 5.7: Ferrule Mounting

The allowable interference between a ferrule and a hub is calculated using the basic equation for thick-walled cylinders:

$$I = \frac{\sigma \cdot D_s}{W} \cdot [\frac{W + v - s}{E_h} + \frac{1 - v_s}{E_s}] \tag{5.12}$$

$$W = \frac{D_h^2 + D_s^2}{D_h^2 - D_s^2} \tag{5.13}$$

Here, I is the diameter interference and σ is the yield stress. D_h and D_s are the diameter of the hub and the ferrule respectively. E and v are the modulus of elasticity and Poisson's ratio respectively.

The ferrule is mounted by cooling the ferrule and heating the structure to a sufficient dimension to fit the ferrule and then cooled down to lock the ferrule. As shown in the equation below, the coefficient of thermal expansion of the materials can be used to estimate the change in diameter due to temperature.

$$D - D_o = \alpha \cdot (T - T_o) \cdot D_o \tag{5.14}$$

where D, D_o and α are the diameter at current temperature, diameter of the initial temperature and CTE respectively. Temperature of 493.15K would be required to create a increase of 0.05mm. Although, this design does suffice the recommended specs, test on prototypes is required, since coefficient of friction is dependent on many other operating factors.

- **SM-2 Mirror**: The method for mounting the SM-2 Mirror is shown in the figure 5.3. It can be seen that three bonding pads were placed on each side of the SM-2 structure. For determining the bonding area, analytical formula (referred from [48]) used below was used.

$$Q_{min} = \frac{W \cdot a_G \cdot FS}{J} \tag{5.15}$$

where W is the weight of the structure which was derived from the simple geometry calculations. a_G is the maximum acceleration factor (i.e. 150G for launch conditions) and FS is the factor of safety for the bonding. J is the tensile strength of the bond used. The bond dimensions were then extracted using the simple formula shown below where d is diameter of the bond pad. The bond size of 0.1mm was used at each bond pad with a diameter of 1.5mm.

$$Q_{min} = \pi \cdot (\frac{D}{2})^2 \tag{5.16}$$

- **Outer structure**: As shown before, the binocular-like module that has two tube structures and an intermediate part holding them was designed.

Here, the weight and the dimensions of the tube structure are determined by the optical components present, their respective mounting strategies, and the properties of the material. Also, the deflection from gravity is usually the parameter that influences the lens barrel dimensions. The defection (δ) considered for a single tube structure is given by:

$$\delta = \frac{W_L \cdot L^3}{3 \cdot E \cdot I} \tag{5.17}$$

Here, W_L, L, E, and I are the weight of the lens, distance of the lens from alignment support, Young's modulus of the structure, and the moment of inertia of tube structure, respectively. Considering that the tube radius(R) is around 10 mm, the thickness and the weight of the barrel structure is calculated using the formula shown below (referred from [49]).

$$t = \frac{W_L \cdot L^3}{3 \cdot \pi \cdot R^3 \cdot E \cdot \delta} \tag{5.18}$$

$$W_{ts} = \frac{2}{3} \cdot \frac{W_l \cdot \rho \cdot L^4}{\delta \cdot E \cdot R} \tag{5.19}$$

After acquiring the desired dimensions for the structure, it was important to derive the parameters for aligning the structure. As shown in figure 4.9 before, a threading method was employed. This technique provides a distinct advantage in terms of volume and accessibility for post-processing methodologies. Also, this technique does align with the sensitives found in chapter 3.3. Finally, since the tube structure designed here is rotationally symmetric, the threading technique provided the required orientation in the x-y plane. Here, an M8 size thread was considered because it provides sufficient area for aligning the lens into the structure without damaging it. Here, The male and female threads are made of the same material, relative tensile ratio is one. To ensure

that the thread doesn't fail, a minimum length (L_e) and the thread area (Tensile- A_t and Shear- A_{ss}) were derived using the formula below (referred from [38]). Here, D , P and d_p are the basic diameter, screw thread pitch and PCD of the thread respectively. The minimum length necessary to maintain the a connection was derived to be around 5.48mm.

$$A_t = \frac{\pi}{4} \cdot (D - 0.938 \cdot p)^2 \tag{5.20}$$

$$L_e(min) = \frac{2 \cdot A_t}{0.5 \cdot \pi \cdot (D - 0.64952 \cdot p)} \tag{5.21}$$

$$A_{ss} = 0.5 \cdot \pi \cdot d_p \cot L_e \tag{5.22}$$

The next alignment technique employed here is between part 3 and part 4. For determining the bond dimensions, the same methodology which was used for SM-2 mirror was employed. The bond size of 0.1mm was used at each bond pad with a diameter of 1mm.

5.3. Model Setup

To construct a detailed design, the CAD program SolidWorks has been chosen. A parametric model has been created such that design variables can easily be changed once verified through analysis. The model was created by combing all the part designs that include all the components and the module outer structures. The four different parts were indicated by different variants of silver for the graphic purpose. The lens and the mirrors are indicated by green color and blue color, respectively. The dimensions used here were derived from the above calculations shown in section 5.2. Since it was difficult to illustrate the 3d model with all the features included, first angle projection is used for visualization. The first rough assembly design is as follows:
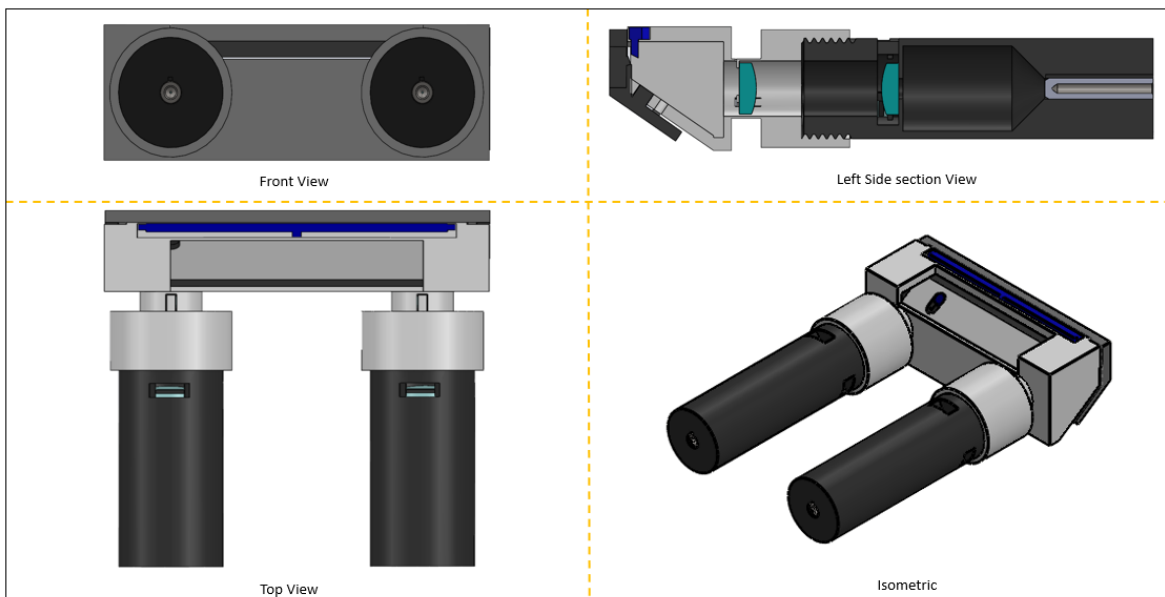
Figure 5.8: Initial Model setup

From the design generated from the detailed design, it was found that the system's volume was higher than that specified in the requirement. As a result, part 3 of the module was overlapping with the M1 mirror of the spectrometer. The current module also faced another problem. The shape of part 3 was a concern as it would fracture the SL-2 lens when impacted by high stresses. As shown in the figure below, design modifications were made to eliminate these problems. Here, only the isometric view of the module was demonstrated, as there were no design changes made inside the module. Firstly, support structures were added around the SL-2 mounting. This would eliminate the damage to the lens. Also, the shape of the third part was optimized to eliminate the volume concern. Also, fillets

are added to the current structure to eliminate the overhang problem while manufacturing it with SLM. This was very useful while estimating the manufacturing tolerances, shown in the next chapter.
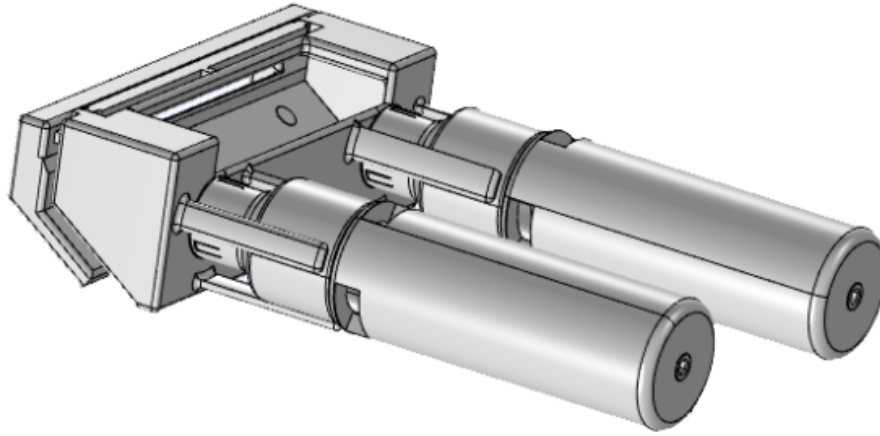
Figure 5.9: Modification on the current module design

Performance Analysis

6.1. Structural and Thermal Analysis

This section will evaluate the current proposed optomechanical design for the lens mounts (SL-1 and SL-2) and the overall integrated module. Since it was very difficult to see the combined effect of the bonding and flexure assembly in case of both the lenses, a FEM analysis was performed, using COM-SOL Multiphysics.

- **SL-1 Lens**: The initial step associated with the procedure is the conceptualization of structure using SolidWorks, which incorporates the functionality of the mounting structure, including the interfaces and the bonding channels. The materials were added appropriately to the corresponding components and interfaces, as shown in table 4.1. Since this simulation aimed to determine the deformations and stresses acting upon the system while applying load, a solid mechanics module with thermal expansion and gravity sub-node were considered for the study. The purple region shown in the figure 6.1 below illustrates the fixed constraint. To start a simulation and realize how the model performs, we use a physics-controlled coarse mesh. This was mainly done to reduce the computational time and concentrate on the initial performance.
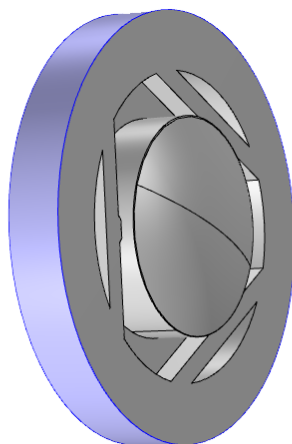
Figure 6.1: Fixed constrain applied on SL-1 mount structure

If a temperature difference of $\Delta T = 0.1$ K is applied to the lens mount system, the flexures, adhesive bond and the lens will expand. The resulting steady state thermal expansion due to a change of 10 K (from 293 K to 303 K) is shown in Figure 6.2a for the lens mount. The lens will

experience a equal force from all the flexure-bond system which will lead to a defocus by the outward movement of the lens structure. The stress due to this thermal expansion is depicted in Figure 6.2b. It can be seen that the maximum stress generated on the module is < 5 Mpa which is very low.
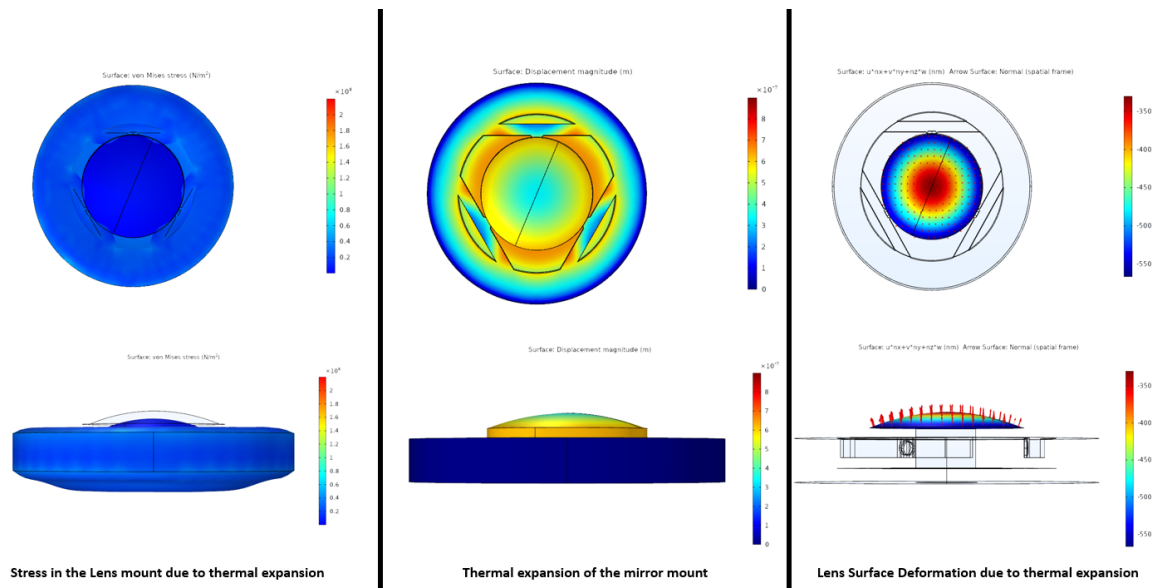
Figure 6.2: Impact on SL-1 lens due to steady state thermal expansion Δ = 10K

As shown in the figure 6.3 below, even with a temperature change of 60 K (from 293K to 233 K), the stress on the lens and the flexure was < 18 MPa and < 150 Mpa respectively. The bond pads on the other hand had a huge peak of stress in both the cases, but this shows that the forces transferred into the lens are minimized by a huge factor. It was found that though the displacement is within the limit for the 10 K change, it was very high for the 60 K change. This shows that the mount system is capable of performing in the operating conditions range and can sustain the extreme conditions without any break age.
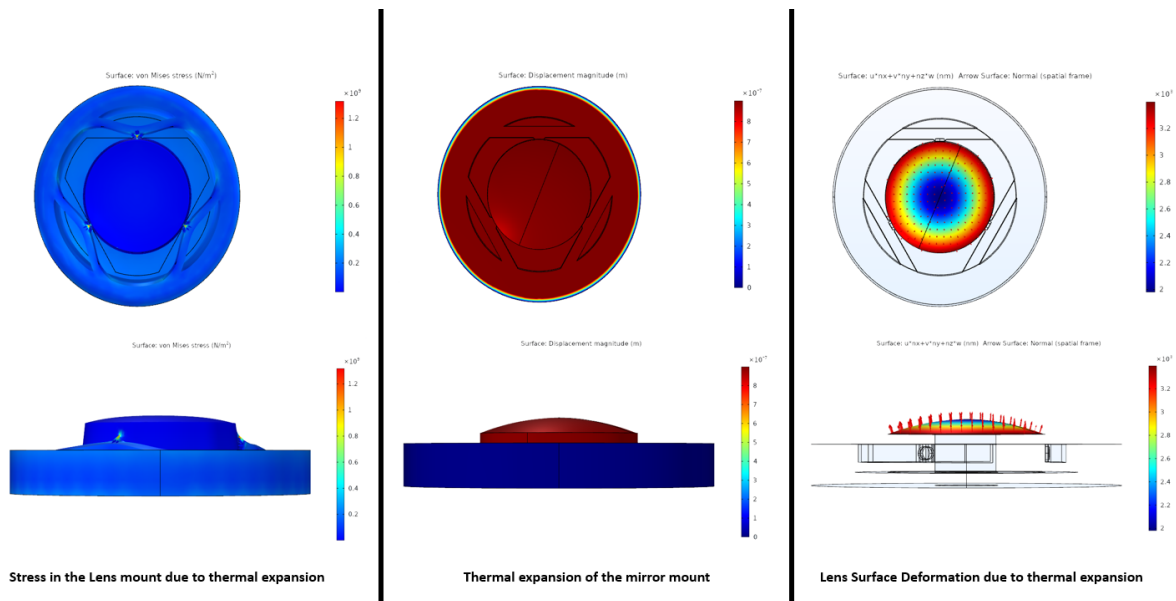
Figure 6.3: Impact on SL-1 lens due to steady state thermal expansion Δ = 60K

Figure 6.3 shows the static deformation due to gravity (2G in all the directions). The lens are moved down with about 0.016 nm. As this is a static situation and the mirrors are mostly moved outward, it does not influence the calibration measurements as it is way below the sensitivity value. The associated stress of the lens and the flexure was $< 2e3$ N/m^2 and $< 4e3$ N/m^2 respectively, which is very low. This clearly shows that the designed mount is under the specifications.
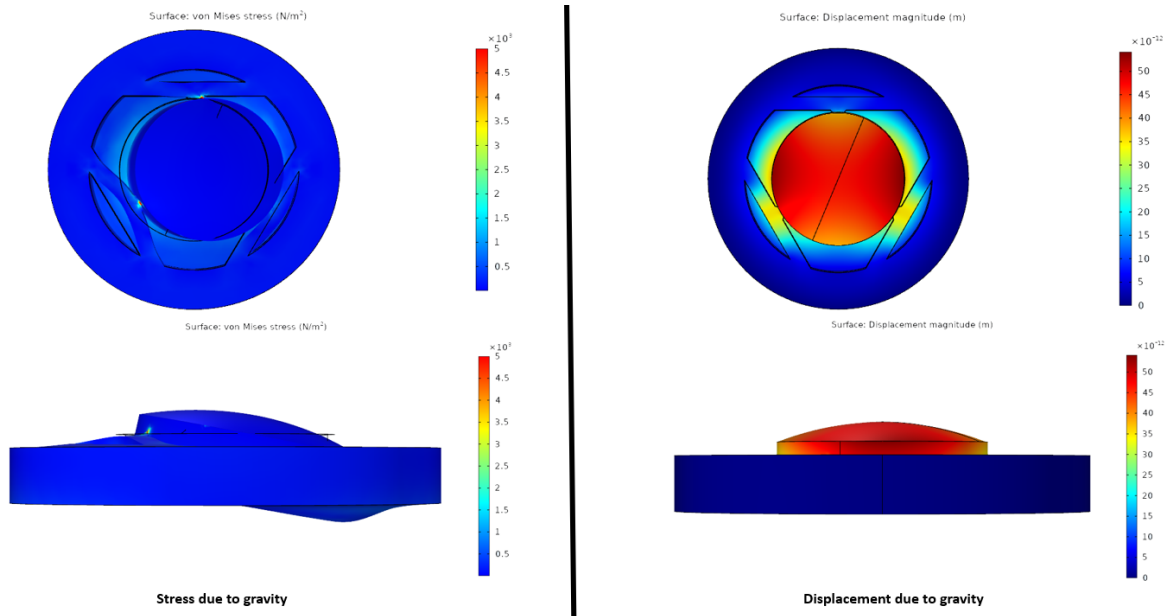
Figure 6.4: Impact on SL-1 lens due to Gravity (2G in X-axis)

- **SL-2 Lens**: The same steps mentioned above were used for the modelling of the SL-2 lens. The purple region shown in the figure 6.5 below illustrates the fixed constraint, while modelling for the COMSOL simulation.
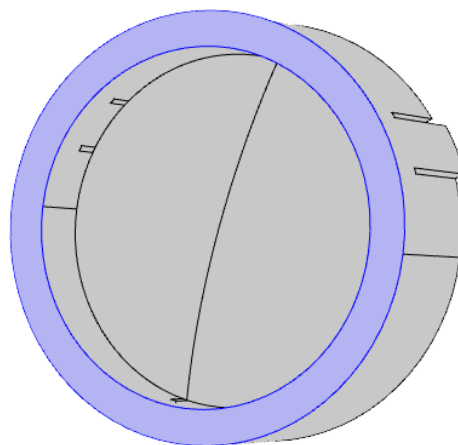
Figure 6.5: Fixed constrain applied on SL-2 mount structure

If a temperature difference of $\Delta T = 0.1$ K is applied to the lens mount system, the flexures, adhesive bond and the lens will expand. The resulting steady state thermal expansion due to a change of 10 K (from 293 K to 303 K) is shown in Figure 6.6a for the lens mount. The lens will experience a defocus by the outward direction. The stress due to this thermal expansion is depicted in Figure

6.6b. It can be seen that the maximum stress generated on the module is < 8 Mpa which is very low.
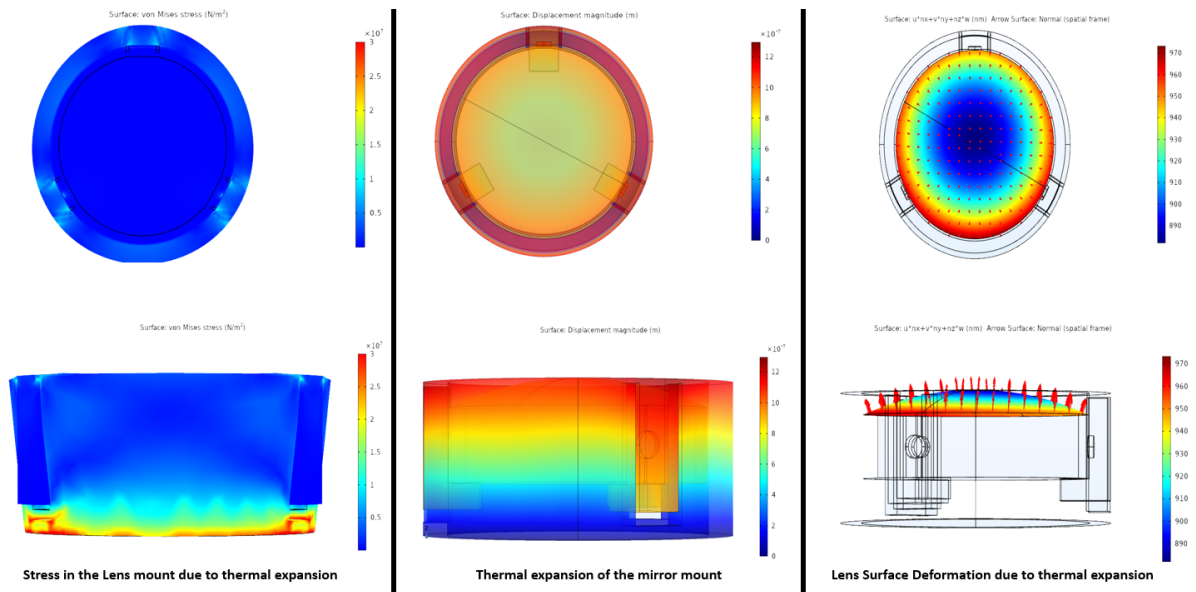
Figure 6.6: Impact on SL-1 lens due to steady state thermal expansion Δ = 10K

As shown in the figure 6.7 below, even with a temperature change of 60 K (from 293K to 233 K), the stress on the lens and the flexure was < 28 MPa and < 40 Mpa respectively. The bond pads on the other hand had a huge peak of stress in both the cases, but this shows that the forces transferred into the lens are minimized by a huge factor. It was found that though the displacement is within the limit for the 10 K change, it was very high for the 60 K change. This shows that the mount system is capable of performing in the operating conditions range and can sustain the extreme conditions without any break age.
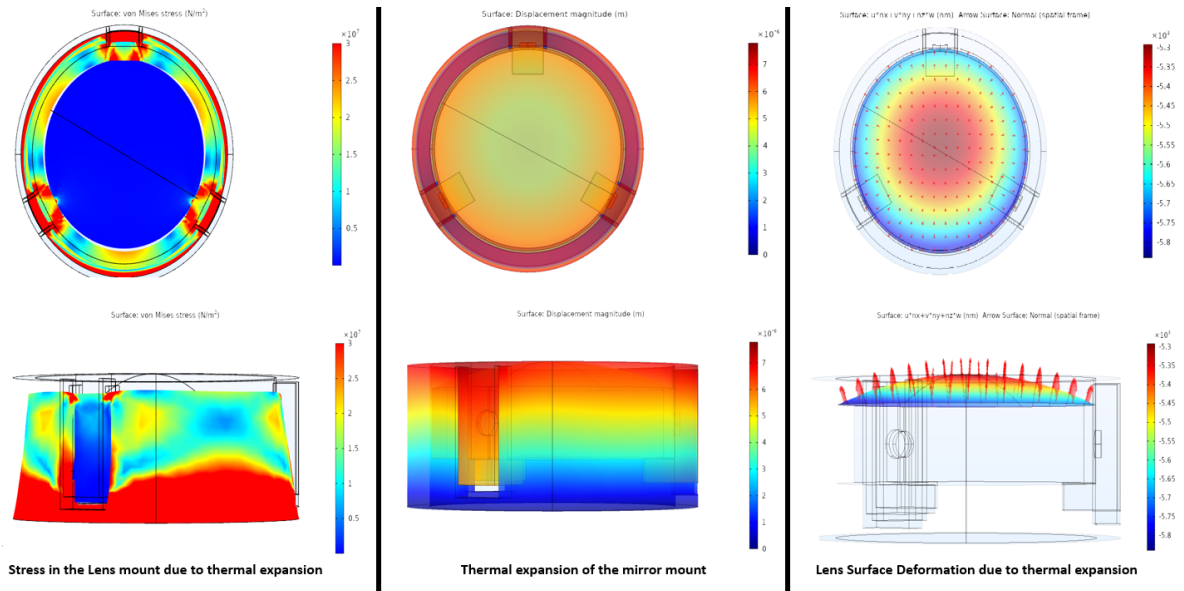
Figure 6.7: Impact on SL-2 lens due to steady state thermal expansion Δ = 60K

Figure 6.8 shows the static deformation due to gravity (2G in all the directions). The lens are moved down with about 0.03 nm. As this is a static situation and the mirrors are mostly moved

outward, it does not influence the calibration measurements as it is way below the sensitivity value. The associated stress of the lens and the flexure was < 2 Mpa and < 6 Mpa respectively, which is very low. This clearly shows that the designed mount is under the specifications.

Stress due to gravity   **Displacement due to gravity**
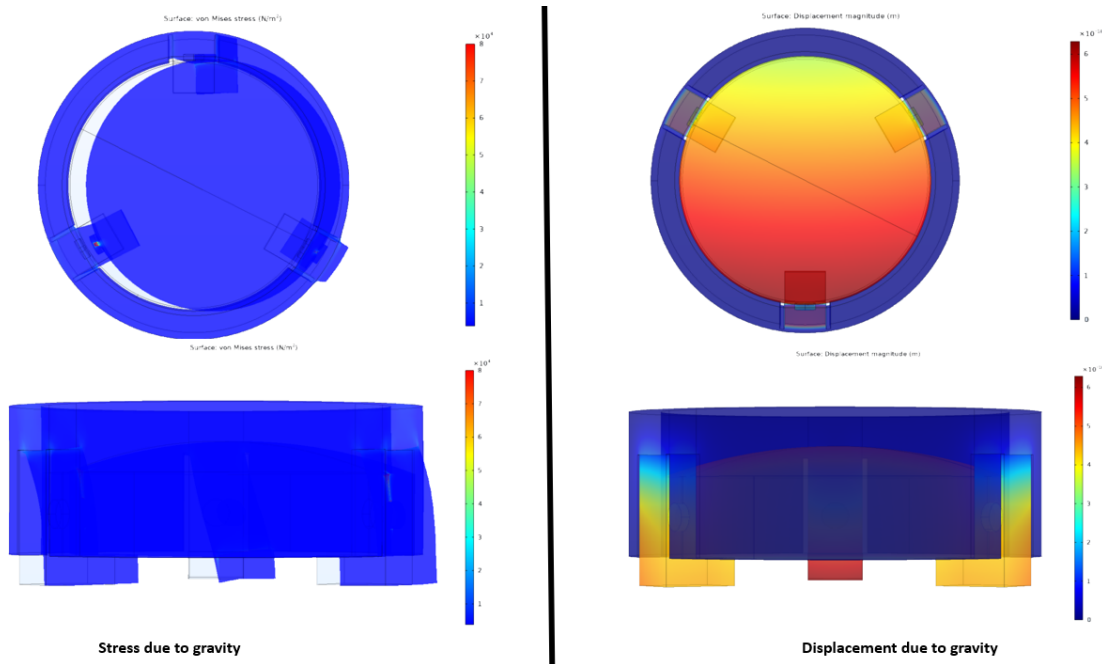
Figure 6.8: Impact on SL-2 lens due to Gravity (2G in all the orthogonal directions)

Now that the lens mount do match the current requirement, the interest have now transferred towards the overall module. As described in the requirements should the design have a higher eigenfrequency of 600Hz. While this already was taken into account during the design the individual components, a combined effect was yet to be determined. For this the least eigenfrequency was considered. The eigenmode is shown in the figure 6.9.

Eigenfrequency=252.84 Hz   Surface: Displacement magnitude (m)
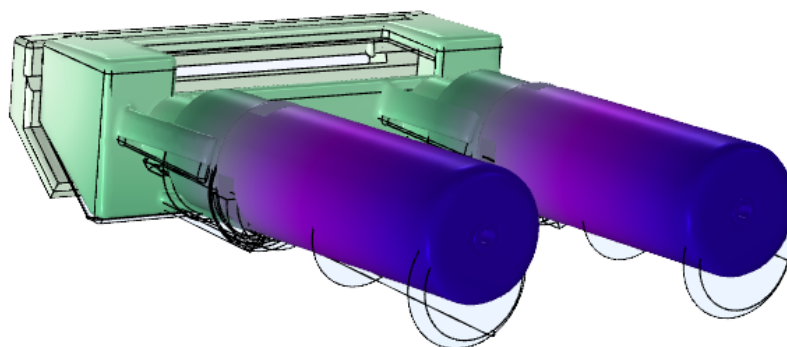
Figure 6.9: Eigenfrequency of the current module

It was noticed that the natural frequency was much to lower compared to the current design. To improve the current design, few changes were required to be made. For determining the root cause

for the lower frequency, kinetic and elastic energy of the module were derived. As shown in the figure 6.10 below, it was noticed that the material near the ferrule was very high, whereas the surface area near the central part of the part 3(connecting both the part 1 module together) was very lower. Also, it was also found that the area connecting part 1 and 3 were very high.
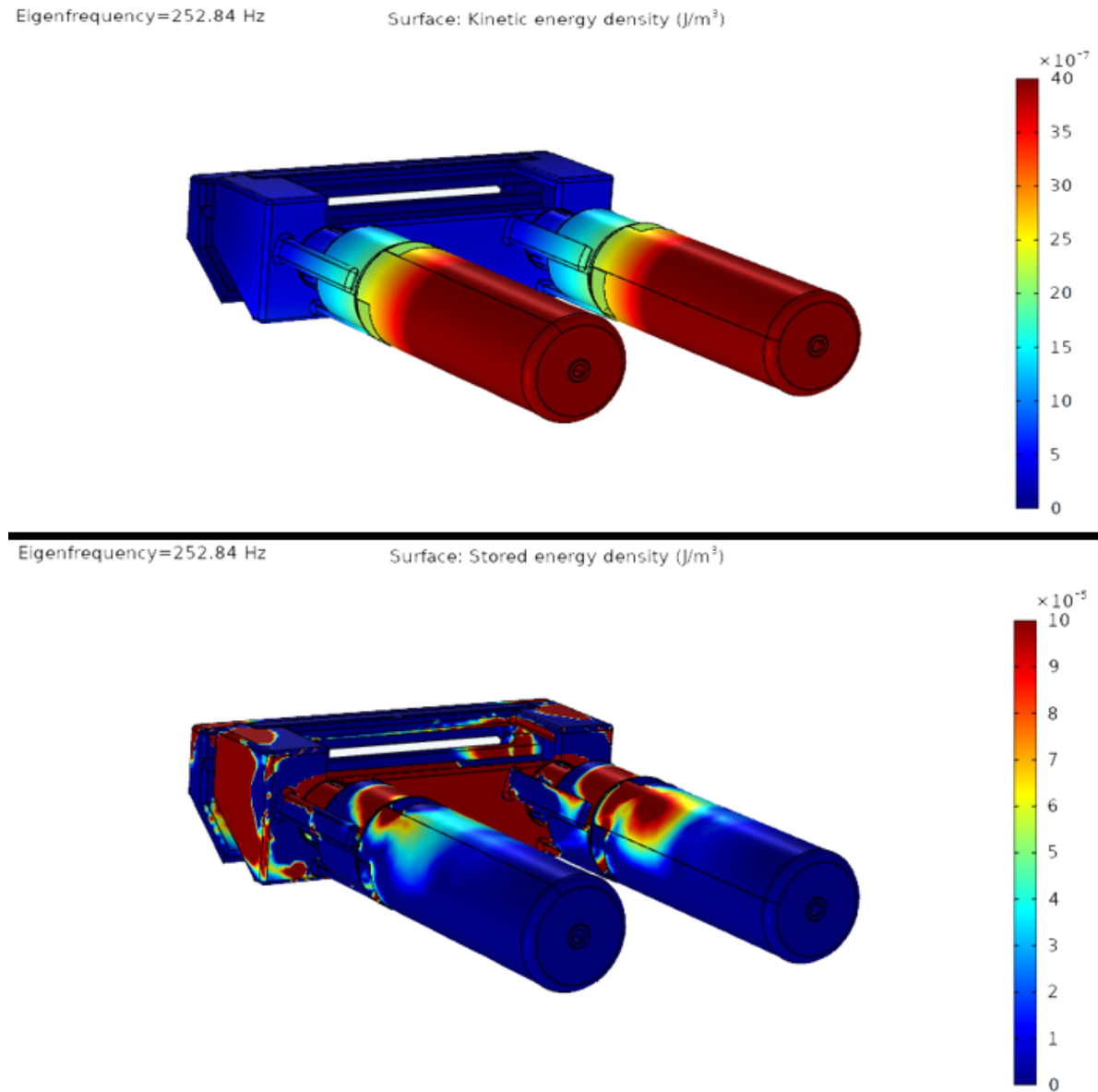
Figure 6.10: Kinetic and Elastic energy of the current module

A few iterations were made by tweaking the structure of the module without affecting the mounts and interfaces of the components. As shown in the figure 6.11 below, the material around the ferrule was substantially reduced. Three support structures were provided to maintain the thermal center. There was an increase in the central region of the part 3 in terms of area. The current dimensions of the proposed flexure (To prevent the stress development and fracture of SL-2 lens) were also reduced to increase the stiffness. Finally, a small modification was made between the intersection of the part 1, 2 and 3. A total of 12 eigenmodes were derived from the simulation. It was seen that the modified module has the lowest eigenfrequency of 772.29 Hz, which does suffice the requirement. Although higher value of natural frequency than required, it does indicate that their are less chances that this frequency will be excited during operation.

Eigenfrequency=772.29 Hz   Surface: Displacement magnitude (m)
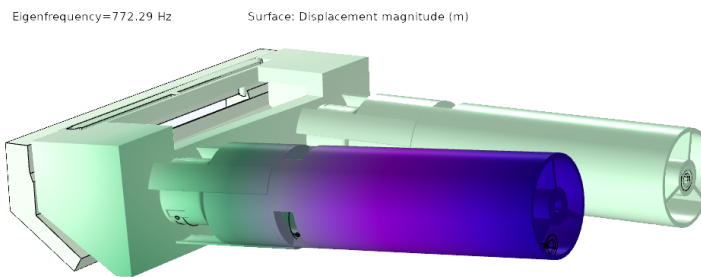
Figure 6.11: Eigenfrequency of the modified module

As previously discussed, the most stress rise during homogeneous temperature change in the environment. This stress mainly arises due to the difference in the CTE of the materials. The von Mises stresses can be plotted by heating the model, and the locations with the largest stress are displayed in red. It is important to note that the stress developed in each of the part should be less than the yield strength. Since, the lens have a yield strength of 54 Mpa, this will be the most critical part to consider. Also, it is important to note that the safety factors shown in table 3.8 must be respected while modelling. In Figure 6.12 is the von mises stress given in the complete assembly for both the case (Homogeneous temperature of 10K and Gravity impact of 2G). It can be seen that the amount of stress developed is lower than the allowed Yield stress (Including the safety factor) and will therefore survive the operating conditions of the mission.

(a) Thermal hom 10K   Surface: von Mises stress (MPa)

(b) Grav Y   Surface: von Mises stress (MPa)
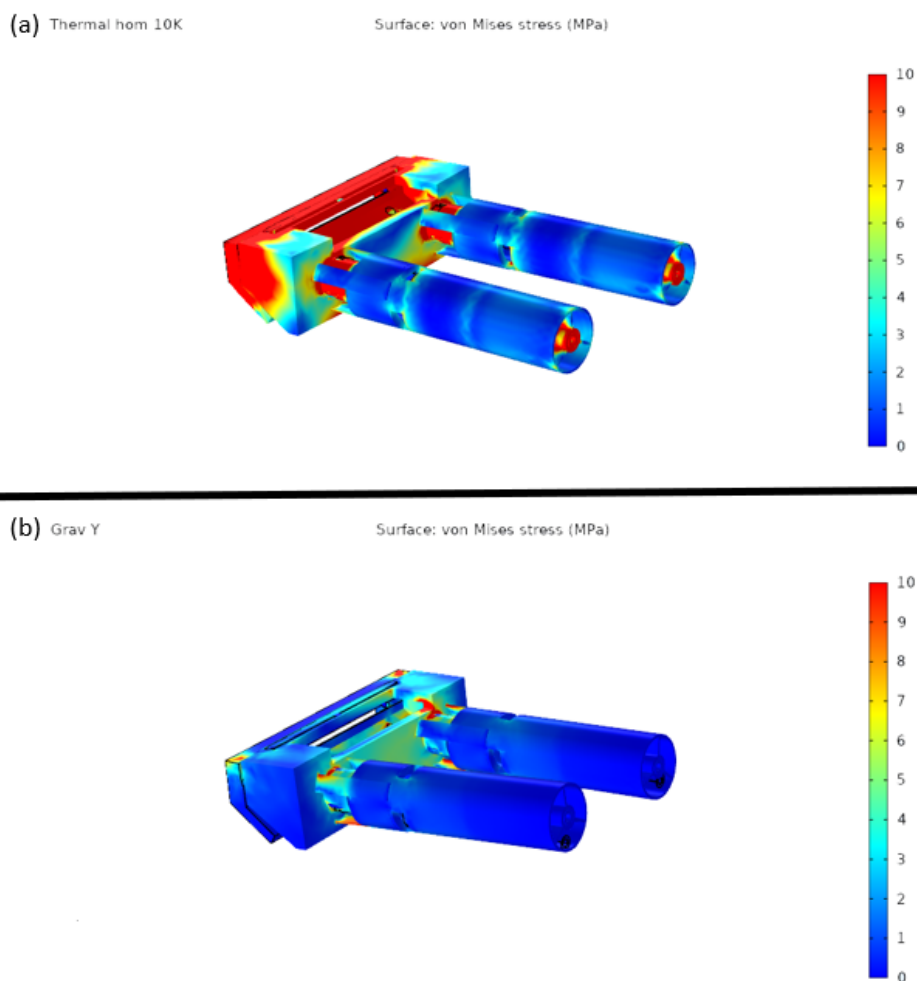
Figure 6.12: Von Mises Stress a)Homogeneous temperature change b)Gravity release

6.2. Manufacturing Tolerance Error Budget

Optomechanics is the engineering of preserving the proper shapes and positions of functional elements in an optical system. Manufacturing tolerances (due to the manufactured interfaces and assembly process) are generally the prime influencers of these parameters. Since the system has a coupled effect on the final result, a small perturbation of a single component will cause an extra aberration which can comprise the end product. As a result, relative alignment of the system is very important. Now that the stresses and the displacements of the overall module is verified, relative displacement of each component within module is yet to be determined.

Since, there are a lot of changes made in the module compared to the one selected from the concept design phase, a second phase of the error budget was required. Since, the last error budget considered was only constrained to mechanical interface tolerances, two new aspects were taken into account. So the goal for the current and the next section is to conduct a system performance analysis to see the effect of optical sensitivity under manufacturing and operational conditions, respectively. It is important to remember that the error budget does not include errors generated by integration with the CHAPS instrument, rather only restricted to Module alone.

The manufacturing tolerances budget is an improvised version of the previous error budget, with an inclusion of optical manufacturing tolerances and assembly process. Here, an assumption is made to fix the position of the slit as the reference element and formulate an error relative to that point. From section 3.3, the sensitivities are already derived. As shown in the figure 6.13 below, the tolerance deviations of each component are stacked up and multiplied with the respective sensitivities to predict the performance of the component. The quadratic summation of these performance will determine the overall module performance. To verify the performance results with the budget, Root Sum Squared (RSS) method was employed. RSS is a statistical method which describes the variations based on the normal distribution. Since, most of the individual parts and features developed by manufacturers occur near the center of tolerance range with very few exceptions, RSS helps in increasing the tolerance limits. This can be indeed resulting in a reduced manufacturing and inspection cost. Also, it is more accurate and less conservative in predicting variations. Finally, RSS provides sensitivities and contributions to enable efficient design direction.
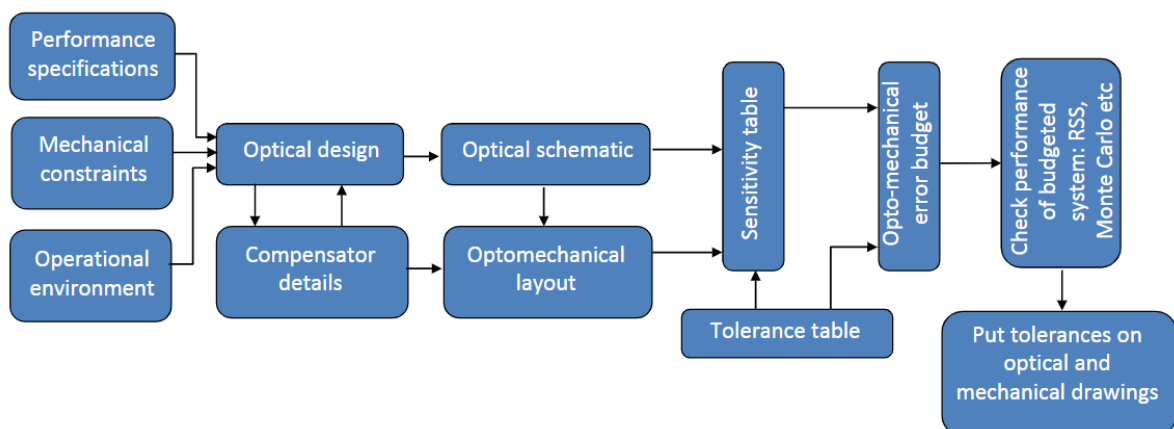
Figure 6.13: Tolerance Flow Chart [48]

From the requirements, it was evident that 50 microns tolerance is acceptable for each axis. The figures 6.14, 6.15 and 6.16 provided below are the error budgets for all the directions (Translation, Rotation and Focus respectively).

ID	Description	Tol TX[μm]	Tol TY[μm]	Tol TZ[μm]	Tol RX[mr]	Tol RY[mr]	Tol RZ[mr]	Remarks
	SM-2							
1	Position accuracy of Hole for SM2 on part B	10	0	10	0.4	NA	NA	Used for aligning the SM-2 w.r.t to slit on Part
2	Angularity of the SM2 surface	0	2	2	NA	NA	NA	To maintain the angle of the mirror surface
3	Flatness of the support surface for SM2 on Part B	10	10	0	0.07	NA	NA	
4	Flatness of the projected structures that are attached to p	0	0	10	0.07	NA	NA	Projections are a part of Part C
5	Cylindericity of the SM2	5	0	5	NA	NA	NA	
6	Flatness of the projected strucures that are attached to pa	10	0	10	0.07	NA	NA	Projections are a part of SM2
	Total	18.02775638	10.198039	18.1383571	0.41797129	0	0	
	Sensitivity(Y)	0	0	0	0.2	0.2	0	
	Error Budget(Y)	0	0	0	0.083594	0	0	
	SM-1							
1	Position accuracy of Hole for SM1 on part B	10	10	10	0.4	NA	NA	
2	Angularity of the SM1 surface	0	2	2	NA	NA	NA	To maintain the angle of the mirror surface
3	Cylindricity of SM1	5	0	5	NA	NA	NA	
4	Flatness of the projected structures that are attached to p	10	0	0	0.14	0.07	NA	
5	Position accuracy of SM1 on Part C	10	10	10	0.4	NA	4.44	
6	Angularity of Part C	0	2	2	NA	NA	NA	
7	Angularity of Part B	0	2	2	NA	NA	NA	
	Total	18.02775638	14.5602198	15.3948043	0.58275209	0.07	4.44	
	Sensitivity(Y)	0	0	0	0.2	0.2	0	
	Error Budget(Y)	0	0	0	0.11655	0.014	0	
	SL-2							
1	Cylindericity of the tube structure	10	10	0	NA	NA	NA	
2	Position of the tube on Part B	10	10	0	NA	NA	NA	
3	Position of vertical flexure w.r.t edge of part B	0	0	10	0.07	0.177	NA	
4	Diameter of the SL2	25	25	0	NA	NA	NA	
5	Center thickness of optics	0	0	50	NA	NA	NA	Claimed by Edmond optics
6	Flatness of vertical flexure	0	0	10	0.07	NA	NA	
	Total	28.72281323	28.7228132	51.9615242	0.09899495	0.177	0	
	Sensitivity(Y)	0.6	0.6	0	-0.06	-0.06	0	
	Error Budget(Y)	17.233688	17.23369	0	-0.00594	-0.01062	0	
	SL-1							
1	Cylindericity of the tube structure	10	10	0	NA	NA	NA	
2	Threading between Part A and B	20	20	0	NA	NA	NA	
3	Flatness of the aperture that aligns SL1	0	0	10	0.07	NA	NA	
4	Flatness of the flexure for SL1	0	10	0	NA	NA	NA	
5	Diameter of the SL1	25	25	0	NA	NA	NA	
6	Center thickness of optics	0	0	50	NA	NA	NA	Claimed by Edmond optics
	Total	33.54101966	35	50.9901951	0.07	0	0	
	Sensitivity(Y)	0.7	0.7	0	0.2	0.2	0	
	Error Budget(Y)	23.478714	24.5	0	0.014	0	0	
	Aperture							
1	Concentricity error of aperture hole	10	10	0	NA	NA	NA	
	Sensitivity(Y)	0.3	0.3	0	0.01	0.01	0	
	Error Budget(Y)	3	3	0	0	0	0	
	Fiber							
2	Concentricity error of fiber ferrule	10	10	0	NA	NA	NA	
3	Angularity of the fiber ferrule constraint	0	2	2	NA	NA	NA	
	Total	14.45994467	14.5976025	2	0.01	0.01	0	
	Sensitivity(Y)	1.2	1.2	0	0.15	0.15	0	
	Error Budget(Y)	17.351934	17.51712	0	0.0015	0.0015	0	
	Grand Total	33.901911	34.70014	0	0.144241	0.017636	0	

Figure 6.14: Manufacturing Error Budget - Translation

| ID	Description	Tol TX[μm]	Tol TY[μm]	Tol TZ[μm]	Tol RX[mr]	Tol RY[mr]	Tol RZ[mra]	Remarks
	SM-2							
1	Position accuracy of Hole for SM2 on part B	10	0	10	0.4	NA	NA	Used for aligning the SM-2 w.r.t to slit on Part
2	Angularity of the SM2 surface	0	2	2	NA	NA	NA	To maintain the angle of the mirror surface
3	Flatness of the support surface for SM2 on Part B	10	10	0	0.07	NA	NA	
4	Flatness of the projected structures that are attached to part	0	0	10	0.07	NA	NA	Projections are a part of Part C
5	Cylindericity of the SM2	5	0	5	NA	NA	NA	
6	Flatness of the projected strucures that are attached to part B	10	0	10	0.07	NA	NA	Projections are a part of SM2
	Total	18.0277564	10.198039	18.1383571	0.41797129	0	0	
	Sensitivity(T)	0	0	0	0.2	0.2	0	
	Error Budget(T)	0	0	0	0.083594	0	0	
	SM-1							
1	Position accuracy of Hole for SM1 on part B	10	10	10	0.4	NA	NA	
2	Angularity of the SM1 surface	0	2	2	NA	NA	NA	To maintain the angle of the mirror surface
3	Cylindricity of SM1	5	0	5	NA	NA	NA	
4	Flatness of the projected structures that are attached to part	10	0	0	0.14	0.07	NA	
5	Position accuracy of SM1 on Part C	10	10	10	0.4	NA	4.44	
6	Angularity of Part C	0	2	2	NA	NA	NA	
7	Angularity of Part B	0	2	2	NA	NA	NA	
	Total	18.0277564	14.5602198	15.3948043	0.58275209	0.07	4.44	
	Sensitivity(T)	0	0	0	0.2	0.2	0	
	Error Budget(T)	0	0	0	0.11655	0.014	0	
	SL-2							
1	Cylindericity of the tube structure	10	10	0	NA	NA	NA	
2	Position of the tube on Part B	10	10	0	NA	NA	NA	
3	Position of vertical flexure w.r.t edge of part B	0	0	10	0.07	0.177	NA	
4	Diameter of the SL2	25	25	0	NA	NA	NA	
5	Center thickness of optics	0	0	50	NA	NA	NA	Claimed by Edmond optics
6	Flatness of vertical flexure	0	0	10	0.07	NA	NA	
	Total	28.7228132	28.7228132	51.9615242	0.09899495	0.177	0	
	Sensitivity(T)	0.212	0.212	0	0.035	0.035	0	
	Error Budget(T)	6.089236	6.089236	0	0.003465	0.006195	0	
	SL-1							
1	Cylindericity of the tube structure	10	10	0	NA	NA	NA	
2	Threading between Part A and B	20	20	0	NA	NA	NA	
3	Flatness of the aperture that aligns SL1	0	0	10	0.07	NA	NA	
4	Flatness of the flexure for SL1	0	10	0	NA	NA	NA	
5	Diameter of the SL1	25	25	0	NA	NA	NA	
6	Center thickness of optics	0	0	50	NA	NA	NA	Claimed by Edmond optics
	Total	33.5410197	35	50.9901951	0.07	0	0	
	Sensitivity(T)	0.09	0.009	0	0	-0.035	-0.035	
	Error Budget(T)	3.018692	0.315	0	0	0	0	
	Aperture							
1	Concentricity error of aperture hole	10	10	0	NA	NA	NA	
	Sensitivity(T)	0.05	0.05	0	0.035	0.035	0	
	Error Budget(T)	0.5	0.5	0	0	0	0	
	Fiber							
2	Concentricity error of fiber ferrule	10	10	0	NA	NA	NA	
3	Angularity of the fiber ferrule constraint	0	2	2	NA	NA	NA	
	Total	14.15106	14.2916934	2	0.035	0.035	0	
	Sensitivity(T)	0.03	0.03	0	0.01	0.01	0	
	Error Budget(T)	0.424532	0.428751	0	0.00035	0.00035	0	
	Grand Total	6.809664	6.112434	0	0.143472	0.015313	0	

Figure 6.15: Manufacturing Error Budget - Rotation

ID	Description	Tol_TX(μm)	Tol_TY(μm)	Tol_TZ(μm)	Tol_RX(mr)	Tol_RY(mr)	Tol_RZ(mr)	Remarks
	SM-2							
1	Position accuracy of Hole for SM2 on part B	10	0	10	0.4	NA	NA	Used for aligning the SM-2 w.r.t to slit on Part C
2	Angularity of the SM2 surface	0	2	2	NA	NA	NA	To maintain the angle of the mirror surface
3	Position of SM2	10	10	10	0.4			
4	Flatness of the support surface for SM2 on Part B	10	10	0	0.07	NA	NA	
5	Flatness of the projected structures that are attached to part	0	0	10	0.07	NA	NA	Projections are a part of Part C
6	Cylindericity of the SM2	5	0	5	NA	NA	NA	
7	Flatness of the projected strucures that are attached to part	10	0	10	0.07	NA	NA	Projections are a part of SM2
	Total	20.61552813	14.28285686	20.7123152	0.578532627	0	0	RSS
	Sensitivity(Z)	0	0	2	0	0	0	
	Error Budget(Z)	**0**	**0**	**41.42463**	**0**	**0**	**0**	
	SM-1							
1	Position accuracy of Hole for SM1 on part B	10	10	10	0.4	NA	NA	
2	Angularity of the SM1 surface	0	2	2	NA	NA	NA	To maintain the angle of the mirror surface
3	Cylindricity of SM1	5	0	5	NA	NA	NA	
4	Flatness of the projected structures that are attached to part	0	0	10	0.14	0.07	NA	
5	Position accuracy of SM1 on Part C	10	10	10	0.4	NA	4.44	
6	Angularity of Part C	0	2	2	NA	NA	NA	
7	Angularity of Part B	0	2	2	NA	NA	NA	
	Total	15	14.56021978	18.3575598	0.582752091	0.07	4.44	
	Sensitivity(Z)	0	0	2	0	0	0	
	Error Budget(Z)	**0**	**0**	**36.71512**	**0**	**0**	**0**	
	SL-2							
1	Cylindericity of the tube structure	10	10	0	NA	NA	NA	
2	Position of the tube on Part B	10	10	0	NA	NA	NA	
3	Diameter of the SL2	25	25	0	NA	NA	NA	
4	Position of vertical flexure w.r.t edge of part B	0	0	10	0.07	0.177	NA	
5	Flatness of vertical flexure	0	0	10	0.07	NA	NA	
6	Center thickness of optics	0	0	50	NA	NA	NA	Claimed by Edmond optics
	Total	28.72281323	28.72281323	51.9615242	0.098994949	0.177	0	
	Sensitivity(Z)	0	0	0.84	0	0	0	
	Error Budget(Z)	**0**	**0**	**43.64768**	**0**	**0**	**0**	
	SL-1							
1	Cylindericity of the tube structure	10	10	0	NA	NA	NA	
2	Threading between Part A and B	20	20	5	NA	NA	NA	
3	Flatness of the aperture that aligns SL1	0	0	10	0.07	NA	NA	
4	Flatness of the flexure for SL1	0	10	0	NA	NA	NA	
5	Diameter of the SL1	25	25	0	NA	NA	NA	
6	Center thickness of optics	0	0	50	NA	NA	NA	Claimed by Edmond optics
	Total	33.54101966	35	51.2347538	0.07	0	0	
	Sensitivity(Z)	0	0	2.4027	0	0	0	
	Error Budget(Z)	**0**	**0**	**123.1017**	**0**	**0**	**0**	
	Aperture							
1	Concentricity error of aperture hole	10	10	0	NA	NA	NA	
	Sensitivity(Z)	0	0	0.99	0	0	0	
	Error Budget(Z)	**0**	**0**	**0**	**0**	**0**	**0**	
	Fiber							
2	Concentricity error of fiber ferrule	10	10	0	NA	NA	NA	
3	Angularity of the fiber ferrule constraint	0	2	2	NA	NA	NA	
	Total	14.14213562	14.28285686	2.23161377	0	0	0	
	Sensitivity(Z)	0	0	2	0	0	0	
	Error Budget(Z)	**0**	**0**	**4.463228**	**0**	**0**	**0**	
	Grand Total	**0**	**0**	**141.926317**	**0**	**0**	**0**	

Figure 6.16: Manufacturing Error Budget - Focus

It can be seen that, although the translation and rotation axis does comply with requirements, the focus error budget is orders of magnitude out of the limit. This does show that the current module will require some design modifications. Since the deviation produced was so high, it was crucial to spot the most influential parameters responsible. Figure 6.17 below clearly shows that the optics selected for the module has a very high tolerance.

Optics	Description	Tol_Z	Senstivity(Z)	Error budget
SL-1	Center Thickness	50	2.4027	120.135
SL-2	Center Thickness	50	0.84	42
SM-1	Surface Error	2	2	4
SM-2	Surface Error	2	2	4
Total:				**127.390809**

Figure 6.17: Influential parameters for very high Focus Error Budget (μm)

The module will, therefore, not satisfy the requirements purely with design modifications. Chapter 6.6 will talk more about the different strategies which are feasible for compensating the current focus error.

6.3. Stability Error Budget

6.3.1. Thermo-mechanical stability

Opto-mechanical instruments are very sensitive to temperature effects. Especially in the space environment, the thermal conditions are very rapid in transition. The temperature change can occur mainly due to day and night effects, eclipse at four different timescale of the year, and internal heat sources

installed in the satellite. This can lead to a change in the light path, thus comprising the performance of the instrument. Also, due to the difference in the material, the components can experience stress and high strain. Therefore, it is important to validate the created design for the proper functionality of the system.

Now that the stresses and the displacements of the overall module under thermal influences have been verified (Chapter 6.1), the relative displacement of each component within the module is yet to be determined. Here, a thermal gradient is created from the difference in the heat source (absorption of sunlight) and low temperatures in space. Since the components are experiencing this gradient, it is crucial to maintain the relative positions of the optical components to perform the calibration activity. Here only radiation is considered as the module operates in a vacuum. Technically, the displacement for an element under thermal influences is calculated using the formula shown below.

$$\Delta L = \alpha_c \cdot L \cdot \Delta T \tag{6.1}$$

The terms L AND α_c shown above are the length and CTE of the cell structure. It is also crucial to consider the focal length change in refractive elements (shown in the formula below).

$$\Delta f = \delta_o \cdot f \cdot \Delta T \tag{6.2}$$

$$\delta_o = \frac{\beta_o}{n-1} - \alpha_o \tag{6.3}$$

The terms δ_o, β_o and n shown above are the coefficient of thermal defocus, coefficient describing the variations of refractive index, and refractive index of the lens, respectively. Although it is easy to calculate for each component, it is analytically intensive to determine the effect of the overall module and each element within it. Therefore FEM analysis was used here to derive the values for each of the components. As shown in chapter 6.1, COMSOL analysis was done to determine the effect of each element in the overall module. Here, a single optical component was considered for the first case to determine the respective thermal influences (As shown in the figure 6.18). In this way, all the deformations for the all the components were derived. To determine the overall effect of each component on the slit, an error budget was derived. From section 3.3, the sensitivities are already derived. The deviations from the analysis for each component was then multiplied with the respective sensitivities to predict the performance of the component. The overall summation of these performance determine the thermomechanical stability performance of the current module in x axis. It is important to note that the athermal affects are considered here, but an applied case has a average temperature change of 0K. The same approach is used for all the other axes.

Figure 6.18: Boundary selection the thermomechanical analysis

Since gradient can occur in all three directions, thermomechanical stability was derived for all three cases. For each case, The COMSOL derived values, their respective temperature plot and the derived RSS values are shown below.

- **Thermal Gradient X**:

Table 6.1: COMSOL derived values for thermal gradient load case X (μm and mrad)

Thermal Gradient X	Tx	Ty	Tz	Rx	Ry	Rz
Fiber	-2.25E-01	-2.70E-01	5.18E-01	4.86E+00	-1.22E+00	1.65E+00
Aperture	-6.62E-02	-1.89E-01	3.64E-01	4.64E+00	-7.10E+00	1.68E+00
SL-1 Lens	-5.42E-03	-1.81E-02	3.85E-01	4.66E+00	-7.04E+00	1.66E+00
SL-2 Lens	1.11E-02	-9.87E-02	1.78E-01	5.83E+00	-2.19E+00	2.16E+00
SM-1 Mirror	3.75E-02	-6.09E-02	6.46E-02	5.83E+00	4.63E+00	-7.82E+00
SM-2 Mirror	5.71E-03	5.04E-03	6.34E-02	7.71E+00	-4.80E-01	-4.18E-01
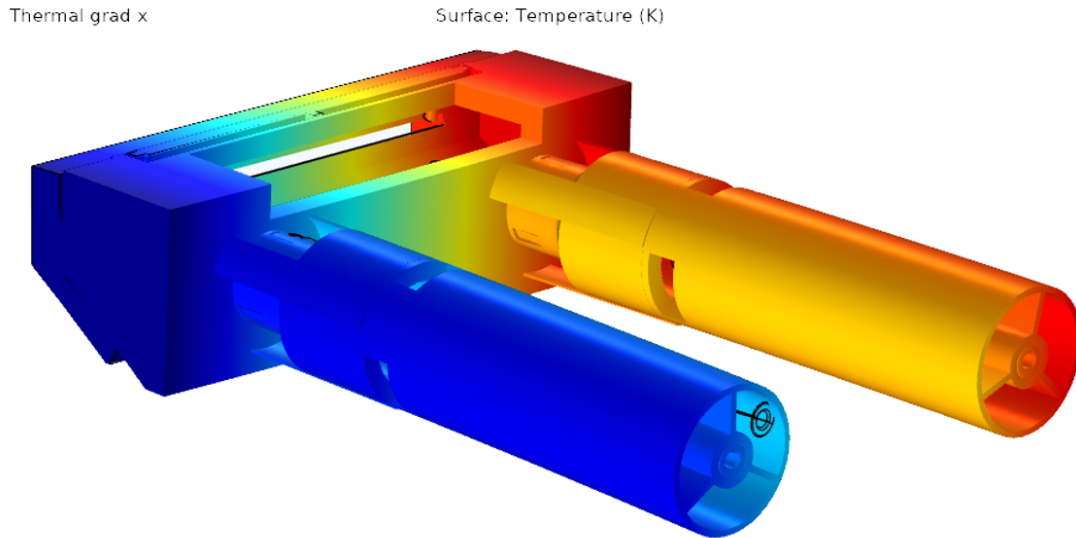
Figure 6.19: Temperature plot of the thermal gradient in X axis

Table 6.2: Total Thermo-mechanical stability for gradient of 3K/m on X axis (μm and mrad)

Thermal Gradient X	Decenter	Tip Tilt	Focus
RSS	**4.89E+00**	**3.09E+00**	**3.15E+00**

- **Thermal Gradient Y**:

Table 6.3: COMSOL derived values for thermal gradient load case Y (μm and mrad)

Thermal Gradient Y	Tx	Ty	Tz	Rx	Ry	Rz
Fiber	2.17E-01	-6.71E-01	3.49E-01	2.13E+01	3.88E+00	-2.07E+00
Aperture	1.52E-01	-3.61E-01	2.46E-01	1.62E+01	3.98E+00	2.05E+00
SL-1 Lens	1.45E-01	-3.33-E-01	2.43E-01	1.61E+01	3.95E+00	2.06E+00
SL-2 Lens	9.26E-02	-1.35E-01	1.23E-01	1.22E+01	3.93E+00	-1.90E+00
SM-1 Mirror	4.70E-02	-3.97E-02	3.91E-02	4.23E+00	6.03E+00	-8.00E+00
SM-2 Mirror	4.04E-02	4.59E-02	5.88E-02	1.19E+01	9.72E-01	-6.34E-00
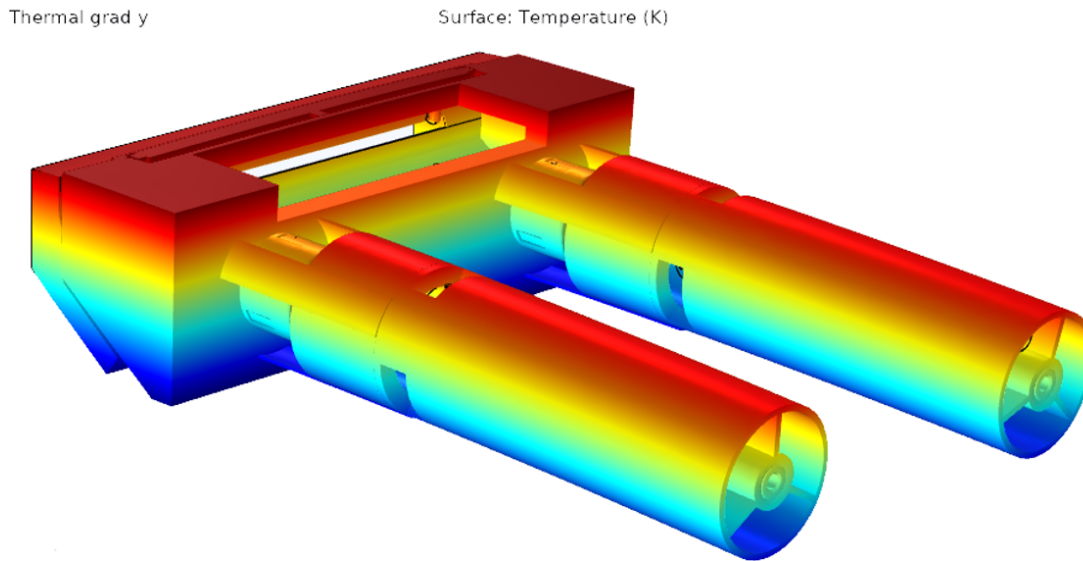
Figure 6.20: Temperature plot of the thermal gradient in Y axis

Table 6.4: Total Thermo-mechanical stability for gradient of 3K/m on Y axis (μm and mrad)

Thermal Gradient Y	Decenter	Tip Tilt	Focus
RSS	**1.11E+01**	**5.22E+00**	**2.16E+00**

- **Thermal Gradient Z**:

Table 6.5: COMSOL derived values for thermal gradient load case Z (μm and mrad)

| Thermal Gradient Z	Tx	Ty	Tz	Rx	Ry	Rz
Fiber	3.59E-01	-6.57E-01	6.16E-01	1.35E+01	7.16E+00	1.13E+00
Aperture	2.40E-01	-4.33E-01	3.46E-01	1.32E+01	7.40E+00	1.18E+00
SL-1 Lens	2.28E-01	-4.10-E-01	3.38E-01	1.32E+01	7.33E+00	1.15E+00
SL-2 Lens	1.30E-01	-2.09E-01	1.20E-01	1.42E+01	7.21E+00	1.26E+00
SM-1 Mirror	4.92E-02	-4.27E-02	3.84E-02	8.35E+00	9.02E+00	-5.40E+00
SM-2 Mirror	3.04E-02	6.97E-03	6.60E-02	1.52E+01	4.62E-01	-1.67E-00
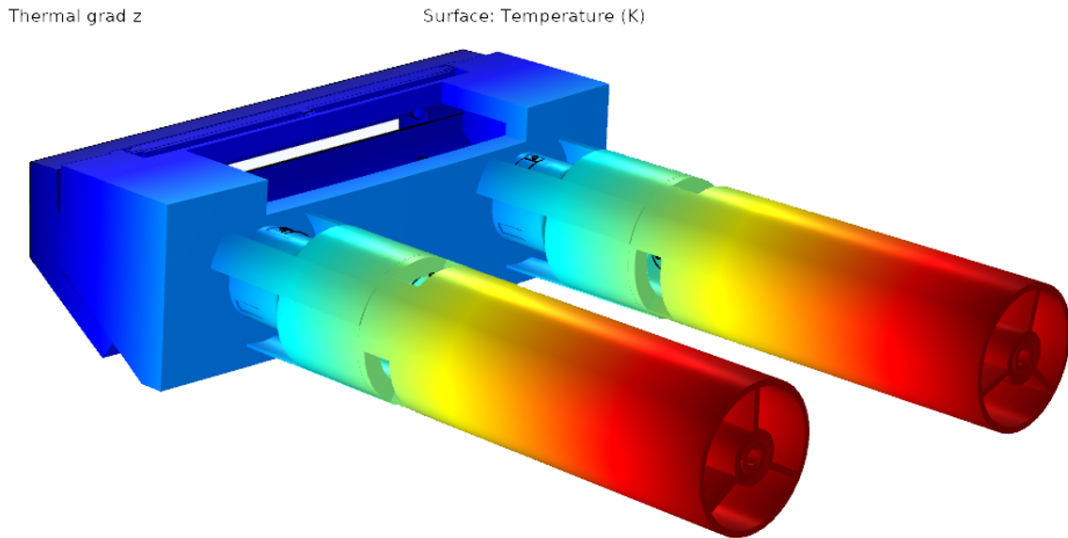
Figure 6.21: Temperature plot of the thermal gradient in Z axis

Table 6.6: Total Thermo-mechanical stability for gradient of 3K/m on Y axis (μm and mrad)

Thermal Gradient Z	Decenter	Tip Tilt	Focus
RSS	1.16E+01	6.04E+00	3.26E+00

6.3.2. Gravity Release stability

Most optical instruments designed for space applications are manufactured at an ambient pressure and temperature in the earth's atmosphere. But when the instrument is launched into the space, there is a change in the environment. The most important factor to be considered here is gravity difference in the operating atmosphere. The instrument will experience microgravity, which makes the object appear weightless. Since there is vacuum, free fall occurs where the gravity cause the object to fall at the same rate.

During this phenomena, the instrument will not experience gravity deformations anymore. Because of the lack of gravity deformations, the overall instrument will deflect compared to its state during calibration on Earth. Since, the module we are dealing here requires micrometer precision, it is important to consider the impact caused on the position of all the components. Therefore, an analysis is created to determine the impact of gravity release on all the components and their respective alignment. The same methodology, shown above in the case of thermo-mechanical stability was used here.

Here, Including a comfortable margin, 2G was considered in each of the axis. For each case, The COMSOL derived values, their respective stress plot and the derived RSS values are shown below.

- **Gravity Release X** :

Table 6.7: COMSOL derived values for gravity release load case X (μm and mrad)

Gravity Release X	Tx	Ty	Tz	Rx	Ry	Rz
Fiber	2.75E-01	-1.80E-01	5.23E-03	4.29E+00	7.49E+00	-2.36E+00
Aperture	1.52E-01	-1.09E-01	5.21E-03	4.28E+01	6.58E+00	-2.37E+00
SL-1 Lens	1.41E-01	-1.01-E-01	5.22E-03	4.28E+01	6.58E+00	-2.73E+00
SL-2 Lens	4.83E-02	-4.16E-02	5.20E-03	4.45E+00	5.26E+00	-2.50E+00
SM-1 Mirror	1.92E-03	2.80E-03	-2.77E-02	-6.37E-01	3.24E-01	-5.77E-01
SM-2 Mirror	7.41E-03	1.14E-02	2.35E-02	1.30E+01	1.58E-00	-1.13E-00

Table 6.8: Total gravity release stability for load 2G on X axis (μm and mrad)

Gravity Release X	Decenter	Tip Tilt	Focus
RSS	**3.80E+00**	**1.03E+00**	**7.93E-02**
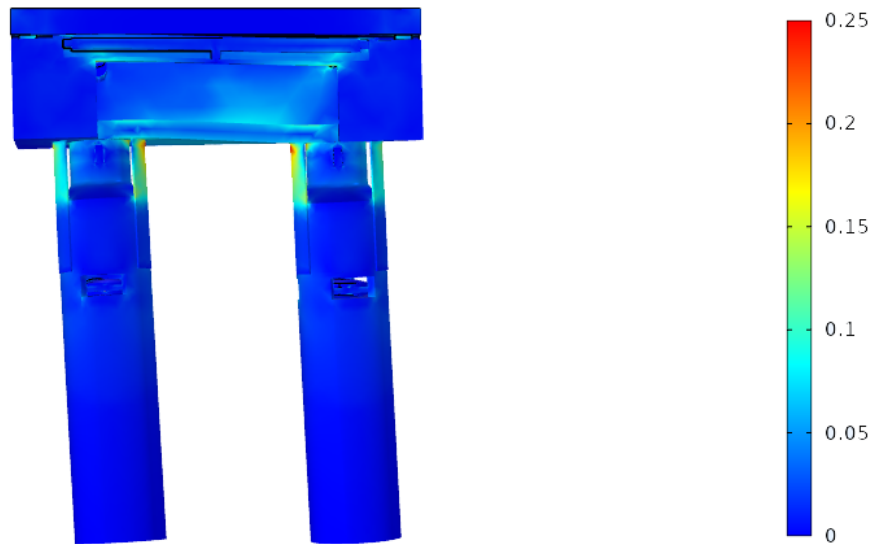
Figure 6.22: Deformation of the Gravity Release in X axis

• **Gravity Release Y**:

Table 6.9: COMSOL derived values for gravity release load case Y (μm and mrad)

Gravity Release Y	Tx	Ty	Tz	Rx	Ry	Rz
Fiber	-1.03E-01	6.20E-01	2.58E-02	-1.42E+01	-3.23E+00	-2.38E+00
Aperture	-4.89E-02	3.85E-01	2.58E-02	-1.33E+01	-3.24E+00	-2.38E+00
SL-1 Lens	-4.33E-02	3.62E-01	2.58E-02	-1.33E+01	-3.24E+00	-2.38E+00
SL-2 Lens	-5.35E-04	1.77E-01	2.64E-02	-1.18E+01	-3.18E+00	-2.62E+00
SM-1 Mirror	1.18E-03	8.57E-03	-3.56E-04	-4.89E+00	1.14E-00	7.10E-02
SM-2 Mirror	4.77E-04	3.72E-02	1.24E-03	-1.24E+01	3.08E-01	-2.58E-00

Table 6.10: Total gravity release stability for load 2G on Y axis (μm and mrad)

Gravity Release Y	Decenter	Tip Tilt	Focus
RSS	9.25E+00	4.48E+00	1.89E-01
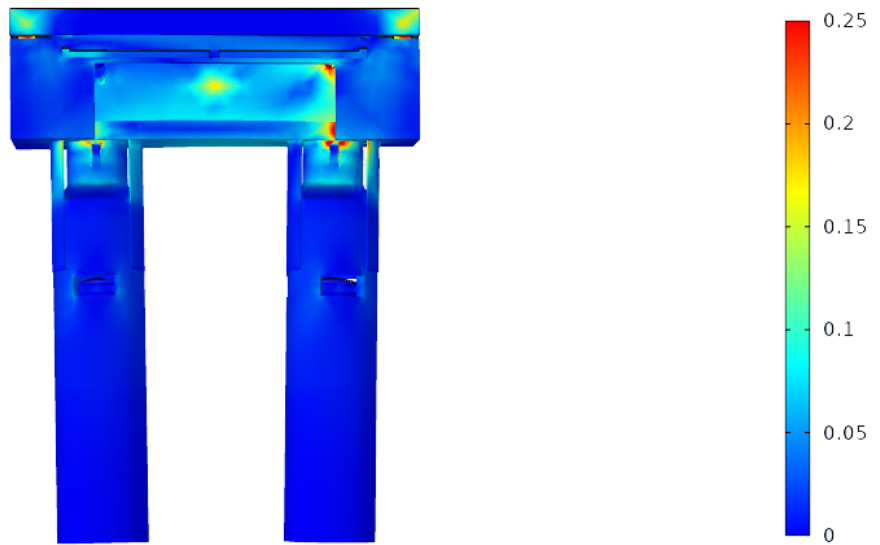
Figure 6.23: Deformation of the Gravity Release in Y axis

• **Gravity Release Z**:

Table 6.11: COMSOL derived values for gravity release load case Z (μm and mrad)

Gravity Release Z	Tx	Ty	Tz	Rx	Ry	Rz
Fiber	1.86E-02	4.15E-02	1.14E-02	-6.84E-01	4.20E-01	-5.73E-01
Aperture	1.17E-02	3.01E-02	1.08E-02	-6.76E-01	4.20E-01	-5.73E-01
SL-1 Lens	1.09E-02	2.90E-02	1.08E-02	-6.76E-01	4.20E-01	-5.73E-01
SL-2 Lens	-5.22E-03	1.96E-02	9.88E-04	-6.66E-01	4.18E-01	-5.70E-01
SM-1 Mirror	2.09E-04	1.25E-03	7.36E-04	-5.74E-01	3.91E-01	2.89E-02
SM-2 Mirror	5.59E-04	3.98E-03	6.70E-03	-1.06E+01	5.53E-01	-2.41E-01

Table 6.12: Total gravity release stability for load 2G on Z axis (μm and mrad)

Gravity Release Z	Decenter	Tip Tilt	Focus
RSS	7.19E-01	4.30E-01	8.66E-02

Figure 6.24: Deformation of the Gravity Release in Z axis

6.3.3. Overall stability

The Table below illustrates the stability values derived from the combined effect of thermal gradient and free fall. It can be seen that the designed module does comply with the stability requirements in both the cases (Linear and RSS).

Table 6.13: Overall Stability of the Designed Module (μm and mrad)

Gradient Direction	Case	Decenter	Tip Tilt	Focus
X Axis	Thermo Mechanical	4.89E+00	3.09E+00	3.15E+00
	Gravity Release	3.80E+00	1.03E+00	7.93E-02
Y Axis	Thermo Mechanical	1.11E+01	5.22E+00	2.16E+00
	Gravity Release	9.25E+00	4.48E+00	1.89E-01
Z Axis	Thermo Mechanical	1.16E+01	6.04E+00	3.26E+00
	Gravity Release	7.19E-01	4.30E-01	8.66E-02
Requirement	Total	<5.00E+01	<5.00E+01	<5.00E+01
Result	**Linear Summation**	**4.12E+01**	**2.03E+01**	**8.92E+00**
	RSS	**1.95E+01**	**9.72E+00**	**5.03E+00**

6.4. Adverse Conditions

Prior to this section, an emphasis was made solely on the analysis of the module under operating conditions. But it is important to note that since the module has to be transported and operated in the space environment, it is critical to consider the worst-case scenarios possible. Although there are many factors imaginable, Two extreme cases were taken for further examination, which is both foreseeable and their behavior is predictable:

- **Acoustic loading during Rocket Launch**: The noise generated at the launch, the liftoff, and the transonic climb phase, creates intense acoustic vibrations that can reach up to a level 0f 180 dB. The generated loads are generally a result of the interactions of the rocket-engine exhaust stream mixing with the atmosphere. These unavoidable and undesirable phenomena can lead to an immense effect on the spacecraft and the payload installed in the system. Therefore, it is crucial to examine the impact created on the current module.

Although this can be done using COMSOL acoustic modeling, the overall designed module being placed within the main instrument, which is further enveloped by the satellite body, has minimized the impact created by the noise. In fact, was found that the noise impact would be orders of magnitude lower than the impact created by the vibration and shock. As of now, the current design does comply with the vibration requirement (results shown in chapter 6.1). The figure below also shows that the stress generated on the system are very low. For this reason, acoustic modeling and analysis were excluded from the research scope.
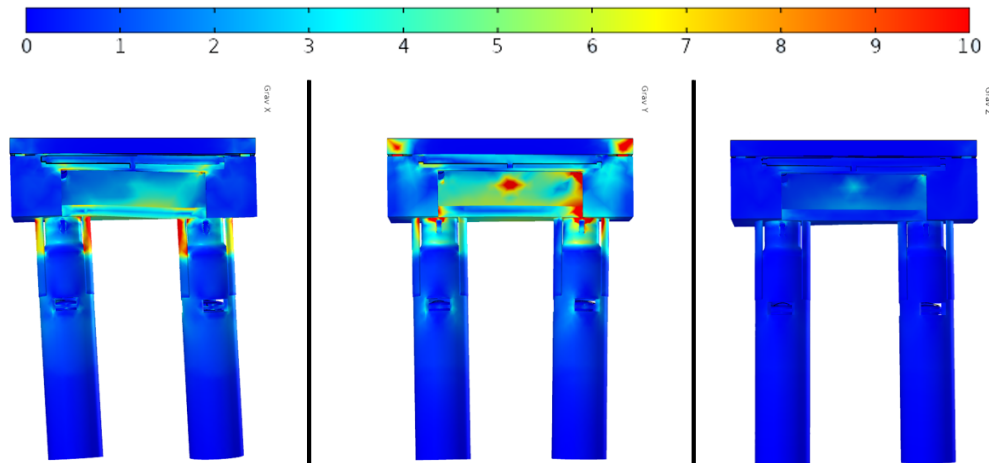
Figure 6.25: Impact on the overall module due to a load of 150G in all the directions (Mpa)

- **Thermal affects due to eclipse cycling**: When the earth or moon blocks sunlight from reaching a satellite, it is said to be in eclipse (As shown in the figure 6.26). When the Sun, Moon, and Earth are aligned in such a way that the Moon's shadow falls on the Earth, it is called a solar eclipse. The shadow of the Moon falls on the Earth-orbiting spacecraft as well. Although the Sun, Moon, and spacecraft are aligned similarly to the Sun, Moon, and Earth in this scenario, the phenomenon is commonly referred to as a lunar eclipse falling on the spaceship. Even though these eclipses occur only a few times in a year with a shorter time interval, once the satellite goes into the shadow, the radiation pressure vanishes, which generates errors in satellite dynamics, and satellite solar sensors lose sight of the sun, causing the thermal control to degrade. In these cases, the spacecraft controller shuts down to conserve energy.
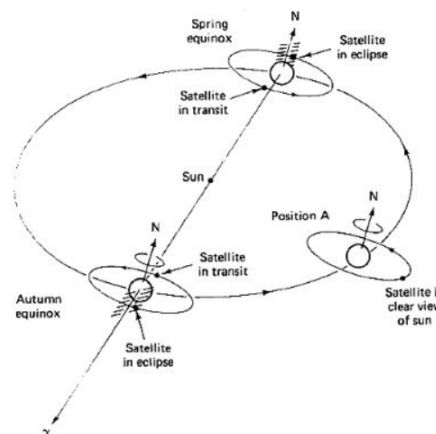
Figure 6.26: Orientation of the satellite during different time periods [37]

With the Calibration module solely dependent on the sun rays for performing the calibration, this

system will not operate for that particular period during the eclipse. Although this is a matter of concern, the real problem is when the thermal control completely shuts down. This will drastically reduce the temperature leading to increased stress and deformation in the components. Therefore, a COMSOL analysis has to be conducted for the examination of the structure at low temperatures. From the previous data collected from similar satellite missions, it was found that the temperature can drop to 233.15 K (ΔT = 60K).
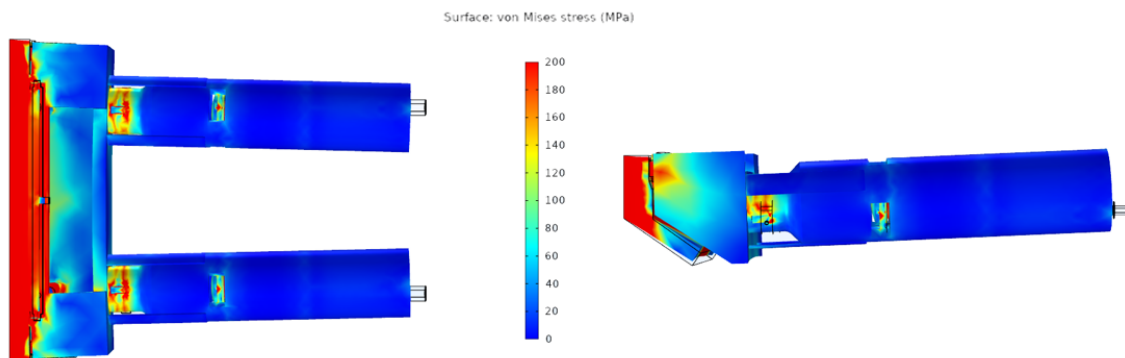
Figure 6.27: Impact on the overall module due to steady state thermal expansion Δ = 60K

The maximum stress experienced by the module is around 230 MPa, as shown in the figure 6.27. Also, as shown in Chapter 6.1, The stress concentration on the lenses (both SL-1 and SL-2) are within the limits. This demonstrates that the stress imposed on the system is entirely within acceptable limits. Even though the optical elements have very high deformations, the system does not fail as the overall module is nonfunctional at the given period and the use of bonding eliminates the hysteresis upto a certain level.

6.5. Cost Estimation

One of the most prominent yet considered trivial tasks for a designer is to evaluate the cost of a design. This parameter can dictate the type of choices and optimization used for a particular solution. The use of Additive manufacturing has been beneficial for trimming the cost by enabling a multi-functional structural housing, which would otherwise not be possible. A total of €10,000 has been allocated for the manufacturing of the part. This includes parts brought from the suppliers,manufacturing of components, and housing structure. Below is a table which provides an overview of the cost incurred for manufacturing and assembly of the designed module. It is important to note that the values are rounded off to the higher numbers as the developed module is yet to be manufactured.

It can be seen that the current module does comply with the cost requirement.

6.6. Focus Compensation

Everything discussed so far has no road blocks from the process of performance specifications to performance analysis, with an exception of the manufacturing tolerances. It is found from the manufacturing error budget that the sensitivities of lens components stated by Edmund optics is way out of limit, which means that it might be impossible to achieve this target with the machining tolerances. Below are some of the strategies which can be implemented to get the design to an acceptable range:

a) **Re-optimize the optical design**: Since we see that the radius and thickness tolerance of the optical system are very high, it is possible to change the design by characterizing the optics received from the Edmund optics. This could disregard the other compensation methodologies, but it is important to note that optics are very sensitive, and a small error while handling can prove the whole exercise a nugatory.

Table 6.14: Total cost of the prototype of the designed system.

Component	Quantity	Total Cost (€)
Lens (SL-1 and SL-2)	4	450
Fiber Ferrule	2	75
Part A	2	150
Part B	1	125
Part C	1	75
3M Epoxy 2216 B/A Grey	1	50
SM-2 Part	1	50
Mirror Finish	4	1000
Milling For interfaces	15	1500
Assembling	1	5000
Laser Cutter For Slit	1	700
Vibro-Polishing For Finishing	1	100
Requirement	34	< 10,000
Total Cost		**9,275**

b) **Relax the current performance budget**: This is a tactic that is perhaps used to eliminate all the additional work required for compensation by increasing the budget. Although it may be simple to employ, it requires a backup of all the documentation generated to validate if the current design would still be viable without any changes. Therefore, it is considered a last resort, as it might tamper with the science product generated by the module.

c) **Request for a tighter tolerance from the manufacturer**: The third compensation strategy would be to reduce the manufacturing tolerances. That way, the current design will suffice if the tolerance is taken below 15 μm. Also, with few design changes, the module would suffice if the tolerance was taken up to 35 μm. But it is important to note that the lead time and the overall cost will increase by a big difference, which would lead to a delay in the current timeline and additional budget allocation, respectively.

d) **Employing a different mounting strategy for lenses**: Sometimes the problem insensitivity is the choice of a mounting strategy. One can try different mechanisms to see if the improvement is possible. Figure 4.2 do provide some different methodologies for mounting the lens. This approach can indeed increase the time for design and assembly changes due to a large number of iterations and validations. Also, some taught has to be given in the print direction, post-processing methodologies, e.t.c. Finally, even if the sensitivity table can be made acceptable, the performance predicted by an RSS might be unacceptable.

e) **Use of a Compensator/Adjustment mechanism for alignment**: In general, there are two ways to achieve the sub micron accuracy: by manufacturing the parts to the required tolerance or use an adjustment mechanism for parts that have loose tolerances compared to the requirements. Compensators are adjustments that can be made to optical components to compensate for errors arising elsewhere in the system. These are either incorporated into the design or can be used as a separate tool while assembling. Although adding such elements is considered favourable, there are a lot of factors (range, ease of adjustments, cross-talk, measurement e.t.c) which have to considered before selecting an appropriate compensator. Reportedly, I can imagine four different compensation strategies possible for the current design:

  • **Off-the Shelf components**: One of the simplest method would be to use a simple off the shelf component like a o-ring or a retainer ring shown in the figure 6.28 below. This could be placed between part 2 and 3 to compensate for the error. Although, it is easy to apply and requires the least time, it does increase the time for assembling the overall component.

Figure 6.28: Aluminium retainer ring

- **Alignment mechanism included in-between the module**: An other method of compensating for the focus error is by using a alignment mechanism in such a way that the current module is not disturbed (As shown in the figure 6.29 below). From the kinetic and eigenfrequency studies conducted before, this would be a perfect location for alignment mechanism. Here, a leaf flexures is introduced in the system which would act like a interface. The actuation is provided by the screw with a differential adjuster. A washer can be provided for the preload purposes and the existing epoxy can be used for the locking of the component.
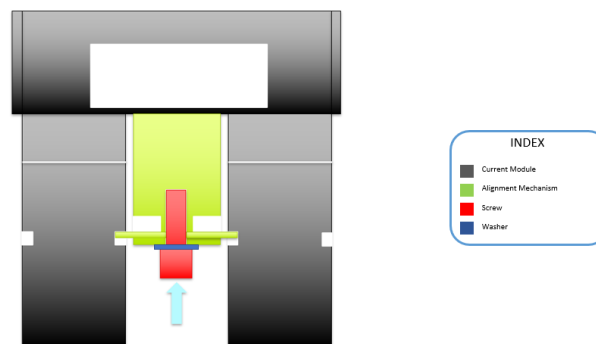
Figure 6.29: Alignment mechanism

- **Small modification in the module for compensator**: This strategy would require a minor design modifications to accommodate the compensator. Here, the part 1 and 2 are combined into a single piece, thus reducing the part count. The threading made earlier is completely eliminated. The alignment accuracy is maintained using a precisely manufactured shim. The module is then locked using a screw to maintain the accurate position. The preload is maintained by a washer at the other end. Although, this strategy requires a design change, the overall features used are pretty much the same. Also, the design is exactly constrained.
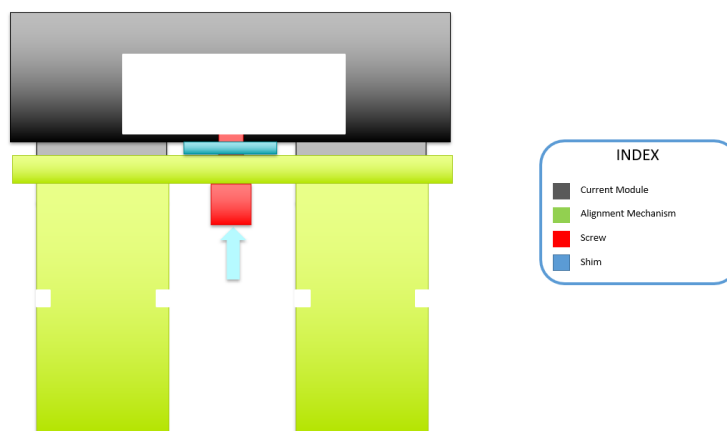
Figure 6.30: Modified Module

- **Compensation using piezoelectric actuators and control system**: Active compensation is one other technique which would provide precise results with high resolution and real time adjustment. The piezoactuator can be placed on the flat side of the optics, near the slots which were provided earlier for post processing. The controller and sensors can be placed below the module and at the slit respectively. Typical disadvantages include hysteresis, creep, non linearity of the actuator. Also, the feedback loop would be very expensive and computationally intensive.

Based on the proposed strategies, it can be seen that all the methodologies do have some positives and negatives. But in conclusion, it is to be hoped that all of them would produce a favorable result. Given the specifications and the current status of the module, it is rational to consider the overall team (optical designer, mechanical engineer, MAIT specialist, system engineer, and other concerned individuals) to strive cooperatively to define the appropriate compensation strategy to meet the system design goals. This will require sufficient analysis and validation as precipitous decisions may produce instruments that reincarnate weaknesses of earlier designs or embody new unintended shortcomings.

<div align="right">

7

</div>

Conclusion, Recommendations and Outlook

7.1. Discussion

The thesis aimed to address the design modeling activities for a spectral calibration module that has to be installed into an Earth-observing satellite and to eliminate the labor-intensive and time-consuming conventional fabrication process of the space products. To avoid the above obstructions and exploit the available design freedom, additive manufacturing technology was used As a result, the goal of this study was to develop a printable optomechanical design of a spectral calibration unit and analyze that to validate it w.r.t the given specifications and constraints. This calibration system that has to be integrated into the instrument for better reliability of measurements. The rapid transition of the operational conditions combined with the high sensitivity of the optical components and tight constraints for a better performance are the main challenges that have to be faced. Although this might seem to be a straightforward task, it is very complicated in practice due to a lack of knowledge regarding the main design drivers or critical items which would have been considered trivial before. Therefore, a preliminary design has been made to understand the behavior of the system and to conceive of a solution for the design problem.

A design process proposed in [24], was used for the development of this preliminary design. It started of by understanding the the basic working principle and the current developments of the opticalnlayout plan. The layout plan is at the heart of every optomechanical design, and it includes an optical element's requisite adjustable degrees of freedom, travel, and resolution, as well as any fiducials. Since there are multiple components involved in the system, it is necessary to analyze the quantitative effect for each deviation concerning the overall performance. Since the performance here is determined by the location and the size of the spot, geometric optical analyses (ie Ray tracing) was considered to determine the sensitivities.

With the knowledge acquired from the sensitivity analysis, design loads and, performance and design constraints, design trade-offs have to be made for designing an optomechanical system. This includes a material selection for each component, followed by their corresponding mounting structures. The housing of the components can be optimized to attain a stiff and stable structure with homogeneous materials and a constrained athermal design to avoid CTE differences and to restore the position when deviations, respectively. However, the space available is low, constraining the employment of better structures for stability. Also, there is always some amount of tolerance present in any manufactured system, which is inevitable. Therefore, compromises and controlling strategies have been utilized for the desired performance and robustness. The employment of additive manufacturing technology has provided a solution by providing distinct advantages in terms of creating complex geometry (like the tube axisymmetric structure or a binocular structure with all mounting features), part count (limiting to

a total of four parts) and homogeneous material usage throughout the structure.

The final phase of the thesis aimed at detailing the design of the overall system with appropriate refinement followed by multi-physics analysis to validate the selected design choices. Since the system is going to work in a for a longer period of time (ie 5 - 10 years), it is also crucial to consider the adverse effects that can be faced by the system and validate the performance in those respective times. The Figure 7.1 shown below, is an illustration of the exploded view of the module module after all the modifications and refinements. The Figure 7.2 below provides the illustration of the calibration module integrated with the CHAPS mirror mountings. This shows that the system is compatible to the given volume requirements without requiring any modification to the current design.
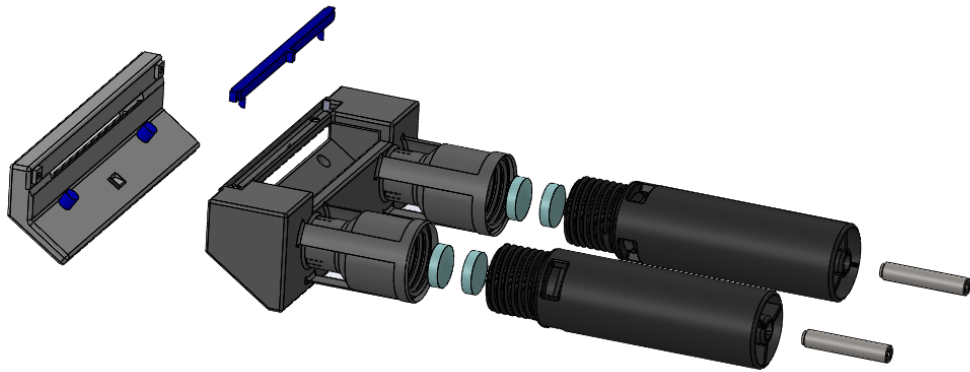

Figure 7.1: Exploded View of the spectral calibration Module
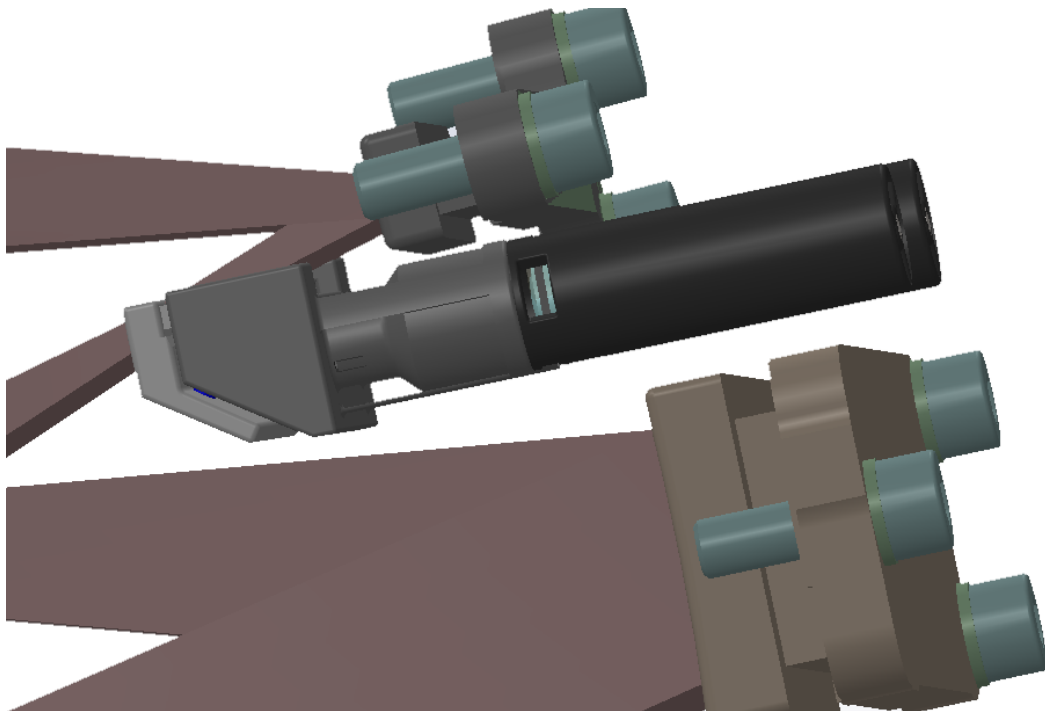

Figure 7.2: Proposed module integrated into the CHAPS instrument

Table 7.1 below recalled corresponding to their verification and validation methods and whether the designed module succeeded to meet each one of those requirements or not. Here, all the validations were made through analytical and simulation results as the manufacturing and design testing would be conducted at the next phase of the optomechanical design process.

Table 7.1: Summary of design requirements, their validation methods, whether each design requirement was met or not

#	Design Requirements	Verification Method	Comply or Not?
1	Eigen Frequency >600Hz	Verified through COMSOL	Comply
2	Stress impact on the optical components	Verified through COMSOL	Comply
3	Thermo-Mechanical Stability <0.05mm	Verified using Error Budget and COMSOL	Comply
4	Total Mass < 200g	Verified within the SolidWorks design	Comply
5	Total Volume <16000 mm^3	Verified within the SolidWorks design	Comply
6	Assembly Tolerance < 0.1 mm	Verified using Error Budget	Not
7	Total Cost <10,000 euros	Intuition and component costs	Comply
8	Adverse Analysis	Verified through COMSOL	Comply
9	No Design Change	Verified through SolidWorks	Comply
10*	Manufacurable with the given expertise	Verified by mentor	Comply

7.2. Conclusion

Based on the research conducted, the following conclusions were drawn:

The first research objective: Design the spectral calibration module for the CHAPS instrument applying kinematic approach to satisfy the stress and the stiffness requirements

- The present design is capable of mounting all the mirrors (which were tightly packed) into a simple six DOF constraint principle (Fig: 5.4), without any need of adjustment mechanisms. Also, there was no need for a optical design change and enough space was provided for a SL-1 lens compensation design.

- The overall eigenfrequency of the proposed module design has its least value around 772.29 Hz. This shows that the proposed module will sustain the vibration and shock impact generated by the rocket launch.

- The fact that the overall designed module is placed inside the main instrument, which is further enveloped inside the satellite body, has minimized the impact created by the acoustic loads. It was found that the acoustic loads impact would be orders of magnitude lower than the impact created by the vibration and shock. For this reason, acoustic modeling and analysis were excluded from the research scope.

- The stress generated on both the lens was orders of magnitude lower than the yield strength of the optics after considering the safety factors (shown in chapter 6.1). Also, the stress generated on the overall component due to homogeneous temperature rise during operation and lunar cycling was less than 12 MPa and 230 MPa, respectively. Also during this rise, it was found that the stress generated on the components was also very low.

The second research objective: Investigate the impact of additive manufacturing for the design of a complex miniature optical system.

- Design guidelines and constraints such as overhang, minimal feature size, overlap, built orientation etc. have been respected while designing the module to prevent errors and damages during post processing. For instance, the part c of the design was not printed because the surface roughness and minimal feature size do not comply with the SM-1 requirements.

- The overall volume of the designed system is 7699 mm^3. The employment of additive manufacturing has been really beneficial for the creating a design with multi-functional capabilities. It was also noticed that the module did not require external adjustment mechanisms, which also contributed for the reduction in the volume. Also, additional volume is available for the modification and focus compensation if required. Finally, this proposed design does comply with the requirements of not interjecting with the M1 mount of the CHAPS Instrument.

- The overall mass of the instrument is around 21g. This is almost an order of magnitude lower than the requirements. This substantial weight reduction would prove to be a valuable asset in terms of overall weight while loading it into the rocket . The use of a monolithic AM housing structure was considered to be major factor for the weight reduction.

- The overall cost of the instrument is around €9250. This only includes the cost of the parts brought from the supplier, manufacturing the structure and post-processing of the module. It can be seen that the value is within the requirement limit.

The third research objective: Perform optical sensitivity analysis to determine the mechanical requirements and design drivers under structural and thermal load cases.

- The manufacturing assembly tolerance of the proposed structure has a very high tolerance in the z-axis translation (i.e. 142 μm). The tolerance in the other axis is all under the limit. The reason for this high tolerance is due to the high manufacturing tolerance quoted by Edmund for both lenses.

- To compensate for the above effect, a few compensation strategies and methods were proposed in chapter 6.6. Finalization of a particular strategy will require a cumulative effort of the team and further analysis.

- The Thermo-mechanical stability of the structure was extracted using an error budget methodology, shown in chapter 6.3. It was seen that the current module was able to maintain a focus stability limit of 50 μm under the gradient temperature effect. This would prove that the system is capable of operating under situation when one side of the satellite is in full sunlight, while the other side is facing deep space.

7.3. Recommendations

From this research, a basic essence of the module and some of the most sensitivity issues have been discovered which will conclude the preliminary phase of the design and this may prove to be very useful for the next phase of the thesis. For the future work, some of the recommendations are provided below which can be implemented if needed:

- Different approaches pertaining to the focus compensation have been discussed in length in the section 6.5. However, to get a concrete decision on the available broad level solutions, it would be beneficial to investigate in detailed and elaborate format. For this a bottom up approach can be implemented where system are specified in a great deal. Further, based on the selected strategy, design enhancements and dimensional analysis should be conducted, to satisfy the top level requirements.

- Due to the short distance and the low angle of incidence between the optical path and the barrel, there might be a possibility of stray light or false images. To avoid this a black coating can be applied in the module, especially near the mirror region. Therefore, selection of a appropriate coating should be done to avoid degradation.

- Now that the module is undergoing the prototype phase, it is important to create a verification plan for ensuring the accuracy in the manufactured parts. This can be done by creating some verification tools to ensure that the pieces are done correctly and making sure that the components can be mounted with all the designed functionalities.

- Testing of the module is one important task that has to be taken up. The figure 7.3 below provide an overview of the typical test sequence flow that should be performed after the manufacturing of the space instrument [16] to interpret the performance. These tests include physical (weight, moment of inertia, and CG), Thermal Cycling (simulations performed by placing the module inside a chamber and by controlling the temperature, useful for time-dependent studies), Thermal vacuum (Very useful for bakeout and demonstrating the integrity) and Mechanical (shock and vibration tests). Of these, thermal cycling is one important test to be performed as time-dependent and hysteresis analysis was not considered in the above numerical simulation. Although it wouldn't be a big risk because of the implemented bond mounting strategies, it would be interesting to see if there are any unforeseen circumstances existing.
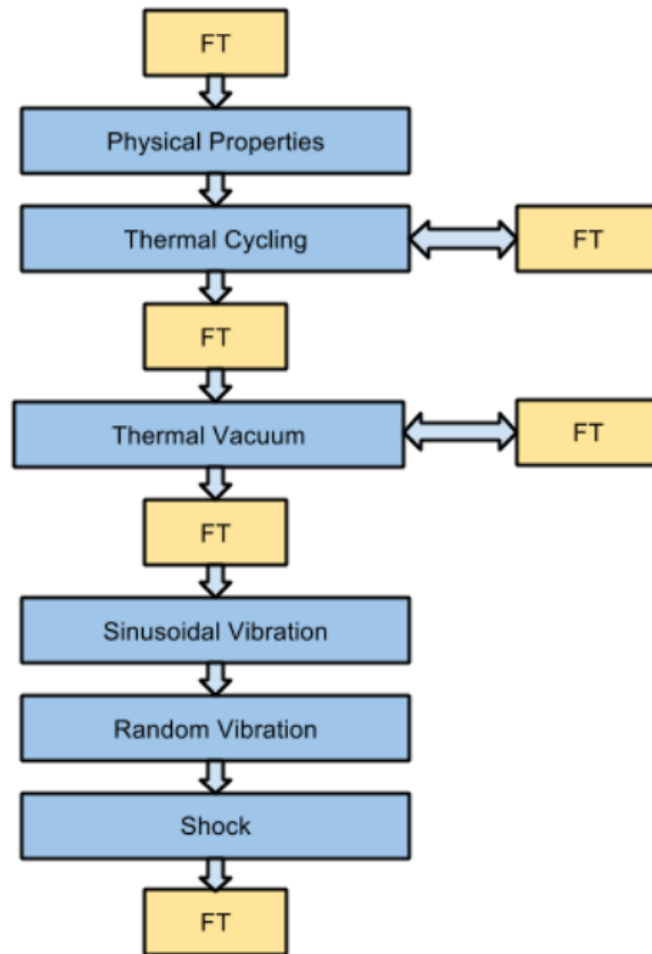

Figure 7.3: Test Sequence Flow [16]

- One of the prime advantages of additive manufacturing is to integrated parts into a single component. As shown above, this was not done mainly to facilitate for post processing methodologies of f the mirrors and lensens. We are not close to printing lenses, but it might be possible to make a design which incorporates internal mirror surfaces using plasma/ electropolishing methodology to clean the surfaces. The figure 7.4 below provides a schematic setup of the electrolyte plasma polishing methodology. Although, it does provide a distinct advantage in creating a single part module, it does create problems in terms of angularity, location, and shape of optical components. Therefore, a detailed comparative study and analysis should be performed to determine the most beneficial design based on current requirements and constraints.
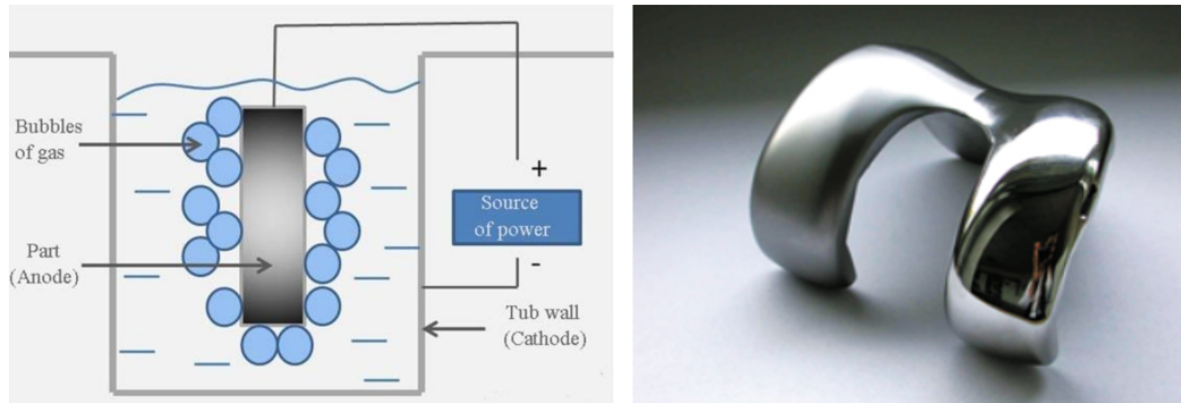
Figure 7.4: Electrolyte plasma polishing [41]

- Finally, the designed module should be integrated into the instrument. As the instrument is not completely designed, there is no current knowledge of the available interfaces and volume. Therefore, a suggestion is made (as shown in the figure 7.5) for integrating the module. Here, three mount interfaces (small protrusions) are created to maintain the position of the module. To constrain all the DOF, three bolts are used in such a way that the thermal center is maintained at the slit. Although, this is an over-constrained design, it maintains the position during dynamic or thermal loads. This is a similar kind of mounting strategy used in the current instrument (i.e. for the telescope mirrors). Although, this does seem a workable design, further investigation is needed to find the optimal mounting strategy.
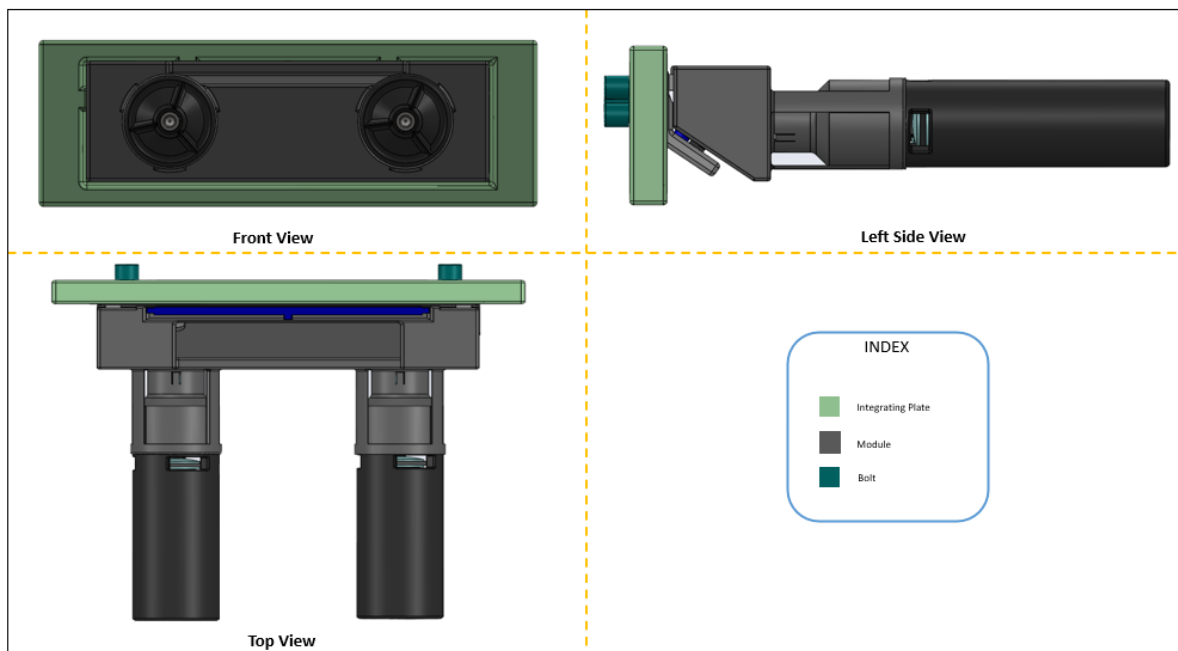
Figure 7.5: Integration of the current module into the CHAPS instrument

7.4. Outlook

Optical instruments for the intended purpose of pollution monitoring, space exploration, communication and surveillance, are turning out to be more complex and simultaneously also miniaturized. Integrating the components into one part is proving to be a substantial solution for tackling this problem. This would reduce the time taken by the engineer to tackle the problems relating to ergonomics and human factor

by providing interfaces in a more convenient places.

Additive Manufacturing offers unique solutions with the possibility of directly manufacturing the component from the design of the CAD.The idea behind this technology is to build up from the synthetic environment and try to replicate the materials and high performance by not using brute force technique to structure them but by nature-inspired methodologies of hierarchical materials, brick and mortar structures, and collaborative building.

As seen from the thesis report, metal additive manufacturing (especially the powder bed fusion) provides a solution not restricting to single component designs but also for an assembly in situations where conventional or off-the-shelf components do not qualify. Also, the quality of the structures is not really disparaged, making it an ideal manufacturing technology for such optical systems. Finally, AM also accommodates the usage of very powerful design tools like topology optimization (TO) for designing non compliant structures [39].

This metal manufacturing process is widely touted as a foundation for the next industrial revolution, especially for the optomechanical and space sector, as it offers profound advantages like shorter lead time, lower wastage of materials, and higher geometric complexity that can be useful for multi-functional and multi-material structures. It can also facilitate good strength, significant mass reduction, and better dimensional homogeneity. For example: [9] provides examples where the mirror and the precision structure is integrated and manufactured as a single monolithic piece. Although it provides clear advantages over other manufacturing methods, it does have some drawbacks. The resultant parts for this technology is not very precise. Their is also no such implementation framework which uses the tools like TO that meet the manufacturing requirements. The most prominent limitation is the restricted overhang. Also, the initial setup cost is more compared to conventional methodologies. Finally, the limited availability of material are available which are compatible to AM.

But, recently their has been a change in this scenario. Active research is going on in the areas of materials development and the situation is also changing. Methods are being created where overhangs are eliminated by means of super magnets and laser (Boeing patent: US20160031156). Also, several software tools are being developed by various organizations which would predict thermal stresses while manufacturing, printing optimized structures with manufacturing compatibility and CAD processing before the initialization of the process. For example, Nettfab Simulation created by Autodesk and [30] created by Mihails Delmans and Jim Haseloff for a printable optomechanics framework. Finally, due to large scaling of this technology, integration of the multiple (pre and post proceesing) techniques into a single system, and outsourcing of large scale productions to well established companies with developed plants are proving to be a valuble step for reducing the cost of the parts and the setup [12]. All these steps and recent initiations have a made a transition in the Metal AM technology which is now seen through the higher Technology readiness level(Powder bed fusion and Direct energy deposition: 8 and Binder jetting and Material jetting:7).

Bibliography

[1] The european cooperation for space standardization. URL `https://ecss.nl/`.

[2] Femci book - miles' equation. URL `https://femci.gsfc.nasa.gov/random/MilesEqn.html`.

[3] Nasa techport. URL `https://techport.nasa.gov/view/96399`.

[4] Issues in the integration of research and operational satellite systems for climate research. URL `https://www.nap.edu/read/9966/chapter/4#12`.

[5] Uv coated plano-convex lens. URL `https://www.edmundoptics.eu/p/6mm-dia-x-18mm-fl-uv-vis-coated-uv-plano-convex-lens/9166/`.

[6] Text book on remote sensing. URL `http://sar.kangwon.ac.kr/etc/rs_note/rsnote/cp2/cp2-1.htm`.

[7] Review Matrix methods in treating decentred optical systems. *Optical and Quantum Electronics*, 17:12, 1985.

[8] Numerical analysis of gradient index lens–based optical coherence tomography imaging probes. *Journal of Biomedical Optics*, 15(6):066027, 2010. ISSN 10833668.

[9] Application and testing of additive manufacturing for mirrors and precision structures. *Material Technologies and Applications to Optics, Structures, Components, and Sub-Systems II*, 9574 (September 2015):957406, 2015. ISSN 1996756X. doi: 10.1117/12.2189202.

[10] Fourier optics, Jun 2020. URL `https://en.wikipedia.org/wiki/Fourier_optics`.

[11] JPE:Driven by passion. PRECISION POINT, To The Point Precision Engineering Knowledge Database. `https://www.jpe-innovations.com/precision-point/`.

[12] Ian Campbell, David Bourell, and Ian Gibson. Additive manufacturing: rapid prototyping comes of age. *Rapid Prototyping Journal*, 18(4):255–258, 2012. ISSN 13552546. doi: 10.1108/13552541211231563.

[13] Electronic Components. Cannon VEAM Fiber Optics Products and.

[14] J. De Vreugd, K. M.B. Jansen, L. J. Ernst, and J. A.C.M. Pijnenburg. Modelling of viscoelastic properties of a curing adhesive. *WIT Transactions on Engineering Sciences*, 57:241–251, 2007. ISSN 17433533. doi: 10.2495/MC070241.

[15] J. de Vreugd, M. J. A. te Voert, J. R. Nijenhuis, J. A. C. M. Pijnenburg, and E. Tabak. Improved stress prediction in adhesive bonded optical components. *Modern Technologies in Space- and Ground-based Telescopes and Instrumentation II*, 8450(September 2012):84504A, 2012. ISSN 0277786X. doi: 10.1117/12.925418.

[16] Endurosat. Test of CubeSat . `https://www.endurosat.com/`.

[17] Chris Van Ewijk. Alignment sensitivity of reflective optical elements and analysis of automated alignment methods. (November):1–44, 2017.

[18] David G Gilmore, David G. Gilmore, and Martin Donabedian. *Spacecraft Thermal Control Handbook*. Aerospace Press, 2002.

[19] James J. Herbert. Techniques for deriving optimal bondlines for athermal bonded mounts. *Current Developments in Lens Design and Optical Engineering VII*, 6288(August 2006):62880J, 2006. ISSN 0277786X. doi: 10.1117/12.680828.

[20] Joseph M. Howard. Optical modeling activities for the James Webb Space Telescope (JWST) project: I. The linear optical model. *Optical Modeling and Performance Predictions*, 5178(January 2004):82, 2004. ISSN 0277786X. doi: 10.1117/12.507735.

[21] Rik Jansen, James P. Day, Rob Vink, Jan de Vreugd, Erik R. van Beekum, Ludger W. van der Laan, Adriaan C. van 't Hof, Wim L. Gielesen, and Jess Koehler. Design and first light of the Sentinel-5 UV1 spectrometer optics. (October 2019):26, 2019. ISSN 1996756X. doi: 10.1117/12.2532400.

[22] Wonseok Kang, Soohwan Yu, Doochun Seo, Jaeheon Jeong, and Joonki Paik. Push-broom-type very high-resolution satellite sensor data correction using combined wavelet-fourier and multiscale non-local means filtering. *Sensors (Switzerland)*, 15(9):22826–22853, 2015. ISSN 14248220. doi: 10.3390/s150922826.

[23] Hagyong Kihm, Ho Soon Yang, and Yun Woo Lee. Bipod flexure for 1-m primary mirror system. *Review of Scientific Instruments*, 85(12), 2014. ISSN 10897623. doi: 10.1063/1.4902151. URL http://dx.doi.org/10.1063/1.4902151.

[24] E. Todd Kvamme, David M. Stubbs, and Michael S. Jacoby. The opto-mechanical design process: from vision to reality. (August 2017):26, 2017. ISSN 1996756X. doi: 10.1117/12.2275671.

[25] Thor Labs. Stainless Steel and Ceramic Fiber Optic Ferrules. https://www.thorlabs.com/newgrouppage9.cfm?objectgroup_id=6313.

[26] Andrew J. S. McGonigle Mary B. Stuart and Jon R. Willmott. "hyperspectral imaging in environmental monitoring: A review of recent developments and technological advances in compact field deployable systems". 19, July 2019.

[27] Chandru B T Venkateswaran R Krishna Murthy T Mayur D Pawar, Bijoy Raha. "opto-mechanical design and analysis of a refractive multi element lens assembly for space applications". 2:77–82, July 2013.

[28] Compliant Mechanism. Design Methods for Compliant Mechanism. https://en.wikipedia.org/wiki/Compliant_mechanism.

[29] Assefa M Melesse, Qihao Weng, Prasad S Thenkabail, and Gabriel B Senay. Remote sensing sensors and applications in environmental resources mapping and modelling. *Sensors*, 7(12): 3209–3241, 2007.

[30] Jim Haseloff Mihails Delmans. µCube A framework for 3D printable optomechanics. https://mdelmans.github.io/uCube/.

[31] Adament Namiki. Feature printed adapters. https://www.ad-na.com/en/product/optical/ferrule-sleeve/singlemode-ferrule.html.

[32] Trent Newswander and Roger A. Paquin. *Materials for optical systems*. 2017. ISBN 9781498761499. doi: 10.4324/9781315153247.

[33] Edmund Optics. Spatial Filter Movement. https://www.edmundoptics.com/f/spatial-filter-movement/11384/.

[34] Roger A. Paquin. Dimensional instability of materials: how critical is it in the design of optical instruments? *Optomechanical Design: A Critical Review*, 10265(December 1992):1026509, 1992. ISSN 1996756X. doi: 10.1117/12.61106.

[35] Gordon Petrie. "airborne pushbroom line scanners: An alternative to digital frame cameras". January 2005.

[36] Gerrit Polder and Gerie W. van der Heijden. Calibration and characterization of spectral imaging systems. *Multispectral and Hyperspectral Image Acquisition and Processing*, 4548:10, 2001. ISSN 0277786X. doi: 10.1117/12.441362.

[37] ques10.   What is Earth eclipse of Satellite?Are there any ways of avoid-
     ing eclipse during lifetime of satellite.   `https://www.ques10.com/p/2938/`
     `what-is-earth-eclipse-of-satelliteare-there-any--1/`.

[38] RoyMech.   Screw dimension calculations.   `https://roymech.org/Useful_Tables/`
     `Screws/Thread_Calcs.html`.

[39] R.P. Hoogeboom. Department of Precision and Microsystems Engineering. *Thesis Topology*,
     (October):5–7, 2016.

[40] Jason Shore, Roy Blows, Andrew Viquerat, Guglielmo S Aglietti, David Gooding, and Guy Richard-
     son. a New Generation of Deployable Optics for Earth Observation Using Small Satellites.
     (September), 2019.

[41] M Smyslova, D Tamindarov, N Plotnikov, Iu Modina, and Irina Semenova. Surface electrolytic-
     plasma polishing of ti-6al-4v alloy with ultrafine-grained structure produced by severe plastic de-
     formation. *IOP Conference Series: Materials Science and Engineering*, 461:012079, 12 2018.
     doi: 10.1088/1757-899X/461/1/012079.

[42] Hai Jun Su, Hongliang Shi, and Jingjun Yu. A symbolic formulation for analytical compliance
     analysis and synthesis of flexure mechanisms. *Journal of Mechanical Design, Transactions of the
     ASME*, 134(5), 2012. ISSN 10500472. doi: 10.1115/1.4006441.

[43] P I William H Swartz, Team Members, Nickolay Krotkov, Lok Lamsal, Frank Morgan, John
     Boldt, Joseph Linden, Scott Janz, Matthew Kowalewski, and Pieternel Levelt. CHAPS-D: The
     Compact Hyperspectral Air Pollution Sensor–Demonstrator. *ESTF2020 Program: IIP-2019
     (80NSSC20K0323)*, 2019:1–6, 2019.

[44] Joe Tansock and Scott Hansen. DigitalCommons @ USU Guidelines for Radiometric Calibration
     of Electro-Optical Instruments for Remote Sensing. 2015.

[45] M.Pd Taufiq Rohman, S.Pd.I. Instrument calibration overall. *Psikologi Perkembangan*, (October
     2013):1–224, 2019. ISSN 1098-6596.

[46] Newport Technologies. Five-Axis Fiber Positioner. `https://www.newport.com/p/9016NF`.

[47] Paul R. Yoder and Frédéric Lamontagne. Optical mounts: Lenses, windows, small mirrors, and
     prisms. *Handbook of Optomechanical Engineering, Second Edition*, pages 269–337, 2017. doi:
     10.4324/9781315153247.

[48] Paul R Yoder and Daniel Vukobratovich.   *Opto-Mechanical Systems Design*.   .   ISBN
     9781482257717.

[49] Paul R Yoder and Daniel Vukobratovich. *Opto-Mechanical Systems Design*, volume 2. CRC Press
     Taylor Francis Group, 6000 Broken Sound Parkway NW, Suite 300 Boca Raton, FL, 4 edition, .

[50] Ugur Ünal. Optomechanical analysis and experimental validation of bonding based prism and
     mirror mounts in a laser system, thesis project. (February), 2012.